Reinforcement Anchorage in Grouted Connections for Precast Bridge Bent Cap Systems

by

Mark Clinton Waggoner, B.S.C.E

Thesis

Presented to the Faculty of the Graduate School of

The University of Texas at Austin

in Partial Fulfillment

of the Requirements

for the Degree of

Master of Science in Engineering

The University of Texas at Austin

May 1999

Reinforcement Anchorage in Grouted Connections for Precast Bridge Bent Cap Systems

Approved by
Supervising Committee:

Supervisor: M.E. Kreger

S.L. Wood

For my parents

Acknowledgements

I would like to express my gratitude to Dr. Kreger, whose guidance and trust allowed me to grow intellectually as I sought out my own ideas and made mistakes that I learned valuable lessons from. I would also like to thank the other project members, Dr. Wood and Dr. Breen, for their insightful suggestions. I must also express my gratitude to our TxDOT contacts, Mr. John Vogel, Mr. Lloyd Wolf, and Mr. Robert Sarcinella, without whom this research would not be possible.

The research presented here was performed with and largely driven by Mr. Eric Matsumoto. I cannot adequately express how grateful I am to Eric for his tireless efforts in pursuing this project, and his valuable leadership and organization in executing the research reported here. I am constantly amazed at the level of energy he brings to the lab every day.

The Ferguson Structural Engineering Laboratory staff were invaluable in the completion of this research. My thanks to Blake Stassney, Mike Bell, Wayne Fontenot, Ray Madonna, Laurie Golding, Ruth Goodson, Regina Forward, and Denise Nealy.

My most heartfelt gratitude goes out to my parents, whose love, support, and encouragement have made this possible. Finally, I would like to thank my fiancé Anne, whose refusal to let me call her every night allowed me to finish this on time.

Mark Clinton Waggoner
May 1999
Austin, Texas

Reinforcement Anchorage in Grouted Connections for Precast Bridge Bent Cap Systems

by

Mark Clinton Waggoner, M.S.E.
The University of Texas at Austin, 1999

Supervisor: Michael E. Kreger

As urban bridge construction in Texas becomes more prevalent, the need to employ progressive construction practices that minimize the impact of a project on the commuting public grows. One method identified by the Texas Department of Transportation (TxDOT) to facilitate rapid bridge erection is through the use of precast bent caps rather than traditional cast-in-place substructures.

Through work with TxDOT engineers and an Industry Review Committee (IRC), details were developed to connect precast bent caps with cast-in-place columns and precast piles. These connection details emphasized economy, ease of erection, and durability. Four primary connection systems were identified:

grout pocket connections, grouted vertical duct connections, bolted connections, and grouted sleeve connections. These systems utilize both straight and upset-headed connection reinforcement.

To address concerns of adequate anchorage capacity in grout pocket and grouted vertical duct connections, pullout tests of upset-headed and straight bars simulating typical grouted connections were conducted. Variables studied included embedment depth, grout type and strength, bar size, loading type, and pocket confinement.

Twenty-four grout pocket pullout tests were conducted. Depending on the embedment depth, the anchorage strength was controlled either by the concrete breakout capacity or the steel strength. The wedging action of the grout pocket produced a favorable confining effect in the grout, but also produced significant cracks at the pocket corners which separated the tensile stress fields, resulting in reduced capacity for upset-headed bars. Anchorage design procedures were developed for straight and upset-headed bars through simple modifications to existing methods.

Eight grouted vertical duct tests were conducted. Bar development lengths were found to be much shorter than what is required in plain concrete due to the confining effects of the duct. Duct anchorages failed when the concrete and duct could no longer restrain the splitting forces in the grout. Because existing methods could not be applied to grouted duct anchorages, a design procedure was developed that limits bond stress to levels that may be easily restrained by the duct and concrete.

Table of Contents

List of Tables

List of Figures

CHAPTER 1

INTRODUCTION

1.1 BACKGROUND

As urban bridge construction in Texas becomes more prevalent, the need to employ progressive construction practices that minimize the impact of a project on the commuting public grows. The cost of traffic delays to motorists due to construction in crowded urban corridors mounts as bridge projects become increasingly large. In addition, concerns about worker and vehicle safety have heightened as traffic volume has increased. These costs associated with traffic control have forced the Texas Department of Transportation (TxDOT) to seek innovative methods to build traditional economic bridge forms.

One method of facilitating rapid bridge erection is through the use of precast bent caps rather than traditional cast-in-place substructures. Already, TxDOT employs precast, prestressed beams and panels in the standard concrete bridge system. Precast bent caps would extend the advantage of rapid erection that precast construction provides. Controlled plant production provides a consistent, high-quality product that allows the opportunity to use high-performance concrete. Repetition of precast cap members in large projects provides a significant opportunity for project economy. In addition, precast bent

caps may be well suited for other difficult construction environments, such as a site over water or a remote site.

Already, precast bent caps have been employed in several projects around Texas due to the advantages they provide over traditional cast-in-place construction. The Pierce Street Elevated Freeway project in Houston required replacement of 1.6 miles of bent caps and superstructure in one of Houston's busiest transportation corridors. The use of precast caps allowed the project to be completed in under 100 days. For the Red Fish Bay/Morris & Cummings Cut bridges near Aransas Pass the contractor chose to use precast bent caps to avoid the difficult process of casting concrete over water. In each of these cases project erection considerations drove the decision to use precast bent caps.

Precast bent caps provide a promising solution to urban bridge construction problems, but the details of creating a viable precast bent cap system must be carefully examined. Erection of precast bent caps requires tight tolerances, and Texas bridge contractors have little experience with precast cap construction. Constructable joint details to connect precast bent caps with cast-in-place columns or piles must be developed that are capable of transferring the expected moments and shears. Of particular concern is the anchorage of the column longitudinal reinforcement in the precast cap, which is typically too shallow to provide a full development length. Connection durability concerns must also be addressed.

1.2 THE BENT CAP SYSTEM: CAST-IN-PLACE VS. PRECAST

In a bridge system, a bent cap serves several purposes. The main function of a bent cap is to provide vertical support to the longitudinal girders. The longitudinal girders typically rest on bearings placed on the bent cap. In concrete superstructure bridges the bearing is usually a neoprene pad, and for steel superstructures the bearing may be either a neoprene pad or steel bearing. The bent cap also contributes to the lateral and longitudinal stability of the bridge. Under lateral loads, such as wind, earthquake forces, or stream pressures, the bent cap and columns act as a moment-resisting frame to provide stability. Under longitudinal forces, such as temperature forces or braking forces, the bent cap transfers shear to the columns, which transfer the load into the foundations as a cantilever.

In Texas, cast-in-place construction is typically used for the entire substructure, including foundations, columns, and bent cap. Two types of bent caps are commonly employed in Texas. Figure 1.1 shows a rectangular bent cap, which is employed when bridge clearance is not an issue. The rectangular bent cap is the most common cap type in Texas, and offers the advantage of being easy to form in the field. The inverted-T bent cap, pictured in Figure 1.2, is most often used in urban environments where bridge clearance is an important consideration. The lower ledge of the inverted-T bent cap allows the main section of the cap to coincide with the depth of the longitudinal girders. This offers aesthetic advantages, producing a smooth, shallow bridge profile. However, the inverted-T cap requires a large, heavy section.

Figure 1.1: Typical Rectangular Bent Cap

Figure 1.2: Typical Inverted-T Bent Cap

Precast bent caps may be adapted to either the rectangular or inverted-T bent cap form. Rectangular caps offer the advantage of being small and light, and would be simple to erect. However, rectangular cap depths are typically between 24 and 42 inches deep, which in many cases does not provide sufficient depth to develop the longitudinal column steel that projects into the cap. Inverted-T caps are often up to 7 feet in total depth, which would provide enough depth to develop even groups of large bars. However, the weight of inverted-T caps may limit the length of bent cap section which could be easily erected. In both rectangular and inverted-T caps, the total cap length may need to be broken into sections to facilitate erection. The sections would then be joined by post-tensioning or a cast-in-place closure.

The logical extension of precast bent caps is to use a completely precast substructure, including columns. However, bridge foundation systems in Texas typically consist of drilled shafts. Since the drilled shafts are usually the same shape as the bridge columns, it is simple to continue forming from the ground level to the top of the column. Therefore, precast columns offer no real construction advantage over cast-in-place columns. The research reported here will focus on connecting a precast bent cap to a cast-in-place column. The same concepts will apply to precast driven piles.

1.3 BENT CAP/COLUMN CONNECTION TRANSFER FORCES

As discussed above, a bent cap is subjected to a number of forces that must be transferred as a moment, shear, or axial load to the columns. Moments and shears must be transferred in both the longitudinal and transverse directions

of the bridge. The types of bridge loads and magnitudes are found in specifications produced by the American Association of State Highway and Transportation Officials (AASHTO). Similar types of loads are specified in both the Standard Specifications for Highway Bridges [1] and the LRFD Bridge Design Specifications [2].

The forces that tend to roll the cap off of the columns in the direction of the bridge axis are pictured in Figure 1.3. The moments and shears produced by these forces are referred to as **longitudinal** moments and shears. There are two principal sources of longitudinal moments and shears: unbalanced dead and live load girder reactions, and longitudinal deck forces due to braking, temperature, and shrinkage. Since the longitudinal girders typically bear on the bent cap at a point offset from the centroid of the column, a longitudinal moment is produced equal to the girder reaction multiplied by the eccentricity of the reaction. This is particularly critical in Inverted-T caps, which have a large eccentricity due to the girder ledge. In most cases, the forward and back spans at a bent produce longitudinal moments that cancel. However, in cases of unequal forward and back-span lengths, unbalanced live loads, or unbalanced erection sequences, a net unbalanced longitudinal moment will exist.

Forces produced when the bent cap and columns act as a planar frame to resist lateral loads are referred to as **transverse** moments. Figure 1.4 shows these forces acting on a portal substructure. Typically in Texas, wind and stream pressure contribute to producing transverse moments and shears, though in other locations earthquake forces must be considered.

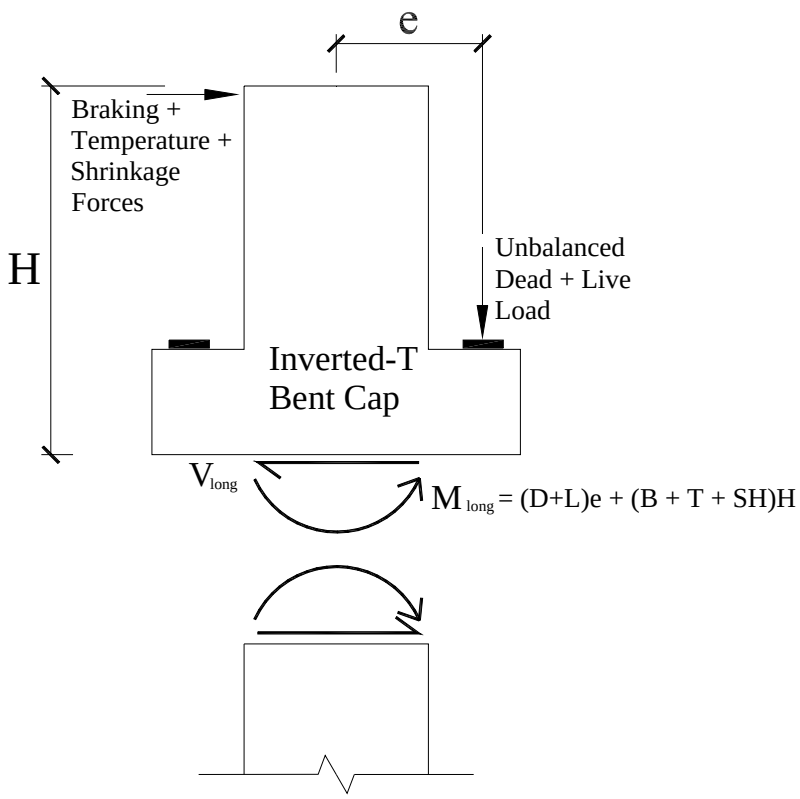

Figure 1.3: Longitudinal Moments and Shears in an Inverted-T Bent Cap

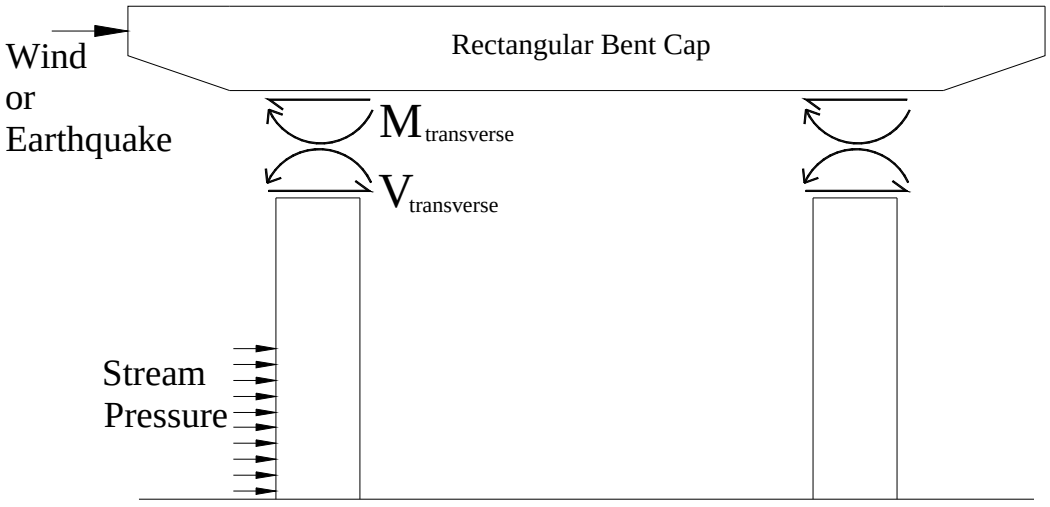

Figure 1.4: Transverse Moments and Shears in a Rectangular Bent Cap

A preliminary study was performed to determine the range of forces that a connection would be required to transfer. The parameters and results are discussed in Reference 3. Through analyzing typical bridge and connection geometries, it was found that significant tension forces could develop in the bent cap-to-column connection reinforcement due to longitudinal and transverse moments. This means that anchorage of the connection reinforcement in the cap will be a primary detailing concern when designing the connection. Shears were found to be generally low compared with the capacity provided by the connection reinforcement through shear friction.

1.4 OBJECTIVES

The overall objective of this research program is to develop reliable, durable, and constructable precast bent cap connection details that are economically competitive with cast-in-place construction. In developing these details, a primary goal must be to identify methods of anchoring connection reinforcement in the precast bent cap. Products such as headed reinforcing bars, U-shaped reinforcing bars, and mechanical bar splices are promising options for providing positive connection anchorage. In addition, issues of durability and constructability must be addressed in order to produce a viable connection.

In developing connection details, design guidelines must be established for the components of the connection. Another objective of this research is to establish design methods for the anchorage systems employed in the connection. Pullout testing of the grouted connection systems developed in Chapter 2 will help establish these design guidelines.

1.5 SCOPE

The research reported here focuses on the reinforcement anchorage aspects of precast bent cap connections. Future research at The University of Texas at Austin will provide recommendations for the design of the entire precast bent cap system, including constructability, durability, and connection issues.

Connection details were developed through working with TxDOT engineers and local precasters. Of the four connection systems identified, grout pocket connections and grouted vertical duct connections were identified for testing. Twenty-four pullout tests simulating grout pocket connections and eight pullout tests simulating grouted vertical duct connections were conducted to determine the anchorage behavior. Test variables included embedment depth, grout type and strength, bar size, loading condition, and confinement steel. These variables were identified to cover the range of expected precast bent cap connection parameters.

Based on these tests, possible modifications to existing design methods for headed and straight bar anchorages are explored. Design recommendations for anchorage of both headed and straight reinforcement in grout pockets and grouted vertical ducts are presented. Specific application of these methods to precast bent cap connections is also discussed.

CHAPTER 2

DEVELOPMENT OF CONNECTION DETAILS

2.1 PREVIOUS PROJECTS

In developing initial precast bent cap connection details, several previous projects that successfully used precast substructures were studied. Precast bent caps were used in two recent TxDOT projects, the Pierce Street Elevated Freeway project in Houston and the Red Fish Bay/Morris & Cummings Cut Bridges near Port Aransas. In each case, issues of constructability drove the decision to use precast bent caps. In addition to these Texas projects, the Florida Department of Transportation (FDOT) has pursued the use of precast substructures as a standard bridge option [4]. Other projects, including a precast pier designed by the Navy and a railroad bridge system proposed by TxDOT, were also evaluated for promising connection concepts.

2.1.1 Pierce Street Elevated Freeway

The 1.6 mile Pierce Street Elevated Freeway on Interstate 45 is one of the busiest transportation corridors in Houston, linking downtown with Galveston island and the southeast suburbs. The original Pierce Street substructure design consisted of cast-in-place inverted-T bent caps and circular columns supporting the typical TxDOT superstructure of precast, pretensioned girders and cast-in-place deck. After 25 years in service, significant deterioration of the concrete

substructure was observed (Figure 2.1). This damage was thought to be primarily due to reinforcement corrosion caused by inadequate concrete cover and runoff from the joints above the bent caps, and was deemed significant enough to warrant replacing the bridge.

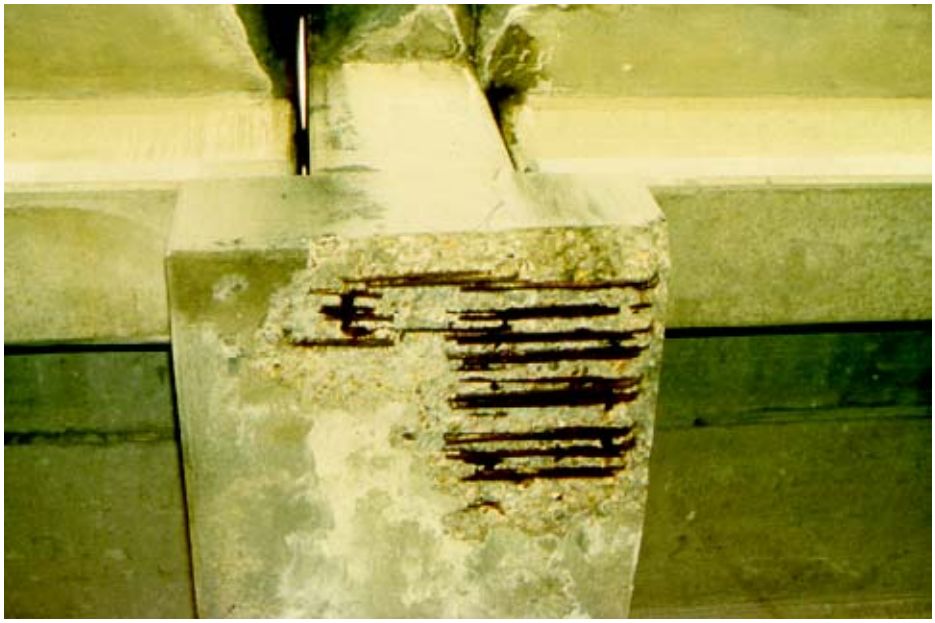

Figure 2.1: Corrosion Damage of Original Pierce Street Bridge

Due to the high volume of traffic carried by Pierce Street, the ability to rapidly erect the bridge replacement drove the design. The existing bridge superstructure and bent caps were removed, and the damaged portions of the column tops were saw-cut, eliminating the need to erect new columns. The bridge replacement consisted of precast inverted-T bent caps supporting precast AASHTO Type-IV girders and a cast-in-place deck with precast panels.

TxDOT Engineers designed a bolted connection to connect each precast bent cap to existing columns. High strength Dywidag bars were grouted into vertical holes drilled in the core of the existing column. These bars were then

proof tested to ensure adequate anchorage to the columns. The precast cap contained vertical ducts in the connection area, and the Dywidag bars were threaded through these ducts to erect the precast bent cap (Figure 2.2). The bent cap was supported by shims on the columns, creating a small bedding layer between the cap and column top (Figure 2.3). This bedding layer was grouted along with the duct and anchorage zone at the top of the cap to complete the connection.

Constructed in 1997, the Pierce Street Elevated Freeway project was remarkably successful in that it was completed in under 100 days, due largely to the use of precast elements. The bolted connection used is well suited to inverted-T caps that must transfer large forces, though durability issues remain. Possible cracking in the grouted areas due to shrinkage and creep could provide moisture ingress paths that could trigger corrosion. Though this connection facilitates rapid erection, the skilled labor and number of construction operations required for the bolted connection make it an expensive option that should be reserved only for cases where transfer of high forces is required.

2.1.2 Red Fish Bay and Morris & Cummings Cut Bridges

The Red Fish Bay and Morris & Cummings Cut Bridges (RFB) are located over the Gulf Intracoastal Waterway along Texas State Highway 361 between Port Aransas and Aransas Pass. The original bridges at this location required replacement due to deterioration caused by the severe salt-water environment. TxDOT designers chose a substructure consisting of a cast-in-place

Figure 2.2: Erection of Pierce Street Elevated Precast Inverted-T Bent Cap

Figure 2.3: Precast Bent Cap Resting on Shims Prior to Grouting

bent cap on precast piles supporting a pretensioned double-tee superstructure [5]. The contractor, in an attempt to minimize the amount of cast-in-place concrete over water, proposed using precast bent caps. This proposal was accepted by TxDOT, and the bridges were built in 1995 using a connection detail for the precast rectangular caps designed by the contractor.

After the precast concrete piles were driven, two U-shaped epoxy-coated #9 bars were epoxy grouted into embedded vertical sleeves in the top of the piles. The precast bent cap was cast with two pockets at the location of each pile connection, as shown in Figure 2.4. The sides of these pockets were inclined to facilitate form removal and lock the field cast portion of the connection in place. The precast cap was lowered over the U-shaped bars and set on friction collars (Figure 2.5), again leaving a bedding layer between the cap and pile. Concrete was cast in the pocket region to complete the connection.

Figure 2.4: Grout Pockets

Figure 2.5: Erection of Red Fish Bay Precast Rectangular Bent Caps

The construction efficiency of precast bent caps on the RFB project was again apparent as the project finished six months ahead of schedule. The connection detail developed for this project provides a simple alternative with few construction operations that is well suited to trestle pile bridges with low force transfer between the cap and piles. However, uncertainties remain as to the force transfer mechanism between the pocket material and parent concrete. The research reported here will address these concerns. Many of the same durability concerns related to bolted connections exist for pocketed connections, especially since the pocket option leaves an exposed seam on the top of the precast cap. During a recent visit to the bridge, the connection region appeared to be in excellent condition with no apparent cracking at the pocket top or bedding layer.

2.1.3 Other Projects

Several other projects have been completed both in Texas and in other states that utilize precast substructures. Most of these projects, such as the Vail

Pass Bridge in Colorado, the Linn Cove Viaduct in North Carolina, and the U.S. 183 Viaduct in Austin [6], utilize precast segmental piers. Projects such as the Lake Pontchartrain Bridge in Louisiana [6] and the Edison Bridge in Florida represent more typical applications of precast bent caps and are thus more relevant to this research program. The following sections summarize precast substructure work that has contributed to ideas for precast bent cap connections in Texas.

2.1.3.1 Florida Projects

The Edison Bridge in Fort Meyers, Florida, pictured in Figure 2.6, utilizes both precast bent caps and I-shaped precast columns [7]. The connection between the columns and cap is achieved using a proprietary grouted sleeve coupler. A typical grouted sleeve coupler, the Lenton Interlock, is pictured in Figure 2.7. This type of connection insures full continuity of column longitudinal reinforcement into the cap and thus provides reliable force transfer. However, the proprietary nature of the hardware used for this connection limits the options for the designer and contractor, which may affect the economy of the construction.

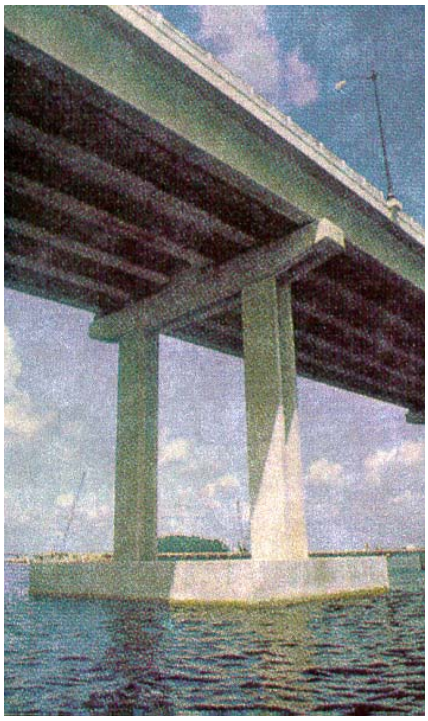

Figure 2.6: Edison Bridge Precast Bent

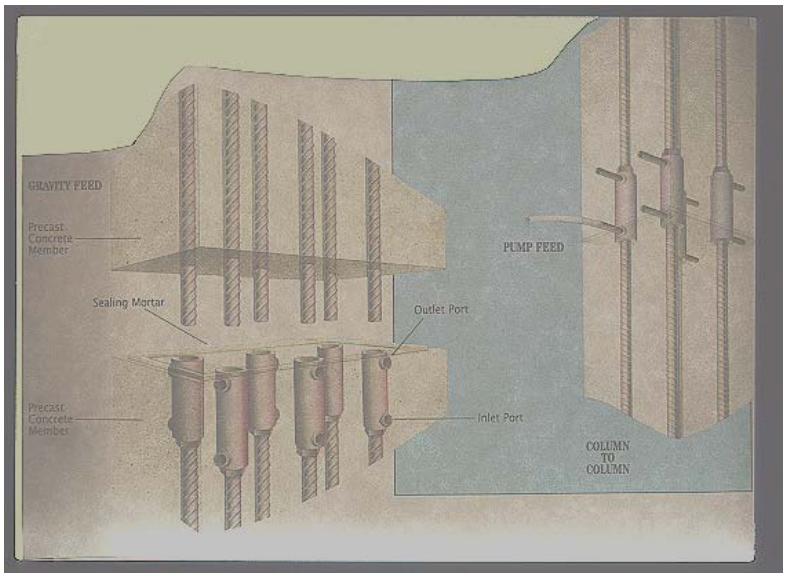

Figure 2.7: Lenton* Interlock *Grouted Sleeve Coupler

An effort is currently underway by FDOT and LoBouno, Armstrong, and Associates to develop standard precast substructure components and connections for use in Florida [4]. The connection concepts the research team has focused on include the grouted sleeve coupler connection and cast-in-place concrete connection, such as that used at RFB. The end result of the research will be a set of standard details, though no testing is planned.

2.1.3.2 Texas State Railroad Bridge Proposal

TxDOT Engineers developed a precast bent cap system in 1995 for a series of railroad bridges. Though the bridges were not built, they offer another option for precast substructures. As shown in Figure 2.8, the precast cap is set over driven steel H-piles and grouted to complete the connection. The superstructure consists of precast box beams. Though considered a viable system,

steel-H piles are rarely used for bridge substructures in Texas and thus this system will not be considered further.

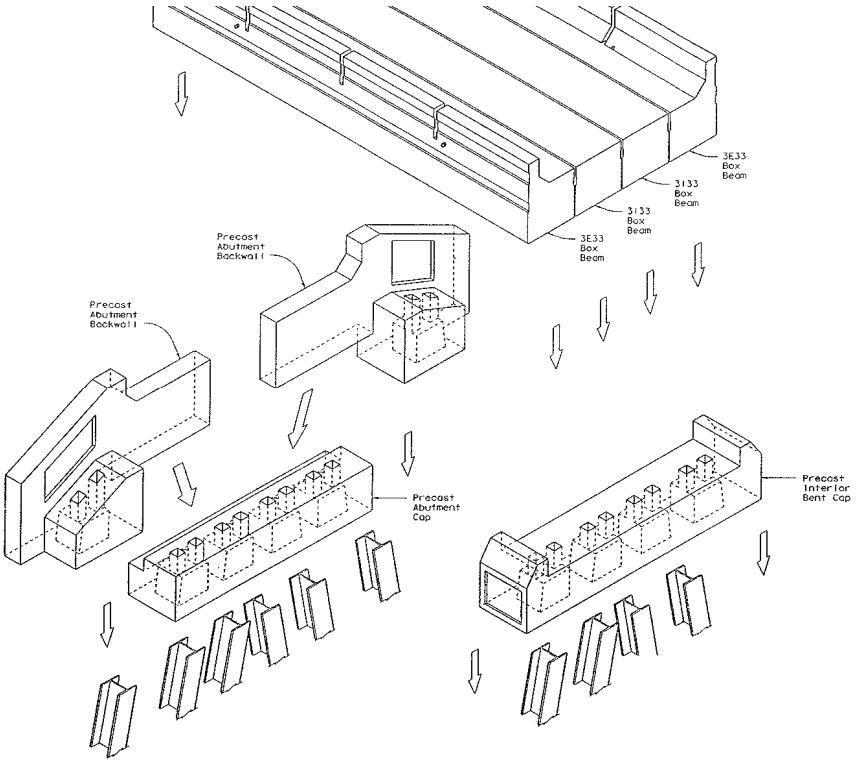

Figure 2.8: Texas State Railroad Bridge Precast Bent Cap System

2.1.3.3 Ingleside Navy Pier

The Ingleside Navy Base located near Aransas Pass, Texas recently completed construction of a pier structure for small marine vessels. Designed by the U.S Navy, the pier substructure is very similar to that of the RFB project. Precast bent caps were set over reinforcement protruding from driven, battered precast piles. The connection was completed by grouting the pocket region, which again has inclined sides.

2.2 PRIMARY CONNECTION CONCEPTS

Based on the previously identified projects and a review of the relevant literature, several precast connection concepts were developed. The connections can be fit into four basic groups:

1. Grout Pocket Connections (Figures 2.9 & 2.10)
2. Grouted Vertical Duct Connections (Figure 2.11)
3. Bolted Connections (Figure 2.12)
4. Grouted Sleeve Coupler Connections (Figure 2.13)

The connections were designed for use with both rectangular and inverted-T caps on cast-in-place columns or precast piles. Table 2.1 shows which column/cap geometries are best suited for each connection.

These connection concepts were developed through several cycles of refinement with input from an Industry Review Committee (IRC) consisting of members of the precast and construction industries, as well as TxDOT engineers. The members of the IRC are listed in Table 2.2. The principal input from the IRC was in the areas of economics and constructability. The IRC members emphasized simplicity of the connection details in order to achieve maximum economy. For example, the number of field operations required for a particular connection should be minimized. In addition, the connection should utilize familiar construction practices and avoid proprietary products. Complex operations such as match-casting and post-tensioning should be avoided. The connection concepts developed from these meetings have been intentionally kept

simple in order to make precast bent cap construction economically competitive with cast-in-place construction.

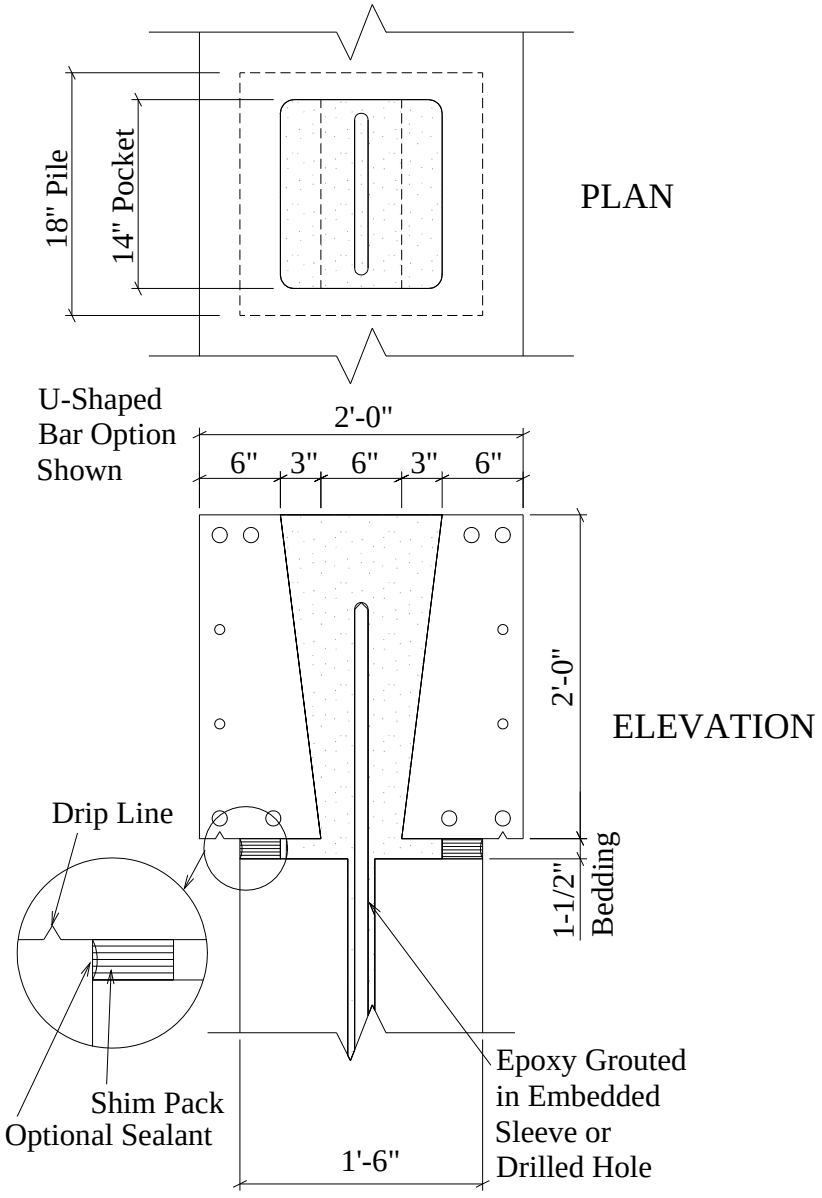

24" Square Cap on 18" Piles Shown

Figure 2.9: Single Line Grout Pocket Connection (SLGP)

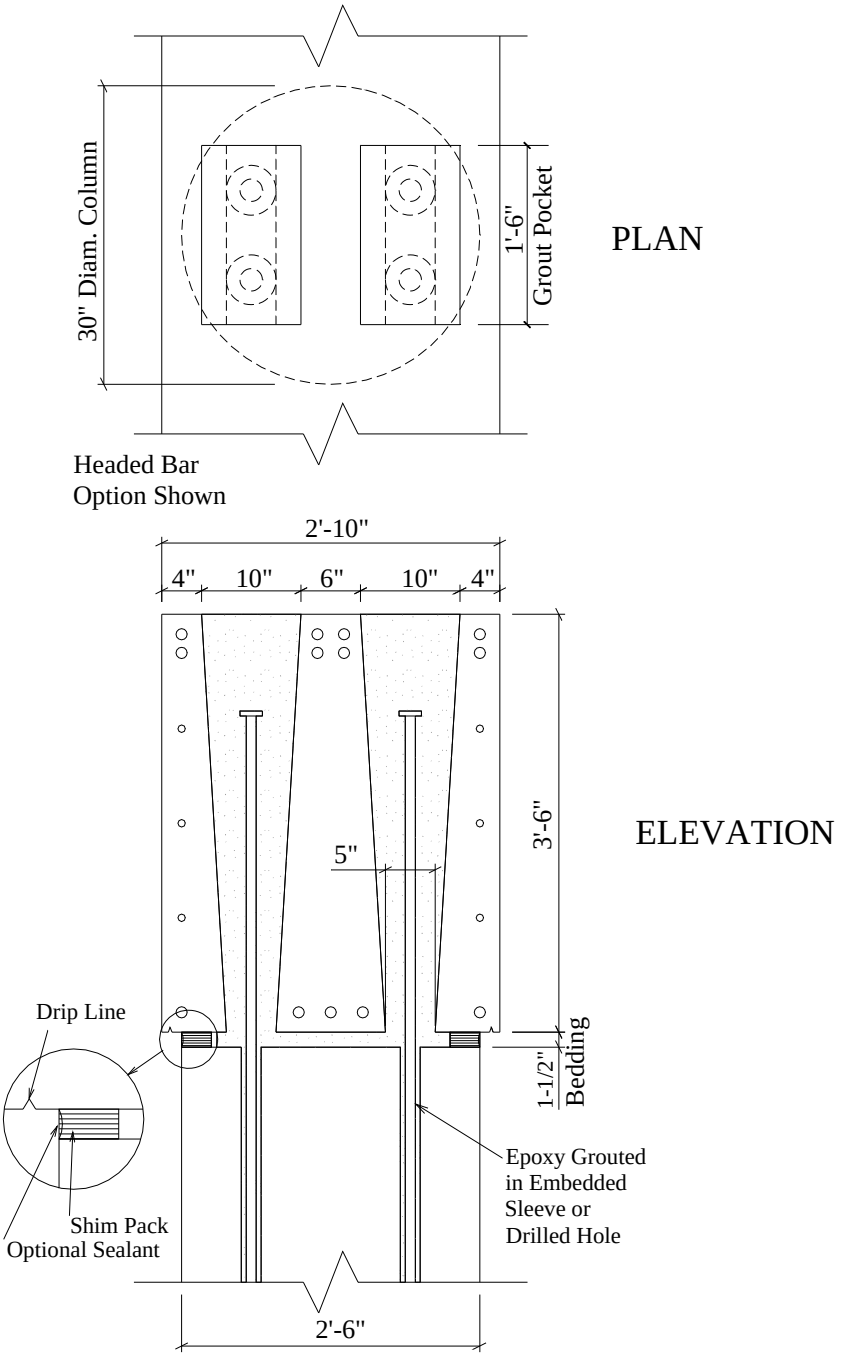

Figure 2.10: Double Line Grout Pocket Connection (DLGP)

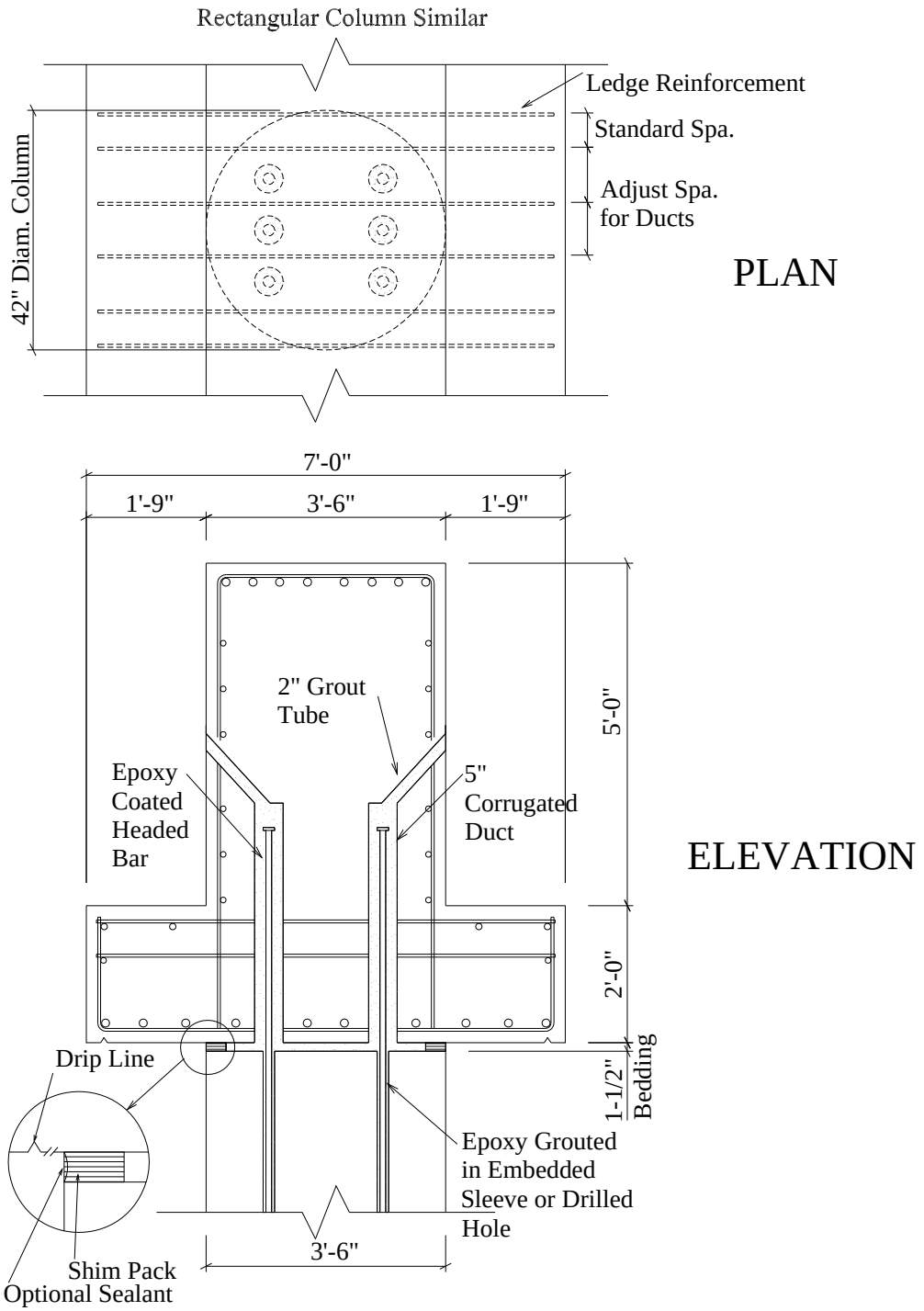

Figure 2.11: Grouted Vertical Duct Connection (GVD)

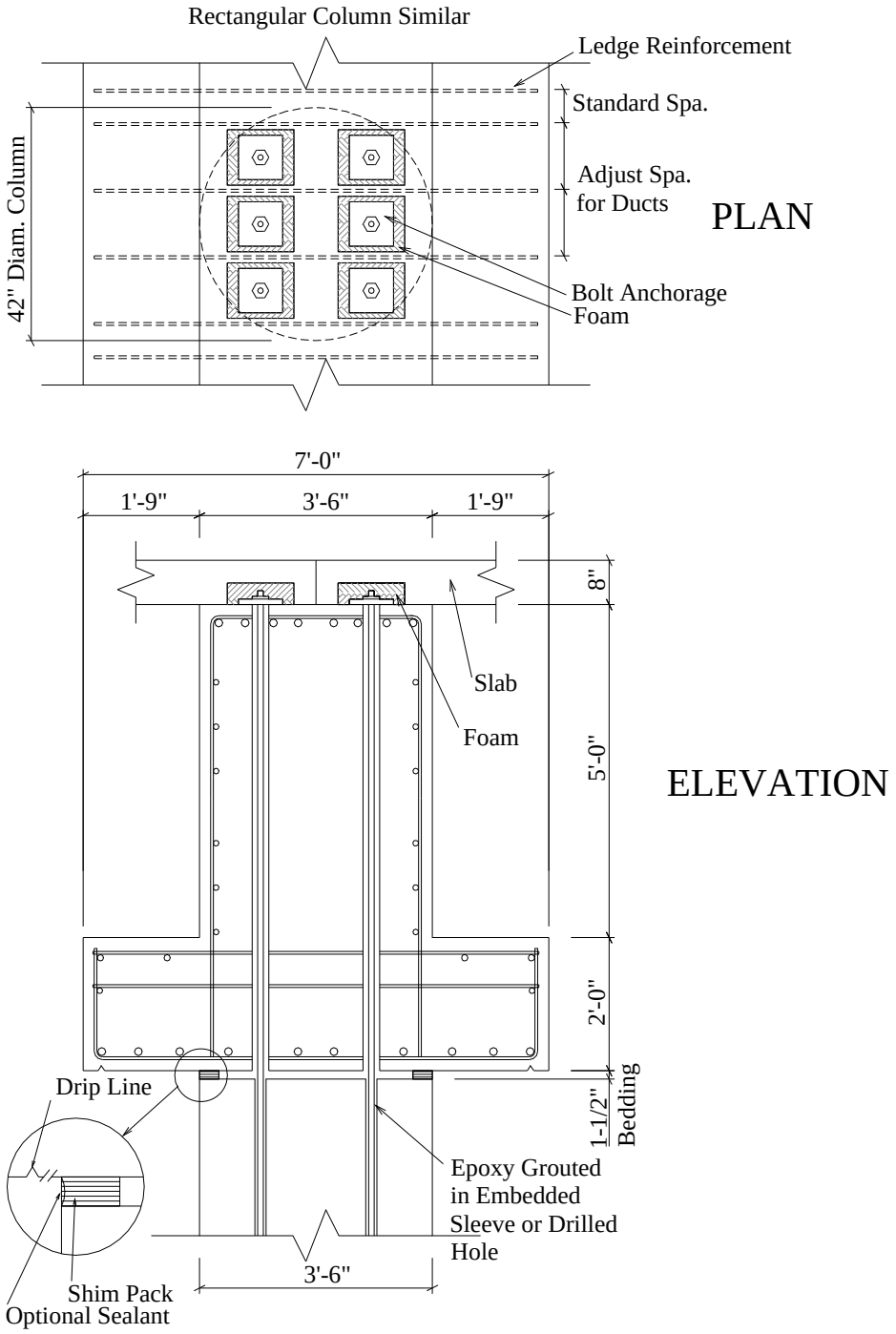

Figure 2.12: Bolted Connection (BC)

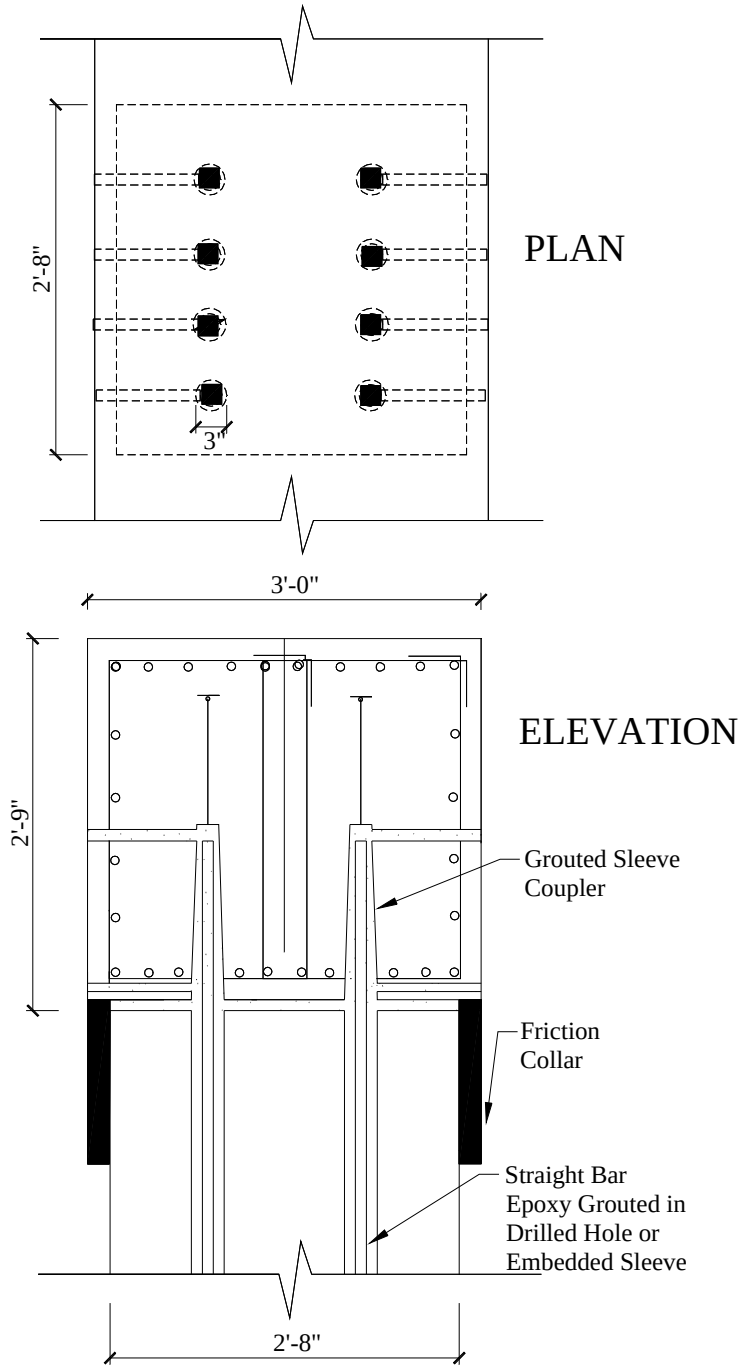

Figure 2.13: Grouted Sleeve Coupler Connection (GSC)

Table 2.1: Applicability of Precast Bent Cap Connections to Various Bridge Types

Column	Trestle Piles		Cast-in-Place Columns	
Cap	***Rectangular***	***Inverted-T***	***Rectangular***	***Inverted-T***
Low Moment	SLGP GVD	GVD	SLGP, DLGP GVD GSC	GVD BC GSC
High Moment	N/A	N/A	DLGP GVD GSC	BC GVD GSC

Table 2.2: Industry Review Committee (IRC)

Charlie Burnett	Champagne-Webber, Houston
Paul Guthrie	Texas Concrete, Victoria
Fred Heldenfels IV	Heldenfels Enterprises, San Marcos
Randy Rogers	McCarthy Brothers, Austin
Carl Thompson	Dalworth Concrete, Houston
Roger Welsh	Assoc. General Contractors, Austin
Robert Sarcinella	TxDOT
John Vogel	TxDOT
Lloyd Wolf	TxDOT

A complete discussion of the development of the connection details is located in Reference 3. The purpose of this research is to determine the force-transfer characteristics of grout pocket connections and grouted vertical duct connections. Bolted connections will be the subject of upcoming research at The University of Texas at Austin involving half and full-scale bent cap-column assemblages. The grouted sleeve coupler connection is considered to be a reliable though expensive option that does not require experimental testing. Future FDOT work should determine the effectiveness of this system.

2.2.1 Grout Pocket Connections

Figure 2.9 shows a typical grout pocket connection between a rectangular cap and precast pile. An inverted pyramidal-shaped pocket is formed in the precast cap. The pocket has side slopes of 5 to 7 degrees along the axis of the cap, and small side slopes at the ends of the pocket. U-shaped bars or headed bars are epoxy grouted into a drilled hole or embedded sleeve in the pile, and the precast cap is lowered over the bars and set on shims, leaving a small bedding layer to accommodate vertical tolerances. After forming around the bedding layer, the pocket and bedding layer are filled with a non-shrink cementitious grout to complete the connection. If headed bars are used, several bars can be fit within each pocket to accommodate longitudinal and transverse moments.

For cases that require transfer of larger longitudinal moments, it may be necessary to locate the connection steel in a more efficient manner. Figure 2.10 illustrates a grout pocket connection with two pockets, hereafter called a double-line connection. Here the steel is located to provide a larger internal moment arm to accommodate the higher transfer forces associated with medium to long span lengths. The taper of the double-line pocket is smaller in order to reasonably fit two pockets into the bent cap section.

The grout pocket connection has several advantages. It utilizes familiar construction practices with simple field operations. The bedding layer and large pocket allow for generous tolerances, which are essential when placing a large precast component such as a bent cap. The inverted pyramidal shape of the grout pocket precludes slippage between the grout and surrounding concrete, and the

wedging action produced by the shape helps to confine the grout around the reinforcing bar, improving bar anchorage. The pocket shape also facilitates easy form removal.

The grout pocket connection also has disadvantages. The presence of shims in the bedding layer may induce cracks as the surrounding grout deforms under creep and shrinkage strains. Since the bedding layer is a key element in the connection load path, care must taken during grouting to ensure that no air pockets are present in the bedding layer. Also, the grout mix must be volumetrically stable. Any grout shrinkage away from the pocket sides could adversely affect the bar anchorage.

The research presented here related to the grout pocket focuses on the force transfer characteristics. Does the connection behave as a monolithic bar anchorage, or does the presence of the pocket influence the anchorage capacity of the bar? What embedment length is required to fully develop the bar, and does the anchorage provide sufficient ductility? The effect of various grout mixes is also examined, as well as various bar options.

2.2.2 Grouted Vertical Duct Connections

The grouted vertical duct connection, shown in Figure 2.11, is a variation on the grout pocket connection using a stay-in-place corrugated duct to form the pocket. A standard 4″ diameter corrugated duct is pictured in Figure 2.14. The duct is embedded in the precast cap, forming a conduit for the straight or headed reinforcing bar protruding from the column. The duct may either extend the full

depth of the cap or partial depth, in which case the connection is grouted through tubes from the side of the cap.

This connection offers many of the same advantages and disadvantages as the grout pocket connection, though tolerances for cap placement are slightly tighter. In this case the duct serves to enhance bar anchorage by confining radial splitting forces from the bar. Duct corrugations anchor both the grout within the duct and the duct within the parent concrete. This research seeks to determine both the possible failure modes for this type of connection and the extent to which the duct confinement enhances bar anchorage for both straight and headed bars.

Figure 2.14: 4″ Corrugated Duct

2.3 BAR OPTIONS

In the connection concepts described above, several options were mentioned for the reinforcing bar connection between the cap and the column. The limited depth of pile caps (typically 24″) and rectangular caps (30″ to 42″) preclude the use of straight bars since the development lengths may exceed the available depth. Deeper inverted-T caps may provide enough depth to develop a straight bar, but the long development lengths of large bars may lead to congestion in the connection region. Therefore, headed reinforcing bars are ideally suited for use in these connections.

2.3.1 Headed Reinforcing Bars

Headed reinforcement consists of a steel plate friction welded or threaded onto the end of a standard deformed bar. Two types of typical headed reinforcing bars are shown in Figure 2.15. Bar anchorage is achieved by a combination of bearing at the plate and bearing on the standard bar deformations. Typical development lengths are therefore much shorter than that of a straight reinforcing bar. More information on types of headed reinforcement may be found in Reference 8.

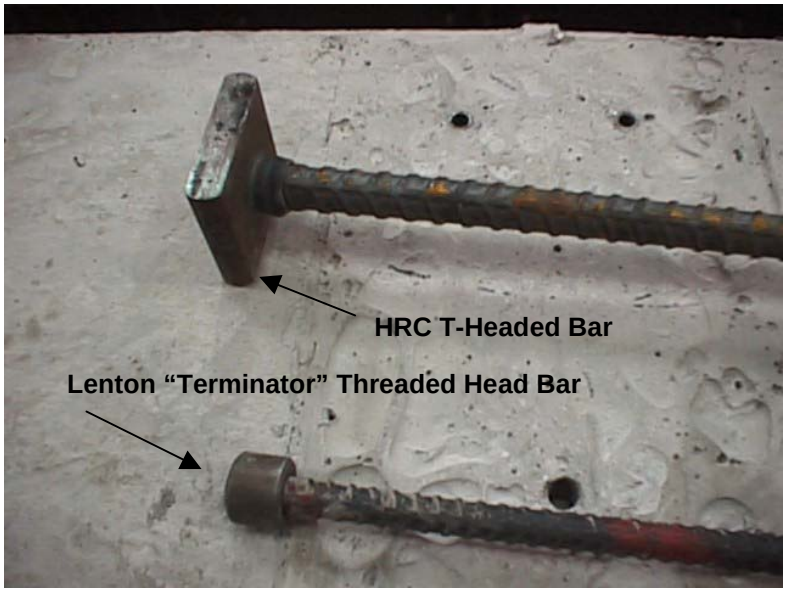

Figure 2.15: Headed Reinforcing Bars

2.3.2 Upset-Headed Reinforcing Bars

Though headed reinforcing bars are ideally suited for use in precast connections, the size of the head limits the tolerances available when erecting a precast bent cap. Headed Reinforcement Corporation of Fountain Valley, California has recently developed the upset-headed bar, which has a knob-shaped

head with a diameter of 1.4 times that of the reinforcing bar diameter. Figure 2.16 shows upset-headed bars for three different bar sizes. The bar head is formed by heating the end of the bar and pressing it into a mold. The smaller head of the upset-headed reinforcing bar makes it an ideal option for the vertical duct and double-line grout pocket connections which require tight tolerances.

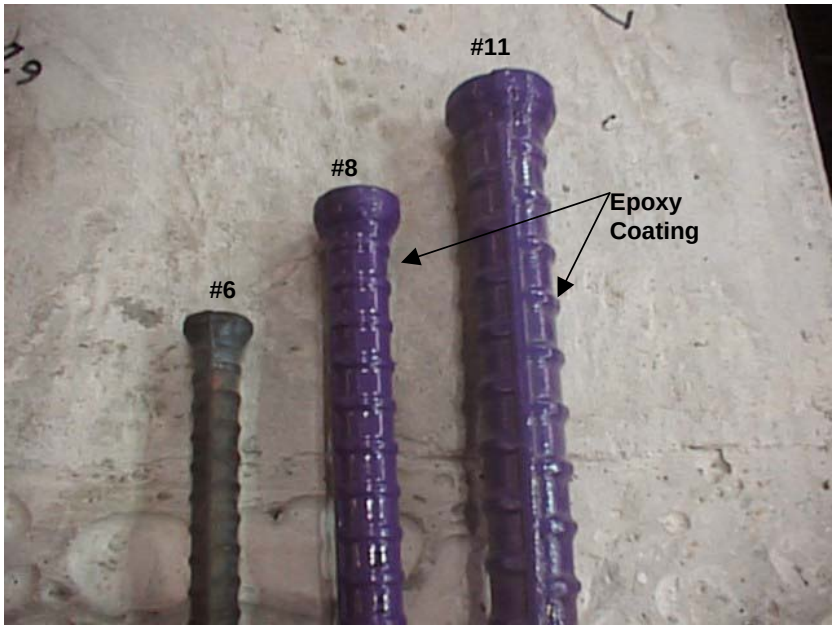

Figure 2.16: Upset-Headed Reinforcing Bars

2.3.2 Straight Reinforcing Bars

Though headed reinforcement may be required in many cases to achieve adequate anchorage, straight reinforcing bars are vastly cheaper since they are not a specialty item. Straight reinforcement also eliminates the tolerance problems associated with headed reinforcement. For these reasons, straight reinforcement should be used wherever possible to simplify the connection. As well as inverted-T caps, some deep rectangular caps may accommodate straight bars as long as

smaller bar diameters are used. Vertical duct connections are promising in that the confinement provided by the duct may allow straight bars to be developed in much shorter lengths.

2.3.3 U-Shaped Reinforcing Bars

The grout pocket connection used in the Red Fish Bay project utilized U-shaped reinforcement. This type of reinforcement provides excellent anchorage and accommodates using standard reinforcement with field bending, but limits the number of bars that may be placed in a pocket. Since the bend diameter of larger bars may be greater than the column core width, U-shaped bars would be limited to cases of low force transfer where smaller bars may be used. Due to this, U-shaped bars were not tested in this research, though the results from headed bar tests may be extrapolated to U-shaped anchorages. Research performed at the University of Kansas by Wright and McCabe [9] compares hooked reinforcing anchorages to headed bar anchorages.

2.3.4 Epoxy Coating

Due to the durability questions associated with grouted connections, epoxy coating of the connection reinforcement should be specified to deter possible corrosion. Deterioration of the connection region could have major implications, as exhibited by the original Pierce Street bridges in Houston. The small expense associated with epoxy coating the connection reinforcement is insignificant compared with the consequences of corrosion, and therefore the research presented here focuses only on epoxy coated reinforcing bars. Research detailing the effect of epoxy coating on bar anchorage may be found in Reference 10.

CHAPTER 3

PREVIOUS RESEARCH AND DESIGN METHODS FOR STRAIGHT AND HEADED BAR ANCHORAGES

3.1 INTRODUCTION

The connections developed in Chapter 2 rely on straight and headed reinforcement to transfer moments between the bent cap and column. Therefore, the anchorage of the connection reinforcement is a key consideration in determining both the strength and stiffness of the precast bent cap system. The behavior of the connection system will depend on the interaction between the reinforcement and the grout, as well as between the grout and parent concrete. Figure 3.1 illustrates the assumed load path for a headed bar in tension in a grout pocket connection.

The behavior of straight and headed anchorages in grout depends on a wide variety of factors, including pocket geometry, embedment length, edge distance, confinement, and grout and concrete strength. Though little research exists for anchorages in grout pockets or ducts, a large amount of research has been performed on anchorage of straight and headed reinforcement in reinforced concrete. Straight bar anchorages have been well researched and the design methods developed from this research are well established in codes such as ACI 318 [11]. More recent research has focused on anchorage of headed

reinforcement [8,9,12], and design methods will appear in future building codes [13].

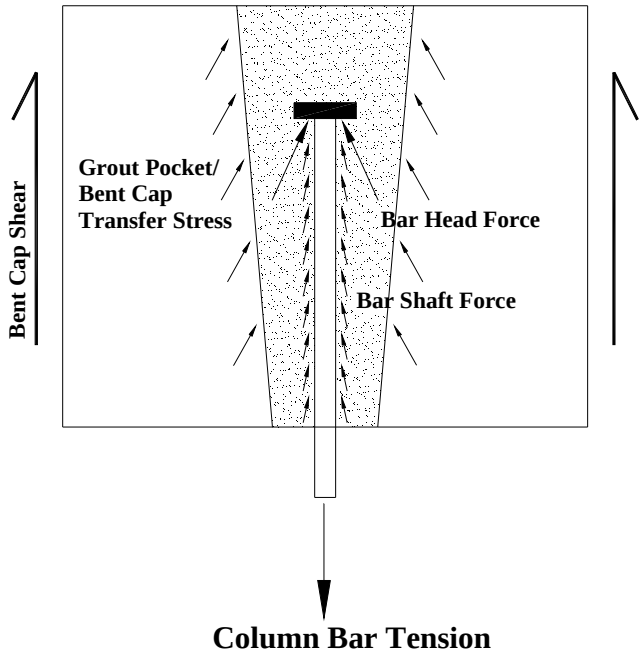

Figure 3.1: Grout Pocket Load Path (longitudinal section through cap)

3.2 BEHAVIOR AND DESIGN OF HEADED ANCHORAGES

Anchorage of headed reinforcement in concrete is accomplished through a combination of bearing along the bar deformations and bearing at the head. In many cases the bar length is short, leaving only the head to anchor the bar. In these cases the headed bar anchorage behaves in a similar manner to cast-in-place anchors such as headed studs, and existing design methods for cast-in-place anchors may be used to predict the behavior. Reference 14 summarizes the vast amount of research that has been performed on cast-in-place anchors. These

design methods will in general under-predict the capacity of headed bar anchorages due to the contribution of the bar deformations.

3.2.1 Potential Failure Modes of Headed Reinforcement in Tension

Research by DeVries at The University of Texas at Austin [8] showed three potential failure modes for headed reinforcement: steel failure, concrete breakout (cone) failure, and lateral blowout failure. A steel failure will occur when the anchorage is sufficient to develop the full strength of the reinforcing bar, and is the desirable failure mode in most cases because of the ductility available in the reinforcement. The strength of the connection is simply:

$$T_{ch} = A_b F_{ub} \qquad \textit{(Equation 3-1)}$$

where: T_{ch} = tensile strength of the headed bar connection

A_b = area of the reinforcing bar

F_{ub} = tensile strength of the reinforcing steel

For design, F_{ub} should be taken as the yield strength, F_y, of the reinforcing bar.

The concrete breakout failure mode corresponds with the formation of a conical fracture surface of concrete emanating from the bar head, as shown in Figure 3.2. The primary factors influencing breakout capacity are the embedment depth (as defined in Figure 3.3) and the concrete strength. The angle α varies from 35 to 45 degrees as the embedment depth increases.

Several methods have been developed to predict concrete breakout capacity. For many years a 45 degree cone model was used by ACI 349 [15] and the PCI Design Handbook [16]. More recently the Concrete Capacity Design

(CCD) Method [17] was developed from the Kappa Method devised at the University of Stuttgart [18]. The CCD Method, described in Section 3.2.2, offers a simpler and more rational design model than the 45 degree cone method, and correlates well with test results.

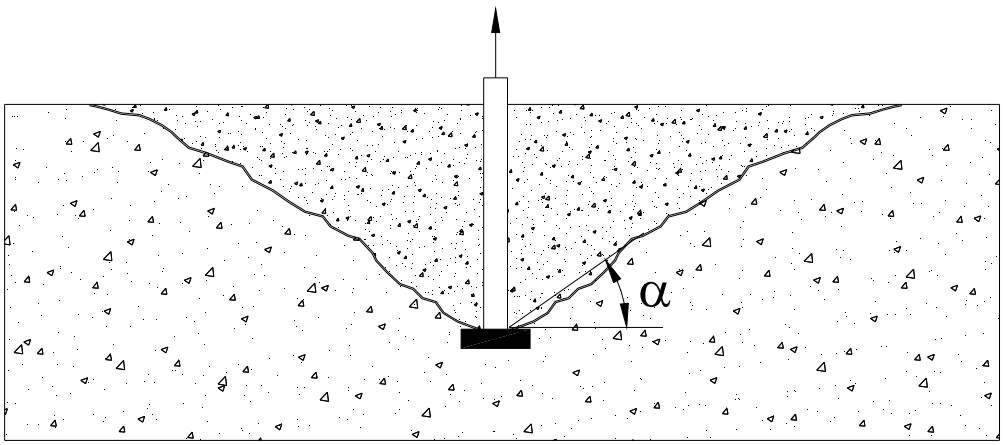

Figure 3.2: Typical Concrete Breakout Surface

Lateral blowout failure occurs when the high bearing stresses at the head of a deeply embeded bar force a cone failure to the side of the member. This type of failure will only control when the bar is sufficiently close to an edge. Due to forming considerations, the details developed in Chapter 2 preclude placing a grout pocket close to the edge of a bent cap. Therefore, lateral blowout failure is not a concern with grout pocket and vertical duct type connections. More information on lateral blowout failure may be found in Reference 8.

3.2.2 Concrete Capacity Design (CCD) Method

The Concrete Capacity Design method [17] calculates the breakout capacity of single and multiple anchors using a physical model derived from observed breakout surfaces. In the CCD method, the angle α in Figure 3.2 is taken as 35 degrees, resulting in the breakout pyramid shown in Figure 3.3. This breakout surface is assumed to resist tensile load with a uniform distribution of stress over the area of the pyramid base. Though the area of the pyramid base will increase with the square of the embedment depth, it has been found from fracture mechanics theory [19] that breakout capacity of the concrete increases in proportion to the embedment depth raised to the 1.5 power. Thus, the breakout capacity is given by:

$$T_o = k\sqrt{f'_c}\,h_{ef}^{1.5} \qquad \textit{(Equation 3-2)}$$

where: T_o = basic concrete breakout capacity

f'_c = concrete cylinder strength (psi in English units, MPa in SI units)

h_{ef} = effective embedment depth (see Figure 3.3; inch or mm)

k = a constant

The constant k in Equation 3-2 represents a collection of calibration factors and constants. Based on a statistical analysis of test results, k was found to be 40 (English units; 15.5 in SI units) for headed cast-in-place anchors. DeVries [8] applied equation 3-2 to 18 headed bar pullout specimens that resulted in concrete breakout failure. He found that Equation 3-2 accurately reproduces

headed bar breakout capacities if the breakout pyramid is measured from the edge of the headed bar, as shown in Figure 3.4.

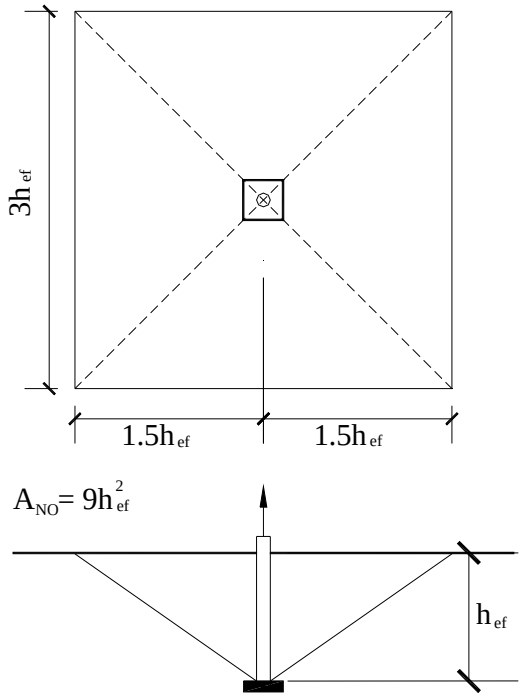

Figure 3.3: CCD Breakout Surface

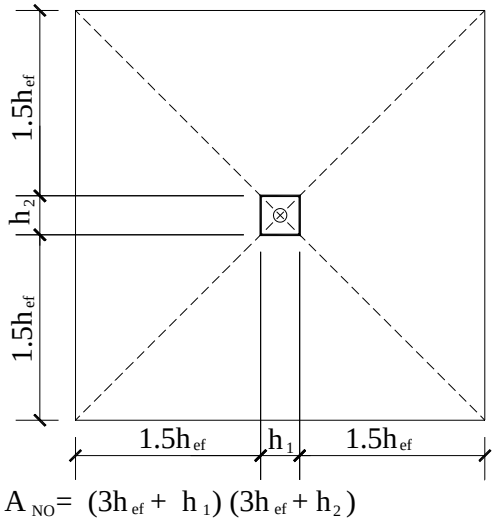

Figure 3.4: Adjusted Breakout Area for Headed Reinforcing Bars [8]

When a headed bar or anchor is near an edge or in a group of bars, the available area to resist tension is reduced. The CCD method accounts for this by modifying the basic capacity given in Equation 3-2 according to the available area. The breakout capacity in this case is:

$$T_n = \frac{A_N}{A_{NO}} \Psi_1 T_o \qquad \textit{(Equation 3-3)}$$

where: T_n = breakout capacity of connection

A_N = available projected area at concrete surface (see Figure 3.5)

A_{NO} = basic breakout surface area = $9h_{ef}^2$

Ψ_1 = tuning factor to adjust for the edge disturbance to the stress state

$$= 0.7 + 0.3\frac{C_1}{1.5h_{ef}} \leq 1.0 \qquad \textbf{(}\textit{Equation 3-4}\textbf{)}$$

where C_1 = minimum edge distance

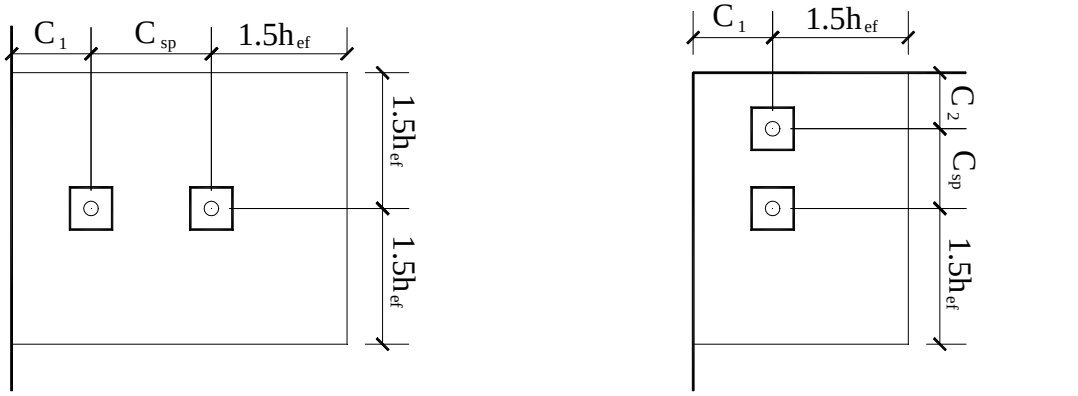

$A_N = (C_1 + C_{sp} + 1.5h_{ef})\ (3h_{ef})$ $A_N = (C_1 + 1.5h_{ef})\ (C_2 + C_{sp} + 1.5h_{ef})$

Edge Bar Group **Corner Bar Group**

Figure 3.5: Adjusted CCD Breakout Area for Bar Groups and Edge Effects

The CCD method is the basis for the proposed Chapter 23 on anchorage to concrete that may be included in future editions of ACI 318 [13]. To provide a 5% fractile breakout strength, the constant k in equation 3-2 is taken as 24 rather than 40 (English units). For embedment depths greater than 11 inches, k is taken as 16 and the term $h_{ef}^{1.5}$ is changed to $h_{ef}^{5/3}$ [13,Commentary]. The breakout capacity may be increased by a factor $\Psi_2 = 1.25$ if analysis shows that no cracking is expected in the concrete member at service levels. The ϕ factor is 0.85 for concrete breakout.

No tests have been reported in the literature on upset-headed bars. DeVries [8] tested T-headed bars with different head sizes, and found little difference in anchorage capacity. One of the goals of this research is to establish whether upset-headed bars behave in a similar manner to T-headed bars.

3.3 BEHAVIOR AND DESIGN OF STRAIGHT BAR ANCHORAGES IN GROUT

Though an extensive amount of research has been performed on straight bar anchorages in reinforced concrete, little work has been done in the area of bar anchorage in grout. However, the equations developed to determine development lengths of straight bars in concrete may serve as a starting point for determining anchorage characteristics of straight bars in grout. Different behavior is expected in grout due to the different physical makeup of grout, which contains large amounts of fine aggregate but lacks coarse aggregate. Thus, the fracture energy criteria required to produce splitting cracks is different than that of reinforced concrete, but the extent of the difference is unknown. One goal of this research is

to determine whether existing design methods apply to anchorage of straight bars in grout pockets.

3.3.1 Design Methods for Straight Bar Anchorage in Reinforced Concrete

The existing ACI 318 design equations for development length are based primarily on research by Orangun, Jirsa, and Breen at The University of Texas at Austin [20] and Darwin and McCabe at The University of Kansas [21]. The development of these equations is well documented and will not be repeated here. Section 12.2.3 of ACI 318-95 gives the development length of a straight bar as:

$$\frac{l_d}{d_b} = \frac{3}{40}\frac{f_y}{\sqrt{f'_c}}\frac{\alpha\beta\gamma\lambda}{\left(\frac{c + K_{tr}}{d_b}\right)} \qquad \textit{(Equation 3-5)}$$

where: l_d = development length (in)

d_b = bar diameter (in)

c = spacing or cover dimension (in)

K_{tr} = transverse reinforcement index = 0 for grout pocket anchorages

α = reinforcement location factor = 1.0 for vertical bars

β = epoxy coating factor = 1.2 for geometry of grout pocket bars

γ = reinforcement size factor

= 0.8 for #6 bars and smaller; 1.0 for #7 bars and larger

λ = lightweight aggregate concrete factor

= 1.3 for lightweight aggregate concrete; 1.0 for normal weight

The value of c/d_b may not be taken greater than 2.5. It is unclear whether the factor λ applies to grout, which has no aggregate.

Since Equation 3-5 is a design equation, certain factors are built into the equation to ensure that it gives 5% fractile development lengths. For comparison with test results, it is desirable to have an equation which gives predictions of the mean strength of a bar anchorage. The best-fit equation developed by Orangun et. al. [20] may be written in the form:

$$l_d = \frac{12{,}250 d_b}{\sqrt{f'_c}\left(1.2 + 3.0\frac{c}{d_b}\right)} \qquad \textit{(Equation 3-6)}$$

for the case of no transverse reinforcement. The value of c/d_b must again be less than 2.5, and the adjustment factors listed in Equation 3-5 for reinforcement location, epoxy coating, bar size, and lightweight concrete apply to equation 3-6 as well.

3.3.1 Bond Strength Tests of Bars Grouted into Existing Concrete

A recent study at The University of Kansas by Darwin and Zavaregh [22] examined the anchorage of bars grouted into small diameter holes drilled into existing concrete. The pullout tests used #5 and #8 bars in holes that were typically ¼ inch larger than the bar diameter. Several types of grout were used, including the cementitious type of grout planned for use in grout pocket connections. Most tests were conducted with a 3 inch distance to an edge. Two

types of failures were observed: failure between the grout and concrete and splitting failure. The best-fit equation determined by the researchers to describe the anchorage strength is:

$$T_n = 30 l_d \sqrt{f'_c} \qquad \textit{(Equation 3-7)}$$

where: T_n = anchorage strength in pounds

l_d = development length in inches

f'_c = concrete compressive strength in psi

Equation 3-7 will be used to evaluate results of grout pocket and grouted vertical duct pullout tests since it is the only existing equation for grouted bar anchorage strength. However, Equation 3-7 will probably not give accurate results since grout pockets consist of a large mass of grout, while the holes used in the Kansas study are much smaller. In addition, the close edge distances used in the Kansas study are probably the primary factor controlling the anchorage strength, and the edge distances in grout pocket connections are much larger.

3.4 TESTS OF DUCT TYPE GROUTED CONNECTIONS

Though grouted duct connections have been used extensively in precast building construction, little data exist regarding anchorage capacity in these connections. Rather, most tests have been conducted on entire precast systems subjected to simulated seismic loads, with little or no instrumentation devoted to anchorage behavior [23,24,25]. The tests discussed below provide an indication that grouted duct connections are extremely promising, but do not provide an understanding of the anchorage behavior.

3.4.1 University of Nebraska Tests

One of the few studies to address duct-type connection anchorage behavior was performed at the University of Nebraska-Lincoln by Einea, Yamane, and Tadros [26]. These tests used steel pipe rather than corrugated ducts. Reinforcing bars were grouted into the pipes and tested by direct pullout. The embedment length of the reinforcement ranged from 6 to 10 inches.

The test results showed that the pipe anchorage provided sufficient strength to yield the #6 bars used in the study. In most cases, the anchorage failed when the steel pipe yielded circumferentially due to the bar splitting forces. An attempt was made to develop a design equation for the anchorage based on the confinement provided by the pipe, but the equation developed from theoretical considerations did not reproduce test results.

Though the Nebraska tests show that duct-type connections are promising, the results do not address the interaction of the pipe or duct with the surrounding concrete in which it will be embedded. Though the bar may develop within the duct, the duct may also pull out of the surrounding concrete. The ridges on corrugated ducts should address this type of failure.

3.4.2 Seismic Tests of Grouted Duct Precast Systems

In the highly seismic environment of New Zealand, grouted duct type connections are a popular choice for precast concrete systems [24]. Research done at the University of Canterbury at Christchurch by Restrepo, Park, and Buchanan [23] examined the ability of grouted duct precast systems to emulate monolithic concrete construction. A series of beam-column assemblies showed

that the connections allow members to develop their full capacities, resulting in good system ductility. No information was reported on duct anchorage behavior.

Similar tests were conducted at Imperial College in London by Zheng [25]. In this series of tests, a precast column was joined by a grouted duct connection at mid-height and subjected to reversed cyclic bending. These tests showed a slightly reduced ductility from monolithic specimens due to cracking at the bedding layer of the connection. The duct anchorages were again adequate to develop the column strength.

CHAPTER 4

OVERVIEW OF TEST PROGRAM

4.1 INTRODUCTION

Overall performance of a precast connection will depend on a number of factors, including anchorage behavior, precast member behavior, loading, and material durability. For the connection systems developed in Chapter 2, anchorage behavior of reinforcing bars in grout is perhaps the least understood of these issues. The anchorage design methods described in Chapter 3 are well established for reinforced concrete, but their applicability to grouted connections are in doubt. In order to determine the anchorage characteristics of grout pocket and grouted vertical duct connections, a series of pullout tests was conducted. Future research will address performance of the entire precast system, including effects of the bedding layer and precast member loading.

The tests that were conducted simulate tension in the connection reinforcement, caused by longitudinal and transverse moments, through direct pullout tests. Tests of single line grout pockets (see Figure 2.10), double line grout pockets (see Figure 2.11), and grouted vertical ducts (see Figure 2.12) were conducted. Upset-headed and straight bars were tested, both as single bars and in groups simulating typical connection arrangements. The following sections describe the primary test variables, testing methods, and test program.

4.2 PRIMARY TEST VARIABLES AND DEFINITIONS

There are a large number of factors that will affect the anchorage behavior of headed and straight reinforcement. In order to limit the number of tests, the following parameters were identified as the primary variables in the test program.

1. Embedment Depth

The embedment depth is the main factor that will determine whether anchorage failure or steel fracture will control. The embedment depth is defined for headed bars (Figure 3.3) as the distance from the top of the bar head to the free surface. For straight bars the embedment depth is simply the length of the bar in grout.

2. Grout

Strength characteristics of the non-shrink grout used for the connections will have a major impact on anchorage capacity. The strength gain with time of a particular grout is important because bent cap connections may be subjected to loads soon after the grout is cast to expedite bridge erection. In addition, the placement characteristics of a grout such as working time, fluidity, and shrinkage compensation mechanism are important to achieving a constructable connection.

A major concern with grouted connections is the volumetric stability of the grout. The grout must also be compatible with the surrounding concrete to accommodate temperature deformations. To address these issues, tests were conducted comparing normal grout mixes to grout mixes extended with small pea gravel aggregate, which provides additional volumetric stability. The grout mixes used for testing are described in Section 4.6.3.

3. Single vs. Multiple Bars

In order to establish the basic characteristics of grouted connection anchorages, the majority of pullout tests were conducted on single bars. However, actual connections will typically consist of groups of bars whose anchorage behavior may or may not interact. A series of tests was conducted with multiple bars at typical spacing in order to examine group effects. The arrangement of the bars is described in Section 4.5.

4. Bar Size

Research by Darwin et. al. [1] at The University of Kansas revealed that straight bar anchorage strengths tend to segregate according to bar size. This is reflected in the 0.8 reduction factor of Equation 3-5 for #6 bars and smaller [2]. To address this effect, #6, #8, and #11 bars were tested.

5. Longitudinal vs. Transverse Moments

Double line grout pockets will be required to transfer significant longitudinal and transverse moments. Tests were conducted for each case to establish the behavior. Figure 4.1a shows a double line connection under longitudinal moment, in which case two bars in the same pocket resist tensile forces. Under transverse moment, as shown in Figure 4.1b, two bars in different pockets resist tensile forces.

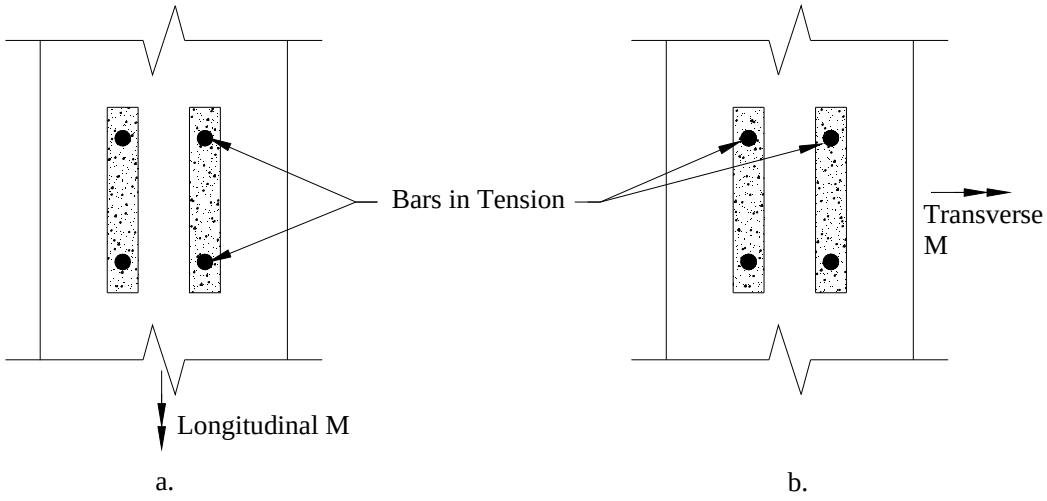

Figure 4.1: Longitudinal vs. Transverse Moments in Double Line Grout Pockets

6. Pocket Confinement Steel

To ensure durability of the precast connections, any cracking detectable at service load levels must be limited to acceptable widths. One way to control cracking in the precast members due to connection forces is to provide reinforcement surrounding the pocket. This steel will be referred to as pocket confinement steel. The pocket confinement steel may also serve to add strength and ductility to the anchorage because it crosses potential failure planes.

Two types of pocket confinement steel were tested. One consisted of welded wire fabric (WWF) mesh placed around the pocket depth. The other type was typical spiral reinforcement placed around the pocket. The specific geometry and placement of the pocket confinement steel is described in Section 4.4.4.

4.3 TEST SETUP

The test setup was designed to facilitate easy testing of many specimens. The basic setup for grout pocket tests is shown in Figure 4.2. Each specimen contained two tests. The grout pockets were cast inverted from what would exist in an actual connection in order to facilitate pulling the bar upwards. The self-reacting frame consisted of two back-to-back C12 x 20.7 channels supported on three W8 x 58 sections, which were bolted into inserts in the concrete specimen. The spacing of the three W8 x 58 sections was established to prevent any confining effects from the support reaction on the breakout capacity. The channels were separated by ½″ threaded rods to maintain a constant 2″ space for the test bar to pass through. Loading frame stiffeners were welded by the steel fabricator at the locations shown in Figure 4.2.

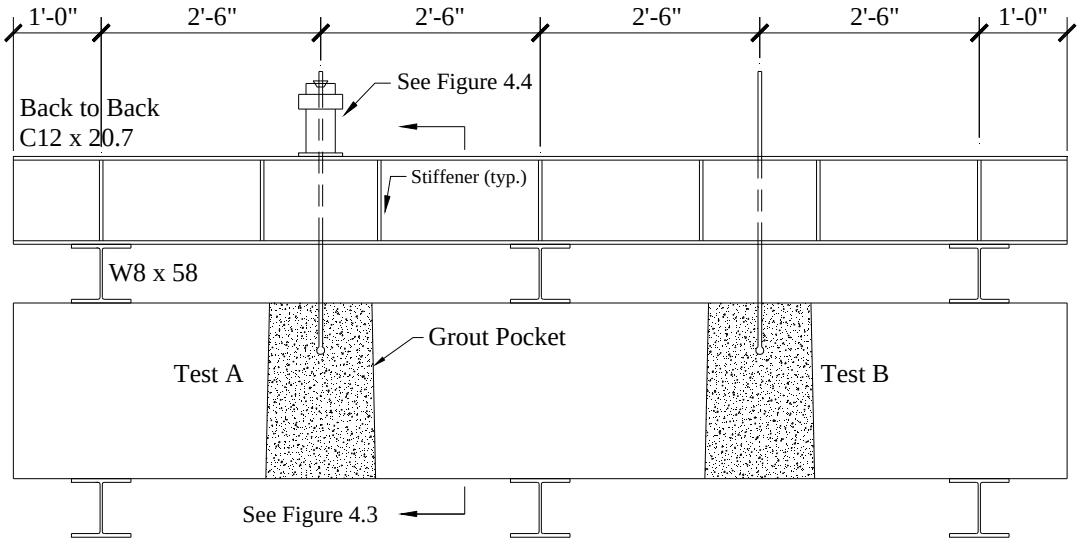

Figure 4.2: Typical Test Setup

The steel for the loading frame was dual certified ASTM A36/A572-Gr. 50. The specimen rested on two wide-flange members which only supported the weight of the specimen and testing frame.

Figure 4.3 shows the arrangement of the loading frame for the various test conditions. For single line grout pocket tests, the channels were centered and bolted to the W8 x 58 support. The test setup for grouted vertical duct specimens was similar to single line grout pocket tests, though the duct specimens accommodate four tests each. Two arrangements were required for double line grout pocket tests. When testing for longitudinal moments, one set of channels was centered over one pocket as shown in Figure 4.3b. For transverse moment cases, two sets of channels were required, as shown in Figure 4.3c.

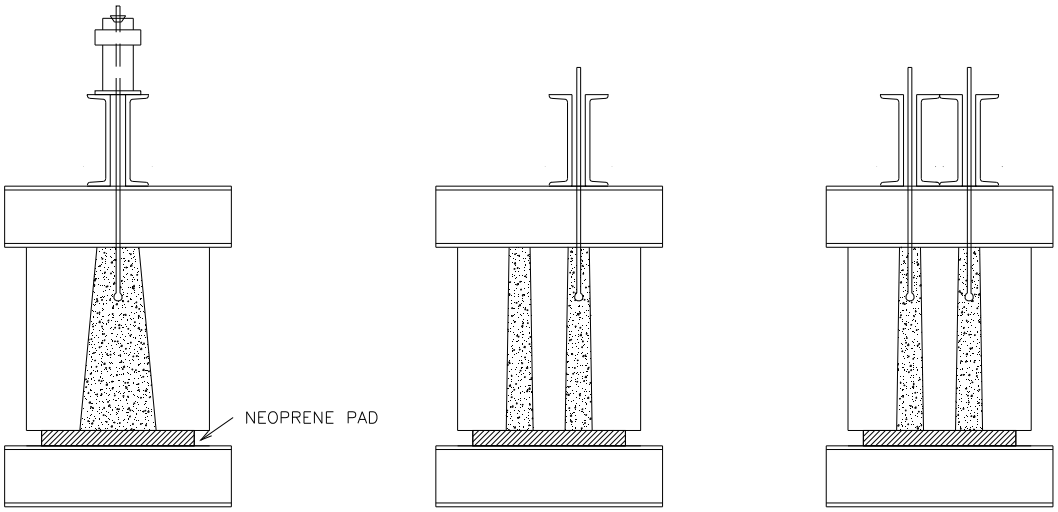

a. SLGP Setup

b. DLGP Setup - Longitudinal M

c. DLGP Setup - Transverse M

Figure 4.3: Loading Frame Setup for Various Test Cases

The test bar was loaded by a hydraulic ram that reacted between the back-to-back channels and a wedge-and-chuck assembly that gripped the test bar. The loading assembly is shown in Figure 4.4. A load cell was placed between the hydraulic ram and chuck to measure the force in the test bar. A typical test setup is shown in Figure 4.5.

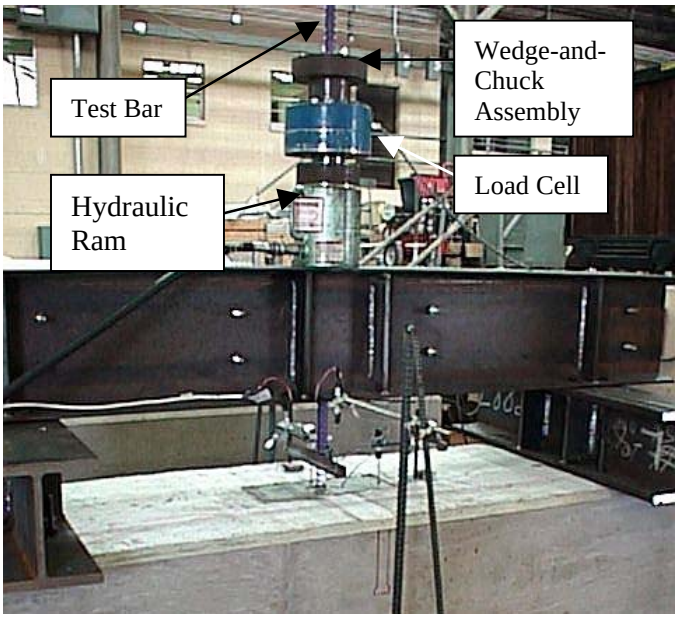

Figure 4.4: Loading Assembly

Figure 4.5: Typical Completed Test Setup

4.4 SPECIMEN DESIGN AND CONSTRUCTION

4.4.1 Single Line Grout Pocket Specimen

The single line grout pocket specimen is shown in Figure 4.6. The specimen was 24″ by 24″ by 12′, and contained two grout pockets. The size of the specimen was chosen to simulate a full-scale precast bent cap on piles or an approximately ¾-scale precast bent cap on cast-in-place columns. Reinforcement was chosen to simulate typical TxDOT bent cap reinforcement patterns, and was checked for the expected loads. The cracking moment of the test section was determined to be less than the maximum applied test moment. To avoid influence on the breakout capacity, stirrups were kept a reasonable distance (12.5″) away from the grout pocket.

Each grout pocket cast into a specimen consisted of a 5-degree taper transverse to the cross-section and a 1-degree taper at the ends. The pockets were created with wooden plywood forms that were sheathed in metal flashing to facilitate form removal. A spacer attached to the wooden forms was used to position the top of the pocket form. Inserts for lifting the specimen and bolting the supports to the specimen were cast into each specimen. Inserts were held in place by threaded rods supported by spacers. The formwork setup is shown in Figure 4.7, and Figure 4.8 shows a reinforcement cage and pocket ready for casting.

Specimens were cast in pairs by placing concrete from a hopper in two lifts, as shown in Figure 4.9. Each lift was vibrated thoroughly, and the surface was finished with a trowel. The forms were covered with plastic sheets while the

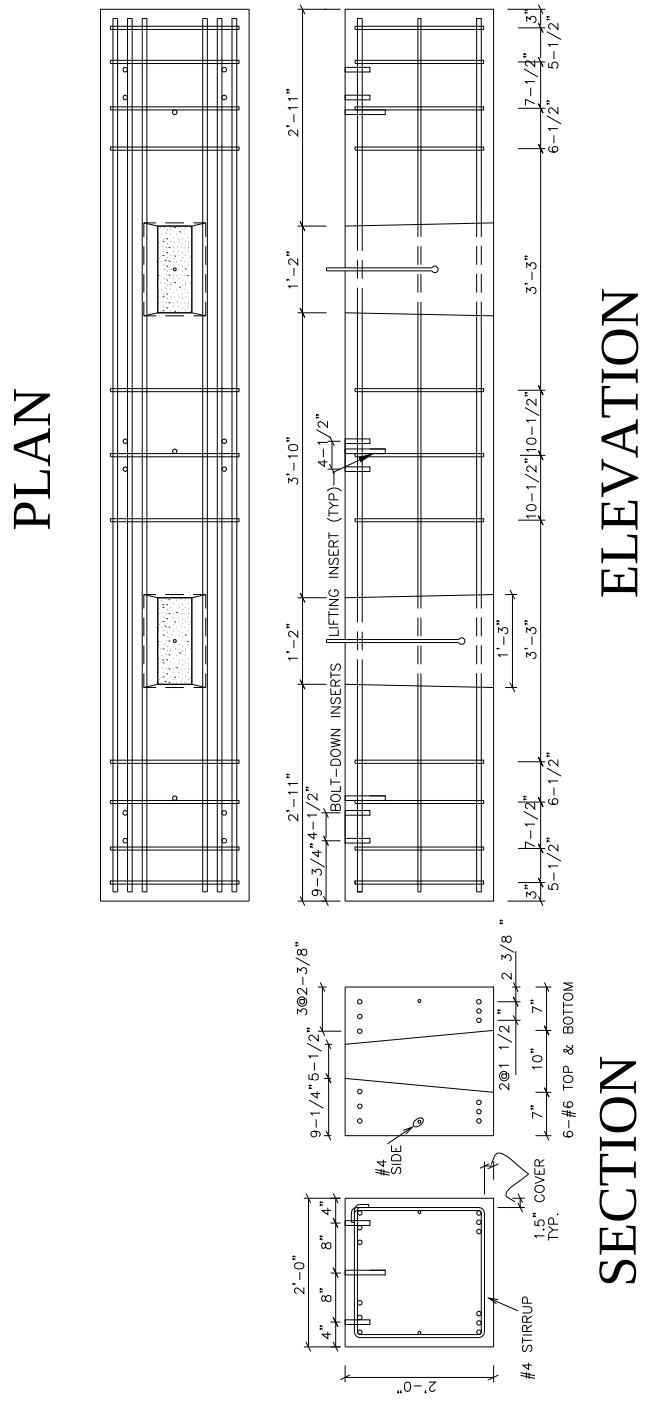

Figure 4.6: Single Line Grout Pocket Specimen

concrete hardened. After a period of four to six hours, wet burlap was placed on the hardened concrete surface, and was kept wet for three days to provide a moist curing environment. The forms were typically removed four to five days after casting.

Figure 4.7: Specimen Formwork

Figure 4.8: Completed Cage Ready for Casting

Figure 4.9: Specimen Casting

After form removal, the specimens were lifted off the casting bed and placed on support blocks. The pocket forms were then removed by pounding the top of the form with a sledgehammer. Due to shrinkage of the concrete around the pocket forms, the pockets were sometimes difficult to remove. Figure 4.10 shows a completed specimen after pocket form removal.

Figure 4.10: Completed Specimen

4.4.2 Double Line Grout Pocket Specimen

Figure 4.12 shows a double line grout pocket specimen. The dimensions are the same as that of the single line specimen, and the double line specimen again represents an approximately ¾-scale precast bent cap on cast-in-place columns. Due to the limited width of the bent cap, to accommodate two pockets the transverse taper of the pockets is small. However, at the ends of the pocket forms the taper is 7 degrees. Construction of the double line specimens was identical to that of the single line specimens. Figure 4.11 shows a completed double line cage with the pocket forms in place.

Figure 4.11: DLGP Specimen Cage

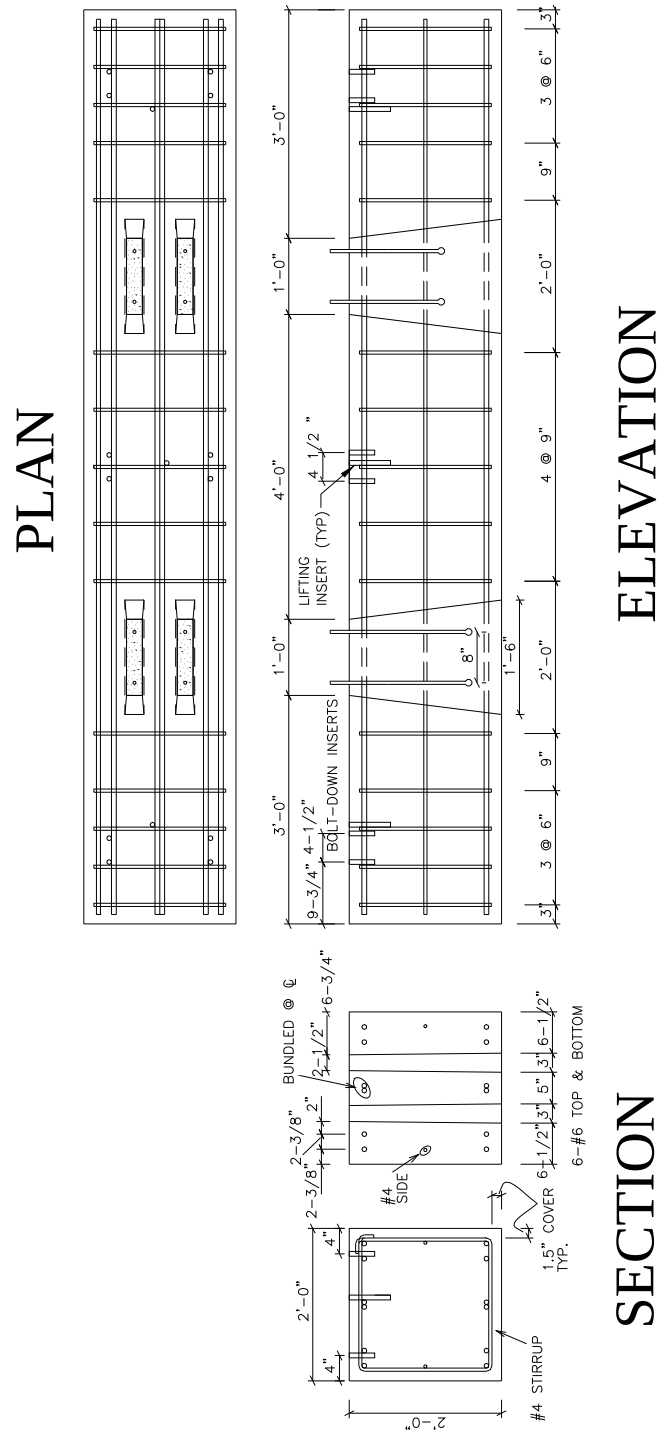

Figure 4.12: Double Line Grout Pocket Specimen

4.4.3 Vertical Duct Specimen

Figure 4.13 shows the vertical duct specimen. Because the failure was expected to be limited to the local duct area, these specimens were fabricated with four tests per specimen. The 24″ x 30″ x 12′ specimen represents a full-scale rectangular or inverted-T cap. Standard 4″ corrugated ducts that extended the full depth of the 30″ member were used for all specimens.

Construction of the vertical duct specimens was similar to that of the grout pocket specimens. The corrugated ducts were sealed at the top and bottom to prevent stray concrete from bonding to the inside surface of the ducts. The ducts were held in place by small bars attached to the longitudinal reinforcement of the bent cap reinforcement cage.

4.4.4 Grout Pocket Confinement Steel

For tests of multiple bars in both single and double line pockets, specimens were fabricated with pocket confinement steel. Confinement consisting of welded wire fabric mesh (WWF) and spiral reinforcement were both used. For single line grout pockets, the WWF confinement was fabricated from a sheet of 4 x 4 x 6 gauge mesh. The mesh was bent at three corners and lapped at the closing corner to form a box that was 17 ¼″ x 12 ¼″ x 18″ deep. Depth of the mesh was limited to 18″ in order to place the confinement steel between the top and bottom longitudinal bars. Spiral steel used for single line grout pockets consisted of a #3 bar with an 18″ outer diameter at a 2.5″ pitch. The proper pitch was achieved by tying the spiral to a vertical bar. Figure 4.14 shows spiral confinement in place around a single line pocket.

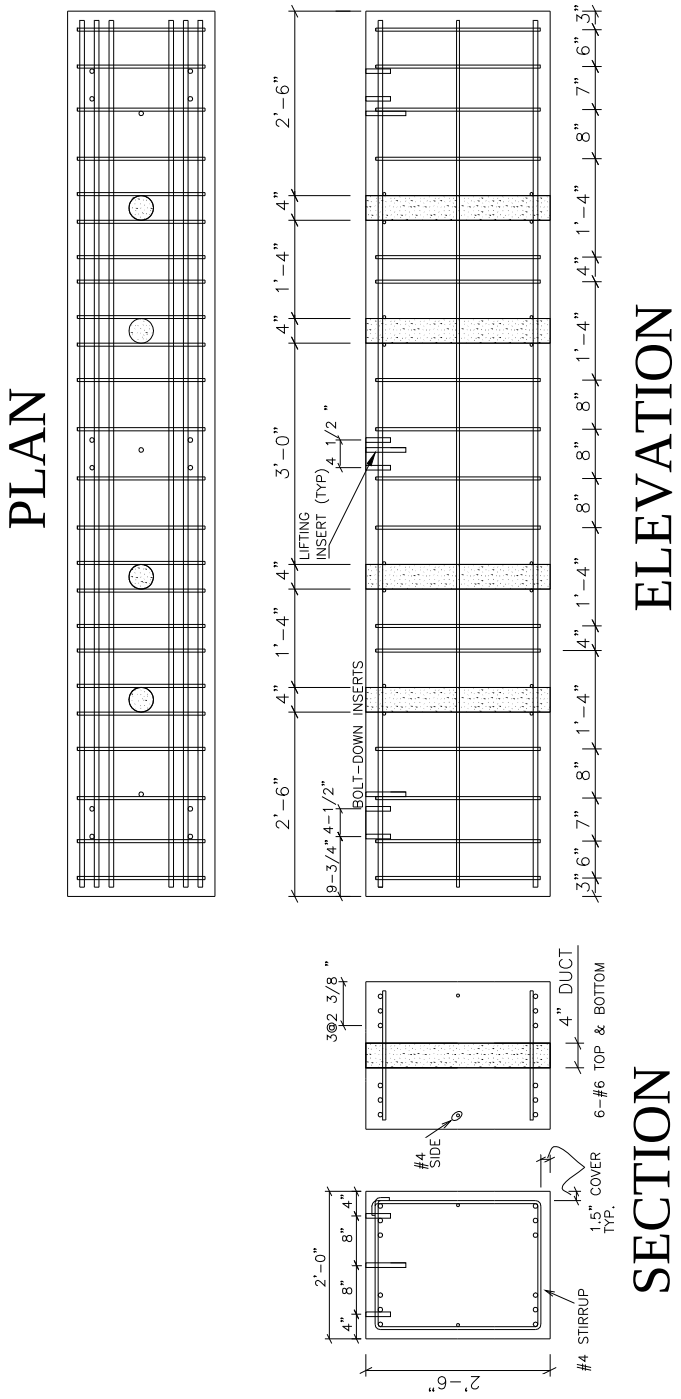

Figure 4.13: Vertical Duct Specimen

For double line grout pockets, the 4 x 4 x 6 ga. mesh was fabricated into a box measuring 15 ½″ x 22″ x 18″ deep. The #3 spiral had an outer diameter of 20-½″ and was again at a 2.5″ pitch. Figure 4.15 shows confinement steel in place in a double line specimen.

Figure 4.14: Spiral Around SLGP

Figure 4.15: DLGP Confinement in Place

4.5 TEST BAR PLACEMENT AND GROUTING

Grouting of test bars in the grout pockets or vertical ducts was accomplished through a series of steps. For the grout pockets, it was necessary to presoak the pocket in order to avoid losing moisture from the grout mix into the surrounding concrete. After forming and sealing the bottom of the pocket, it was filled with water and allowed to soak for a period of several hours before grouting. The water was removed with a vacuum typically one hour before the pocket was grouted in order to set the bar in the pocket.

Test bars were held in place by clamps connected to wood blocks that bridged across the pocket. Figure 4.16 shows a single bar in a single line pocket

ready for grouting. All bars were plumbed in both directions before grouting. Bars for double line pockets and vertical ducts were held in place in a similar manner.

Figure 4.16: Bar Ready for Grouting in SLGP

For tests of single bars, the bar was centered in the grout pocket or duct. The arrangement of bars for multiple bar tests in single and double line pockets are shown in Figure 4.17. The typical spacing between bars in either direction was 8″. For double line pockets, a connection arrangement of two bars in each pocket was simulated. To represent the two bars under compression in the connection, bars were placed in the grout pockets but were not loaded.

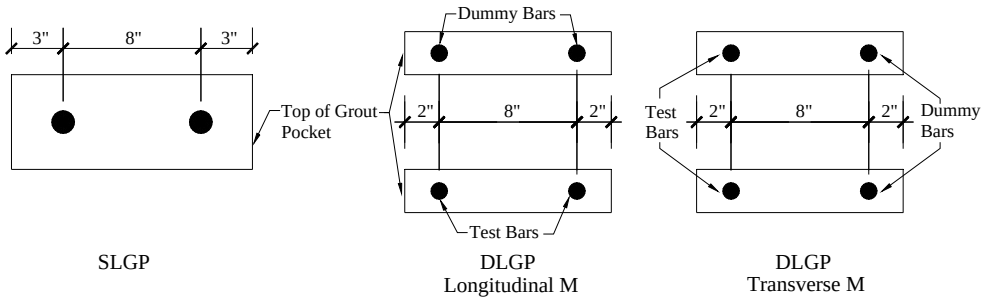

Figure 4.17: Bar Arrangements for Multiple Bar Tests

A prepackaged grout mix was used for each test. The grout was mixed in a paddle-type mechanical mixer in batches of 2.5 ft^3 or less. Care was taken to monitor the ambient temperature during mixing to stay within the grout manufacturer's recommendations for mixing temperature. The grout was mixed for the amount of time recommended by the manufacturer.

After the initial mixing, a flowcone test was performed in accordance with ASTM C827 to ensure proper fluidity of the grout. A standard flow of 30 seconds was used to establish acceptable fluidity. If the grout mix did not meet this, small quantities of water were added and the grout was remixed until it passed.

Grout was poured into the pocket through a funnel attached to a hose. Figure 4.18 shows grout being placed in a single line pocket. The end of the hose was initially placed at the bottom of the grout pocket, and was kept under the surface of the grout in order to keep air from entering into the grout mix. Once the pocket was filled, a curing compound was applied to the surface per grout manufacturer's instructions. The grout surface typically hardened in 3 to 4 hours, and then wet rags were placed on the surface and kept moist for a period of 24 hours. Forms were typically removed after a period of two to three days. Figure 4.19 shows a completed single line test specimen.

Figure 4.18: Grout Placement

Though care was taken to prevent air from entering the grout mix, in many cases air bubbles were noticed on the surface while the grout was still wet. Figure 4.20 shows a typical large air bubble penetrating the grout surface in a vertical duct specimen. Though these air bubble paths left a hole in the surface, they had no noticeable effect on testing. To determine the extent of surface irregularities in the grout pocket, dye was injected into an air bubble hole and small shrinkage cracks on the grout surface of one specimen after surface hardening. After the specimen was tested, the dye indicated that the air bubble hole and shrinkage cracks extended only ¼″ to ½″ into the pocket surface.

Figure 4.19: Completed SLGP

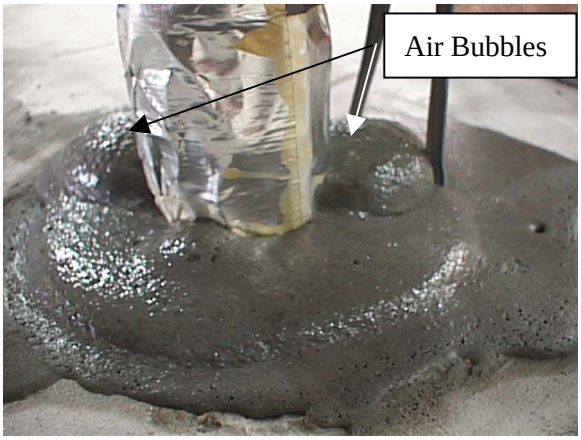

Figure 4.20: Air Bubbles at Grout Surface

4.6 MATERIALS

4.6.1 Steel

Reinforcing steel for the concrete specimens was Grade 60 steel obtained from a local fabricator. The #4 closed stirrups were manufactured by the fabricator. Steel used for the test bars was also Grade 60 steel, and was supplied by Headed Reinforcement Corporation California (HRC). The upset ends of the upset-headed bars were formed by HRC. All test bars were epoxy coated by Fletcher Coatings Company. Abrasion resistant epoxy coating in accordance with ASTM A775 was used. The epoxy coating system utilized the 3M Scotchkote 426 process, which produces a purple-colored coating that is more resistant to incidental cuts than the traditional green coating.

Table 4.1 lists the yield and fracture strength of the test bars. Each size of test bar came from the same mill batch. The lab test values reported in Table 4.1 were obtained by testing the bars under monotonic tension loading with a slow loading rate. Table 4.1 also lists the strengths reported by the steel mill. Since mill tests are frequently conducted under high rates of loading, the results obtained from tests conducted at a slow loading rate are more useful for interpreting results of grout pocket and duct tests, which were also conducted at a slow rate of loading.

4.6.2 Concrete

Concrete was delivered by a local ready-mix company. The mix used for all of the concrete specimens is shown in Table 4.2 and is a standard TxDOT Class C mix with a required 28 day compressive strength of 3600 psi. The mix

Table 4.1: Reinforcing Bar Strengths (ksi)

	Mill Report		Lab Tests	
Bar Size	**Yield**	**Fracture**	**Yield**	**Fracture**
#6	72	101	65	94
#8	74	101	69	97
#11	70	100	59	85

Table 4.2: Concrete Mix Design

	Cement	**¾" Coarse Aggregate**	**Fine Aggregate**	**Water**	**Retarder (oz.)**
Pounds/cubic yard	564	1882	1191	250	24

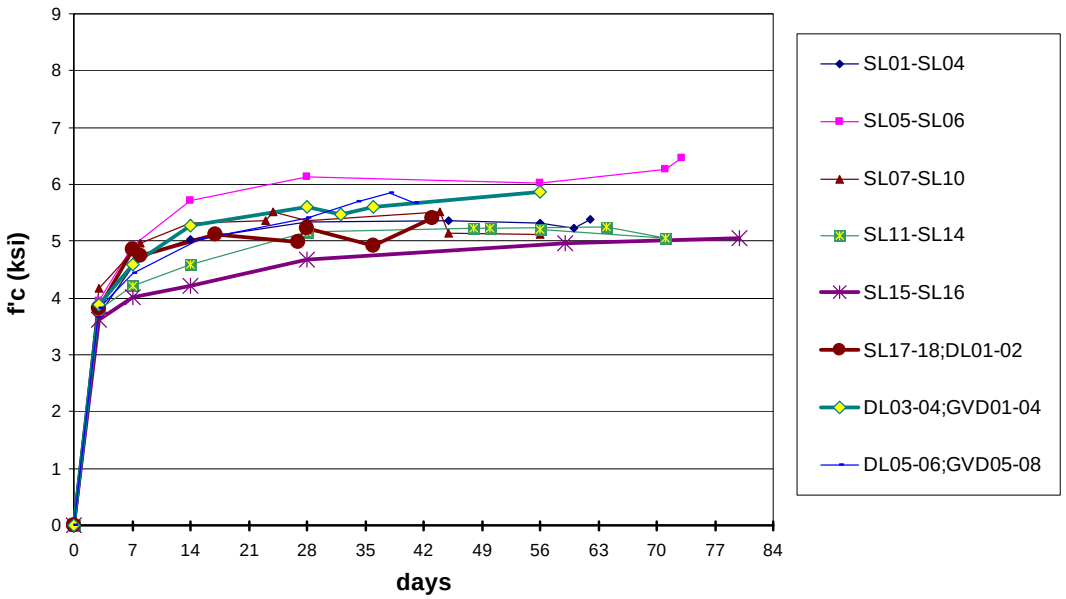

Figure 4.21: Concrete Strength Curves

was ordered with a slump of 4″, but the delivered slump varied. Water was added when necessary to achieve a slump between 3 and 4 inches in order to ensure easy placement of the concrete.

Standard 6″ diameter control cylinders were cast with each batch of concrete and were tested at 3, 7, 14, 28, and 56 days. In addition, three cylinders were tested on the same day that pullout tests were conducted. Figure 4.21 shows strength curves for each of the eight specimen castings. Typical 28 day compressive strengths were in the vicinity of 5000 psi.

4.6.2 Grout

Three types of cementitious non-shrink grout were used in the test program. Each was a prepackaged proprietary grout mix provided by the manufacturer:

1. Masterflow 928 by Masterbuilders (used for the majority of tests)
2. Euclid Hi-Flow by Euclid Corporation
3. Sika 212 by Sika Corporation

Since the grouts are proprietary, no information is available on the specific mix designs. The mixes come in bags of approximately 50 pounds, and were mixed with 10 pounds of water per bag according to manufacturer's instructions. For the mixes that were extended with aggregate, 25 pounds of 1/8″ pea gravel per bag were included in the mix.

Standard 2″ grout cubes were cast with each grout batch in accordance with ASTM C109 and C1107. The cubes were tested at 1, 3, 7, and 28 days. Three cubes were tested on the day of each pullout test. For grout mixes that

were extended with pea gravel, standard 4″ cylinders were used instead of grout cubes. Typical strength curves for each of the three types of grout are shown in Figure 4.22. The values shown in Figure 4.22 and reported in the test results include a 0.8 factor applied to grout cube compressive strengths. This factor provides a correlation between cube and cylinder strengths and accounts for the different degree of end restraint from the loading platens for cube and cylinder specimens. Pullout tests were not conducted until the grout reached a strength at least equal to that of the surrounding concrete specimen.

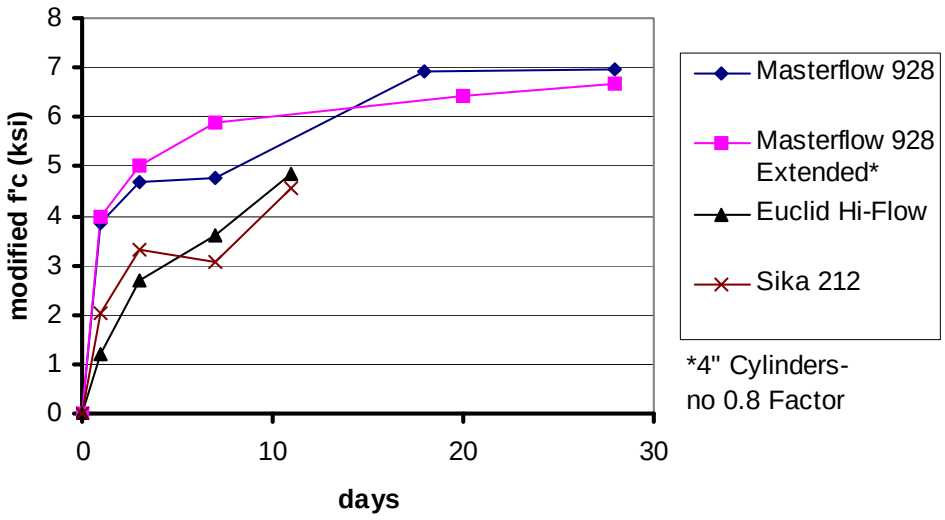

Figure 4.22: Typical Grout Strength Curves

4.7 INSTRUMENTATION AND MEASUREMENTS

Measurements of strain, deflection, and load were taken during each test and recorded using a data acquisition system. Figure 4.23 shows a schematic of the instrumentation system for the grout pocket tests. In addition to these electronic measurements, cracks were marked as they developed on the specimen

surface and were measured with a plastic crack comparator card. The load in the test bar was measured with a load cell as shown in Figure 4.5. Deflections were measured at the bar head, the bar lead end, and across the interface between the grout and concrete.

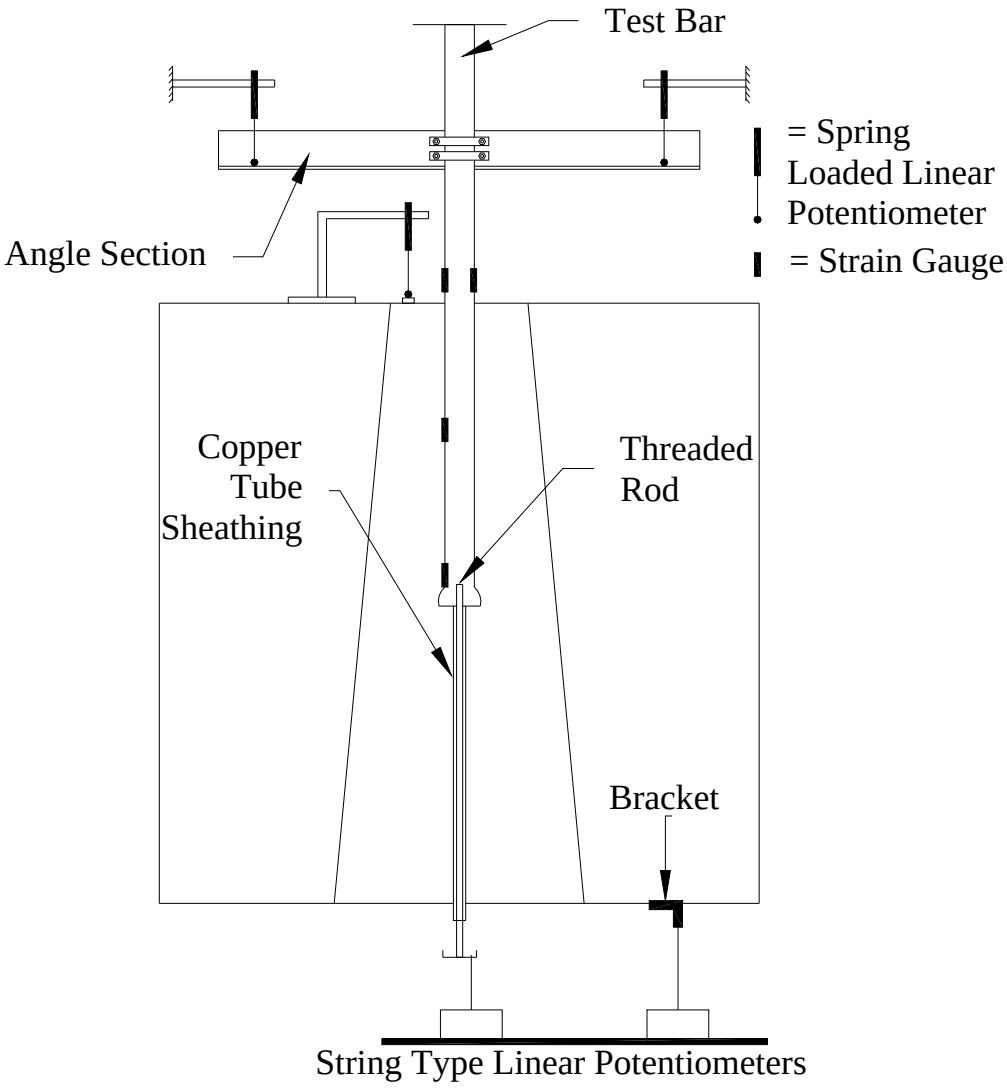

Figure 4.23: Instrumentation Schematic

The bar head deflection was measured through a threaded rod attached to the underside of the bar head. A small hole was drilled into the bottom of the head and threaded, and the threaded rod was screwed into the hole. The threaded rod extended through the bottom of the specimen and was attached to a string-type linear potentiometer that was attached to the laboratory floor. Copper tubing was used to sheath the threaded rod to prevent it from bonding to the grout. Deflection of the specimen was measured at a location adjacent to the threaded rod. A bracket was mounted on the concrete surface and connected to a string type-linear potentiometer that was attached to the laboratory floor. The specimen deflection was subtracted from the measured head deflection to obtain the true head deflection.

The lead deflection was defined as the deflection of the bar just above the specimen surface. A length of angle section was attached to the test bar with two U-bolts such that it extended across the specimen as shown in Figure 4.23. Deflection was measured with spring-loaded linear potentiometers that rested on the angle surface at each end and were attached to rigid stands. Deflections were measured at each end of the angle in order to account for any bending of the bar that might have occurred. The two measured deflections were averaged to find the true lead deflection.

The relative deflection across the grout and concrete surfaces was measured to determine whether slip occurred between the grout/concrete interface. A stand was bonded with silicone to the concrete surface adjacent to the pocket. A spring-loaded linear potentiometer was mounted on the stand, and

the end of the potentiometer rested on a glass slide bonded to the grout surface with silicone. Figure 4.24 shows the instrumentation at the surface of the specimen.

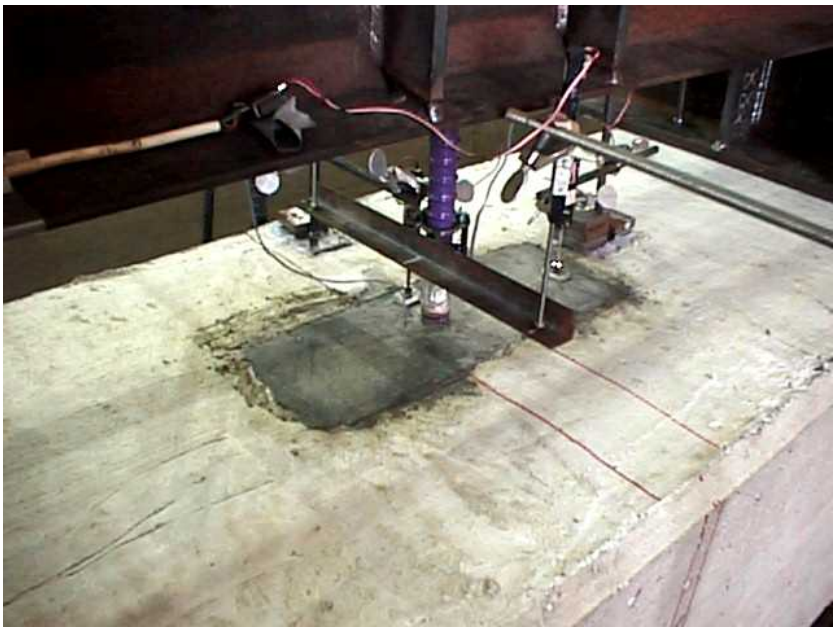

Figure 4.24: Instrumentation at Specimen Top

Test bar strains were measured at several locations along the bar to determine the force in the bar at each location. For headed bar tests, strains were measured just above the head and at the lead end of the bar just above the concrete surface. If the embedment was sufficiently long, additional strain measurements were made along the embedment length. Typically, strains were measured at six inch intervals along the test bar. For straight bar tests, the lead strain was measured but the distribution of additional strain measurements varied depending on the embedment depth. Lead strains were measured with strain gauges on opposite sides of the bar as shown in Figure 4.23 in order to account for any bar bending.

Vertical duct specimens were instrumented identically to grout pocket specimens, though strain gauges were provided to measure the circumferential strains in the duct. Figure 4.25 shows an instrumented duct. Strain gauges were oriented circumferentially at 6, 12, and 18 inches from the top of the duct. At 12 inches from the duct top another gauge was applied so that it was oriented parallel to the deformations in the duct. This gauge was provided to determine whether the duct expanded purely radially or if it expanded along the duct seams.

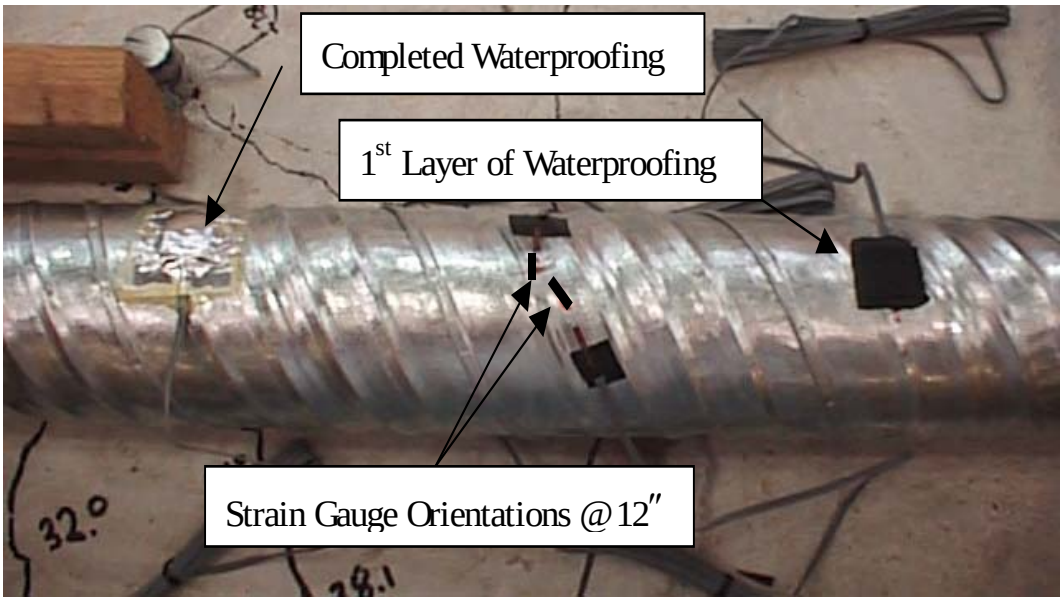

Figure 4.25: Duct Instrumentation

Five-mm long, quarter-bridge strain gauges were used for all strain measurements. Bar deformations were ground off to provide a smooth surface to apply the strain gauge. Care was taken to ensure that the bar section was not significantly reduced. Each strain gauge was protected with two-layer waterproofing consisting of black mastic and foil tape.

4.8 TEST PROCEDURE

The test bar was loaded in 2-kip increments using a hand-powered hydraulic pump. After each load step the voltage of each instrument was recorded and stored by a data acquisition system, and cracks were marked on the specimen. For cases in which the bar anchorage failed, loading continued after the peak load was reached in order to expose the failure surface. A continuous plot of bar load versus lead deflection was made using an electronic plotter to monitor the specimen response during testing.

In a few cases the wedges that gripped the bar to load it slipped before the peak test load was reached. In these cases the bar was unloaded and the wedges were reseated at another location along the bar. The bar was then reloaded to failure. Similarly, in a few other cases excessive bending of the bar in the elastic range was observed. The bar was again unloaded and the loading frame was adjusted to eliminate the bending.

4.9 OVERVIEW OF TEST PROGRAM

Fourteen tests of single bars in single line grout pockets were conducted. These tests are labeled SL01 through SL14. Four tests, SL15 through SL18, were of two bars in a single line grout pocket. Parameters and results for single line grout pocket tests are discussed in Chapter 5.

Six double line grout pocket tests were conducted. One test, DL01, was a test of a connection representing transverse moment transfer in a bent cap. DL02 through DL06 were tests of connections representing longitudinal moment transfer in a bent cap. Double line grout pocket tests are described in Chapter 6.

Eight grouted vertical duct pullout tests (GVD01-GVD08) were conducted, and are described in Chapter 7.

CHAPTER 5

SINGLE LINE GROUT POCKET TESTS

5.1 SUMMARY OF RESULTS

Tests of single and multiple bars in single line grout pockets are summarized in Table 5.1. Subsequent discussion will refer to the Test ID for each test, which is numbered consecutively from SL01 to SL14 for single bar tests and SL15 to SL18 for multiple bar tests. The maximum test load (P_{max}), load at which the bar yielded (P_{yield}), and strength of the grout and concrete on test day are also summarized in Table 5.1.

The behavior observed during single line grout pocket testing consisted of concrete breakout and bar yielding, and in some tests a combination of the two. In cases where the bar yielded, loading was continued into the strain hardening range until a breakout failure occurred or the test had to be stopped due to setup limitations. Loading was generally stopped before the bar reached its fracture strength.

For single bar tests, eight specimens experienced concrete breakout; three of these after the bar had yielded. Six of the specimens experienced steel yielding followed by strain hardening before testing was stopped. The three multiple bar grout pocket tests all resulted in concrete breakout. One control test of 2 bars

cast-in-place in a specimen was conducted for comparison, and also resulted in breakout failure.

Table 5.1: Summary of Single Line Grout Pocket Tests

Test ID	Type	#Bars	Bar Type	Bar Size	Grout	h_{ef} in	f'c conc ksi	f'c grout ksi	P_{max} kips/bar	P_{yield} kips
SL01	SLGP	1	up.-head	#8	MF928	6	5.3	6.9	36	*
SL02	SLGP	1	up.-head	#8	MF928EX	6	5.3	6.4	37	*
SL03	SLGP	1	up.-head	#8	MF928	12	5.3	6.5	60[A]	51
SL04	SLGP	1	up.-head	#8	MF928EX	12	5.3	6.3	61[A]	54
SL05	SLGP	1	up.-head	#8	MF928	9	6.3	7.0	46	*
SL06	SLGP	1	up.-head	#8	MF928EX	9	6.3	7.1	45	*
SL07	SLGP	1	up.-head	#8	MF928	18	5.4	7.0	70[B]	53
SL08	SLGP	1	up.-head	#8	MF928EX	18	5.4	8.5	64[C]	55
SL09	SLGP	1	up.-head	#6	MF928	4	5.5	7.4	21	*
SL10	SLGP	1	up.-head	#6	MF928	8	5.5	7.5	35[D]	28
SL11	SLGP	1	up.-head	#6	MF928	6	5.2	6.9	34[A]	26
SL12	SLGP	1	up.-head	#6	EUHF	6	5.2	6.3	35[D]	28
SL13	SLGP	1	straight	#8	MF928	12	5.2	6.9	56[E]	52
SL14	SLGP	1	straight	#8	MF928	18	5.2	6.9	73[D]	52
SL15	SLGP	2	up.-head	#8	MF928	12	5.0	5.3	31	*
SL16	CIP	2	up.-head	#8	-	12	5.0	-	39	*
SL17	SLGP**	2	up.-head	#8	MF928	12	5.1	6.2	48	*
SL18	SLGP***	2	up.-head	#8	MF928	12	5.1	5.6	50	*

* Concrete Breakout Failure
**Pocket Confined with Spiral
***Pocket Confined with WWF

Notes: A. concrete breakout failure after bar yield
B. stopped test due to grip failure
C. stopped test to prevent grip failure
D. stopped test to prevent bar fracture
E. stopped test due to excessive bar bending

MF928 = Masterflow 928
MF928 EX = Masterflow 928 extended with 1/8" pea gravel
EUHF = Euclid Hi-Flow

5.2 SINGLE BAR TESTS

5.2.1 General Behavior

The general behavior of upset-headed bar anchorages may be illustrated by test SL06. SL06 was a test of a #8 bar embedded 9 inches into a grout pocket using an extended Masterflow 928 mix. Though some details differ for other tests, this test is representative of a concrete breakout failure.

When using headed bars, the embedded length is much shorter than that needed to develop the bar by bearing against the deformations alone. However, anchorage by bearing against bar deformations is stiffer than the bearing capacity at the bar head alone. Therefore, the bar must slip a slight amount before the head becomes effective. The result is splitting cracks emanating from the bar, as shown in Figure 5.1. The first splitting crack occurred at 30 kips for SL06, and was the first cracking observed. The initial splitting crack always extended transversely across the specimen from the bar to the edge of the grout pocket. The crack then gradually grew into the concrete as loading progressed. Orientation of the cracking can be explained by the fact that splitting and flexural tensile stresses coincide in a direction along the specimen axis.

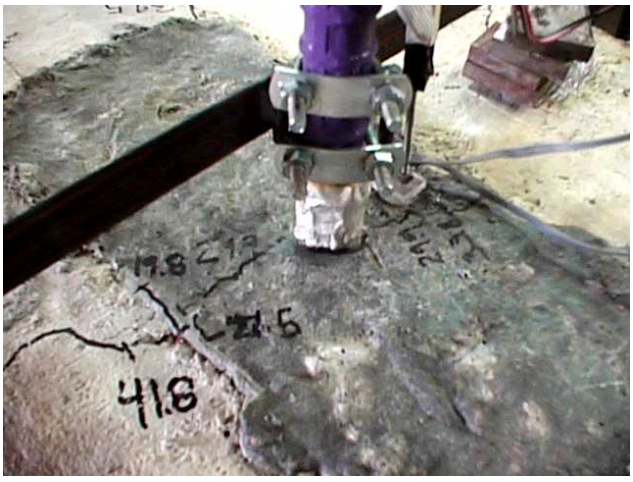

Figure 5.1: Splitting Cracks in Single Bar Specimen

The next significant cracking for SL06 was observed at a load of 40 kips. At this point, cracks began to grow outward from the corners of the grout pocket, as shown in Figure 5.2. These cracks initiated due to the stress concentration at the pocket corners, but extended and participated in the overall breakout surface. Figure 5.3 shows the crack pattern of a pocket near breakout failure. Splitting cracks extended well down the side of the specimen, and corner cracks turned to form a conical surface. Notice that the approximate conical shape that formed is consistent with the theoretical CCD breakout shape [17]. SL06 reached an ultimate load of 45 kips, or approximately 80% of the bar yield force.

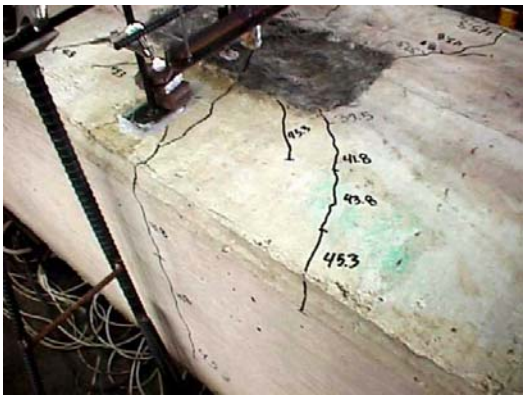

Figure 5.2: Pocket Corner Cracks

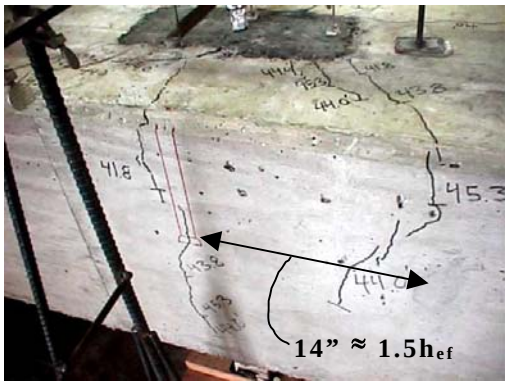

Figure 5.3: Specimen Near Failure

After the peak load was reached, loading continued to expose the full failure surface. In this case, shallow surface cones spalled off the top of the specimen as shown in Figure 5.4. Though the grout remained intact around the bar, it was cracked significantly.

Based on the measured bar strains, the load distribution between the bar head and bar shaft is shown in Figure 5.5. At low loads, the bar shaft resisted the force in the bar nearly entirely. As the bar began to slip relative to the grout, the head resisted an increasing percentage of the load. The share of the load resisted by the head increased to a maximum of 60% at failure.

Figure 5.4: Surface Cone Spalling

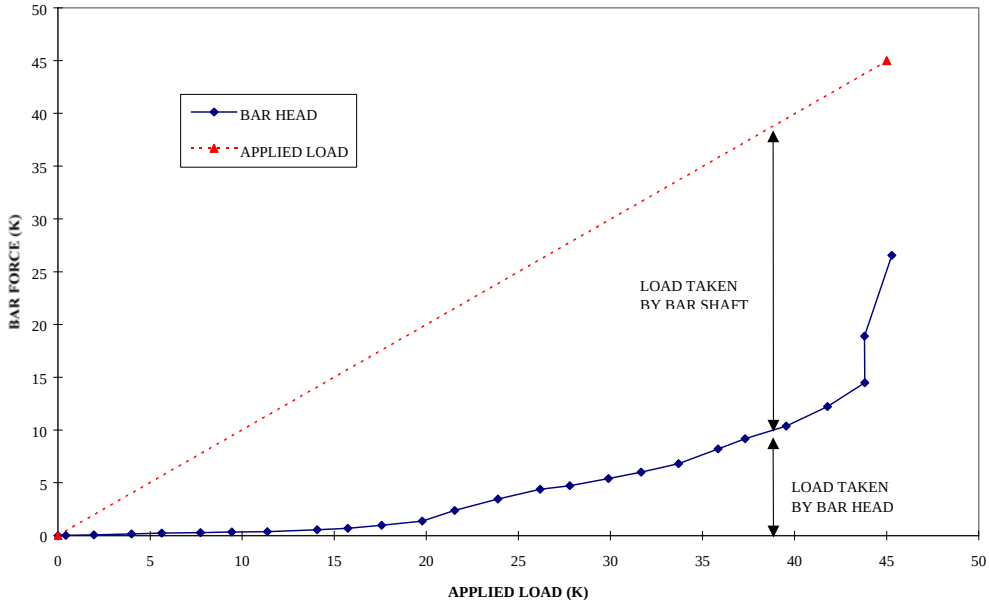

Figure 5.5: SL06 Bar Load Distribution

The load-bar slip response curve for SL06 is shown in Figure 5.6. As was typical for most breakout-type failures, the system deformation was due mainly to the concrete, so little difference was observed between the head and lead bar slip. For deeper embedments in which the bar yielded, the system deformation was due mainly to bar strains. Figure 5.7 shows the load-bar slip response curve for a typical test in which the bar yielded.

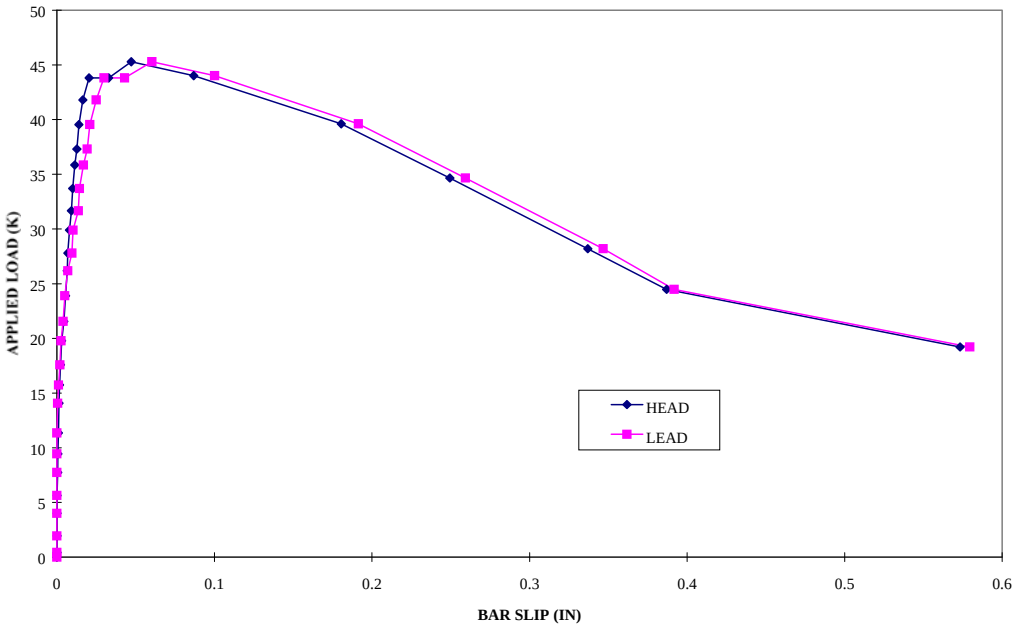

Figure 5.6: SL06 Load - Bar Slip Behavior

Deformation of the grout relative to the concrete was found to be small in most tests. Figure 5.8 shows the relative grout/concrete slip for SL06. The north reading was at the end of the pocket well away from the bar, and showed little movement. The west reading was adjacent to the bar, typically immediately above the splitting crack. Small deformations were observed prior to the peak load. The large relative deformations recorded after reaching the peak load were

due to the breakout failure. As the cracks opened, the pocket surface expanded and the inverted pocket shape no longer restrained the top layers of grout.

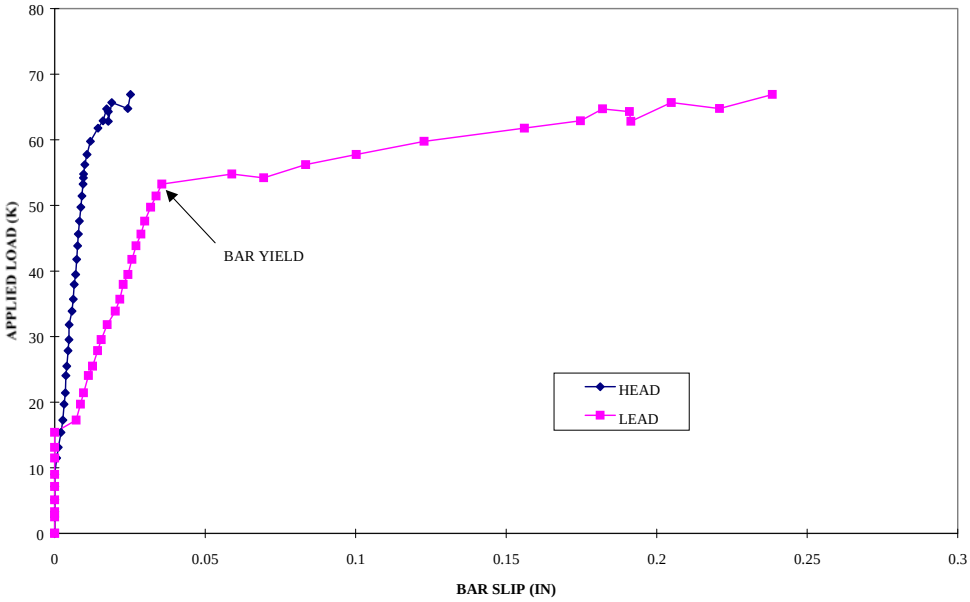

Figure 5.7: SL07 Load - Bar Slip Behavior

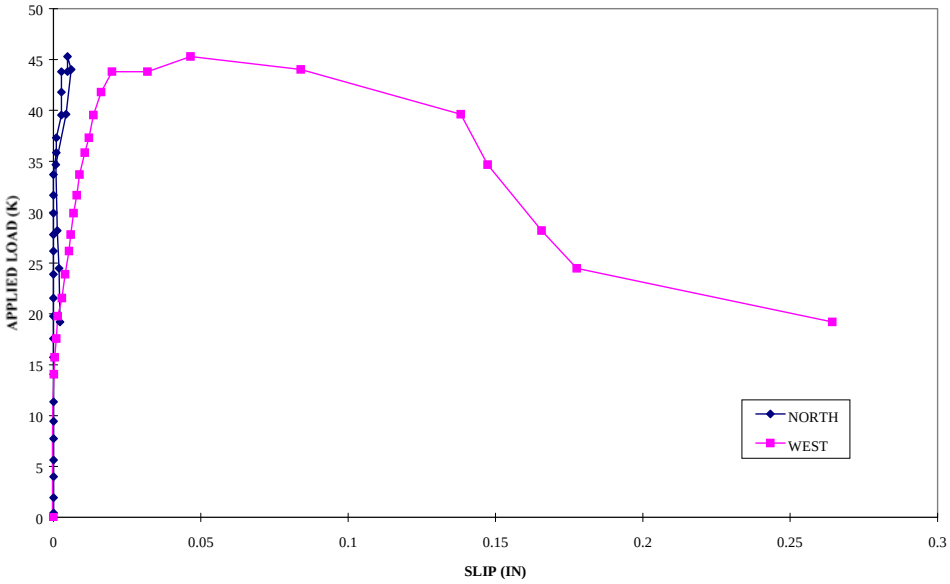

Figure 5.8: SL06 Load vs. Relative Slip Between Grout and Concrete

5.2.2 Effect of Grout Type

5.2.2.1 Extended vs. Unextended Grout

A series of four pairs of tests (SL01 through SL08) were conducted to determine whether using an extended grout mix affects the force transfer characteristics of grout pocket anchorages. Comparisons of unextended and extended Masterflow 928 mixes were performed for embedment depths of 6, 9, 12, and 18 inches.

Virtually no difference in behavior under load between mix types was observed in the tests. As can be seen from the peak loads summarized in Table 5.1, each pair of tests reached roughly the same peak load. Figure 5.9 compares the load-bar slip response of SL01 and SL02, which were tests at a 6" embedment of a #8 upset-headed bar. The behavior is virtually identical.

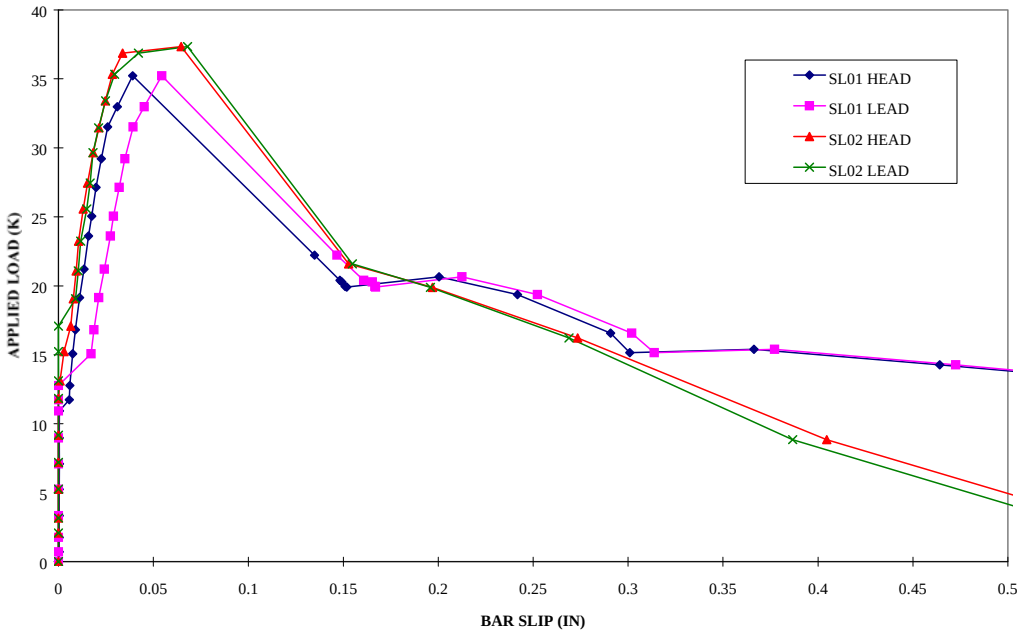

Figure 5.9: Comparison of Extended (SL01) vs. Unextended (SL02) Grout

5.2.2.2 Effect of Grout Type

SL11 and SL12 compared Masterflow 928 to Euclid Hi-Flow for a #6 bar embedded 6 inches. The mixes were placed on the same day and had similar test day cube strengths. The resulting load-deformation curves are shown in Figure 5.10. Though the Masterflow 928 mix was slightly less stiff, the behavior was very similar. The peak loads only differed by 1 kip.

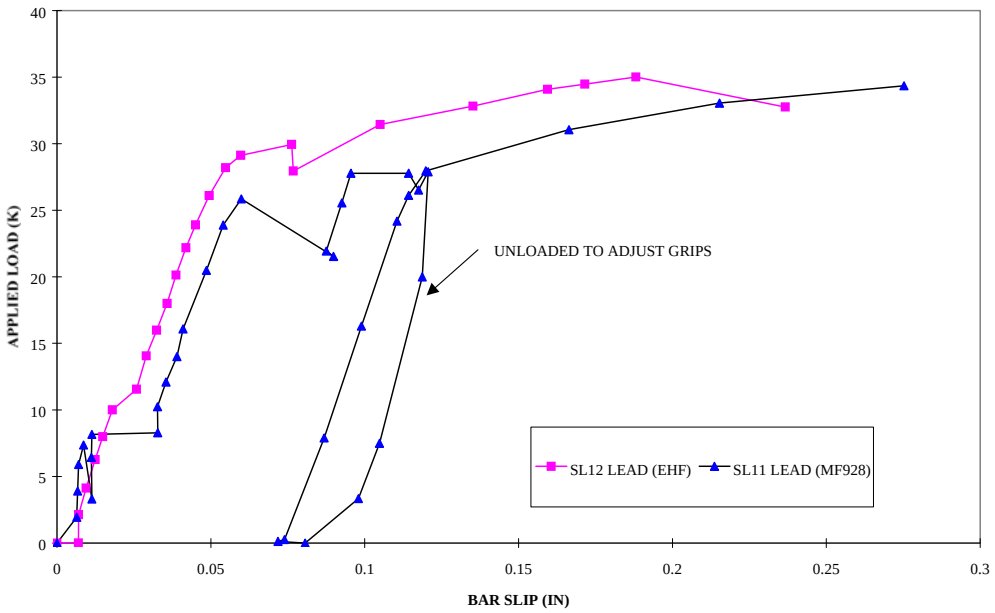

Figure 5.10: Comparison of MF928 Grout (SL11) vs. Euclid HF Grout (SL12)

5.2.3 Effect of Embedment Depth

The primary test variable in the single bar tests was embedment depth. As expected, at greater embedment depths the anchorage capacity of the bars improved. Figures 5.11 and 5.12 show the relationship between embedment depth and pullout capacity for #8 and #6 bars.

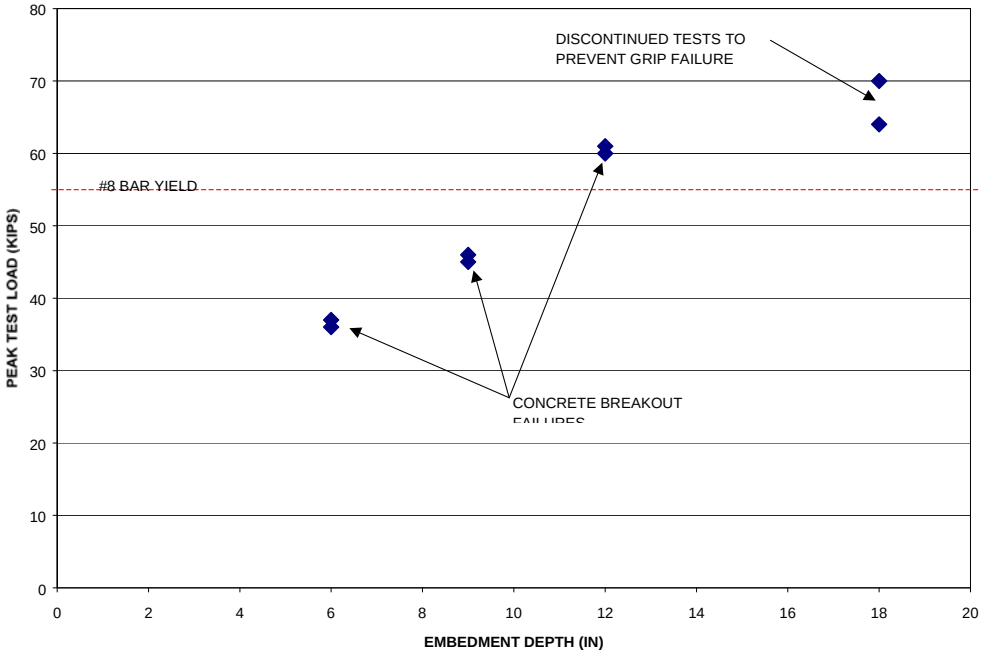

Figure 5.11: Effect of Embedment Depth for #8 Bars

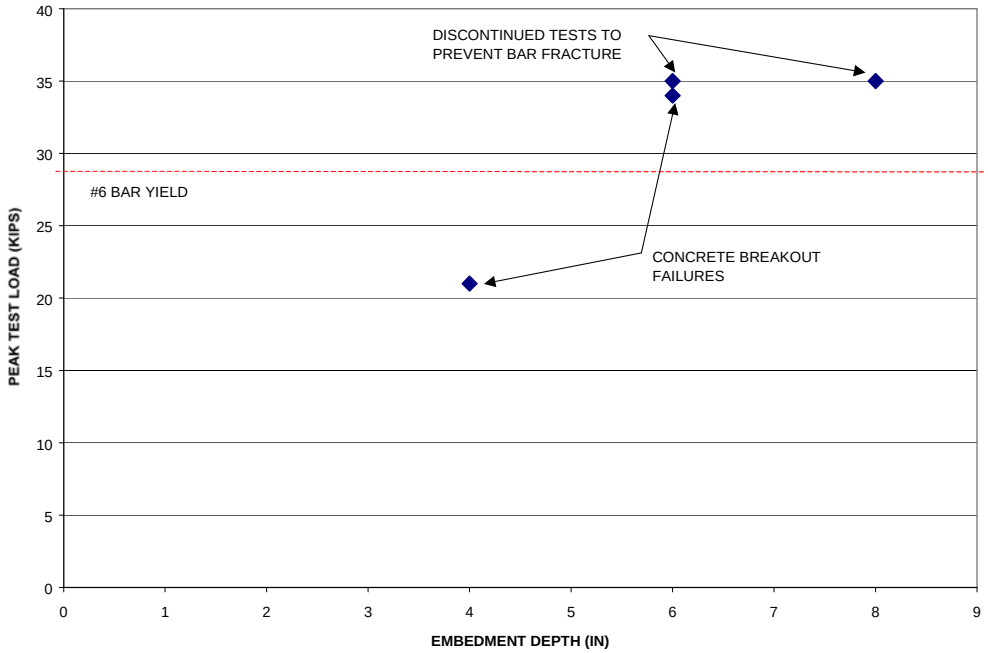

Figure 5.12: Effect of Embedment Depth for #6 Bars

For #8 bar tests, the transition between concrete breakout failure and steel yield occurred at an embedment depth of approximately 12 inches. Tests at 12" embedment (SL03, 04) yielded the bar, but a breakout failure occurred at a slightly higher load. Though a 12" embedment provided sufficient capacity to yield the #8 bar, the behavior was poor at service load levels. Crack widths up to 0.016 inches were observed at a load of 40 kips, a reasonable service load level. The tests at an 18" embedment (SL07, 08) provided much better behavior, with the bar able to reach yield with maximum crack widths of only 0.010 inches. Crack widths at a load of 40 kips were all less than 0.005 inches.

The behavior of #6 bar tests was similar. The transition between concrete breakout and bar yield failure occurred between 4 and 6 inches. Again, the 6 inch embedment provided sufficient capacity to yield the bar, but significant cracking existed at the yield load. Service load splitting cracks reached 0.013 inches. An embedment of 8 inches provided sufficient capacity to yield the bar as well as keep crack widths below 0.013 inches at yield and 0.005 inches at service loads.

5.2.4 Straight Bar Tests

SL13 and SL14 were tests of straight bars in single line grout pockets for embedments of 12 and 18 inches, respectively. Figure 5.13 shows the load-bar slip behavior for the two tests. The 12 inch embedment failed just at the yield load of the bar. The 18 inch embedment provided so much capacity that the test had to be stopped before the bar fractured, but showed signs of imminent anchorage failure when the test was stopped.

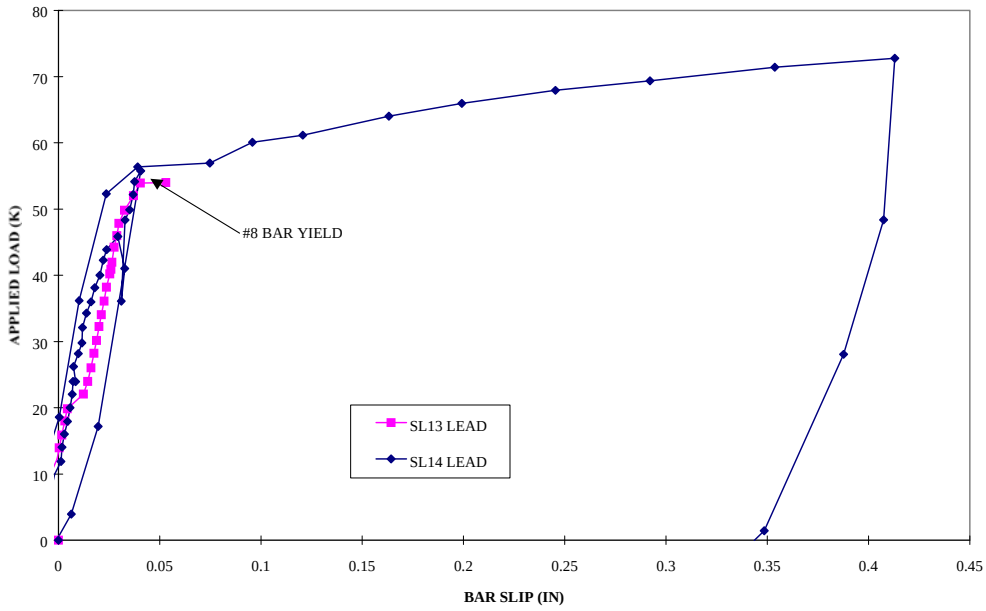

Figure 5.13: Load-Bar Slip Behavior for Straight Bar Tests

Behavior of the straight bars was similar in many ways to the headed bars. Initial splitting cracks formed transverse to the specimen as for headed bar tests, and were again followed by cracking at the corners of the grout pocket. However, as the load approached failure, the cracks did not mobilize a conical failure, but instead new splitting cracks radiated from the bar. The anchorage failed by pulling out a shallow surface cone. Figure 5.14 shows SL13 near the anchorage failure load.

The embedment lengths of 12 and 18 inches are less than the 20 inch embedment required by Equation 3-6 to develop the yield strength of the bar. This can be explained in part by the fact that a bar in a tapered grout pocket experiences lateral confining pressure. As the bar is pulled out of the grout,

wedging action of the grout against the concrete produces a state of triaxial compression in the grout, enhancing bar anchorage. However, it should be noted that during the testing of SL13, a significant amount of bending was observed in the test bar due to loading frame misalignment. Strain differentials up to 1100 microstrain were observed across the bar section at the lead measurement point (see Figure 4.23). The prying effect resulting from the bar bending might have contributed to the enhanced anchorage strength observed for SL13.

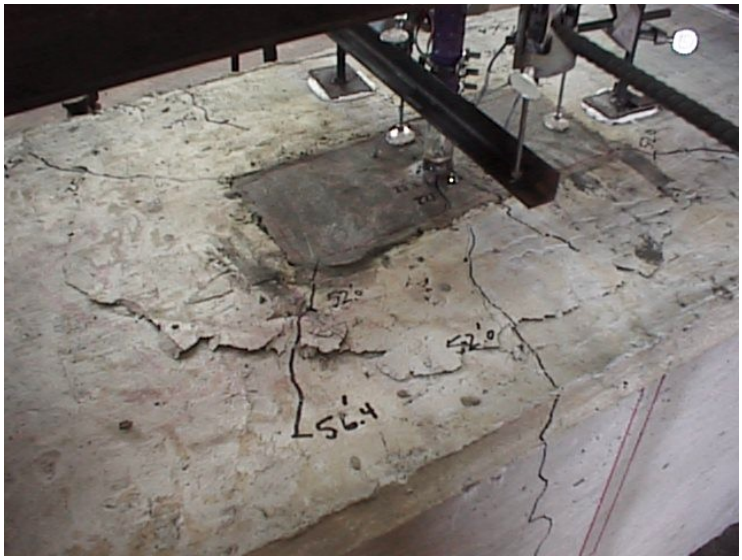

Figure 5.14: SL13 Near Failure Load

5.3 MULTIPLE BAR TESTS

The multiple bar single line grout pocket tests were all of two #8 upset-headed bars with an embedment of 12 inches. SL15 was the control test with no pocket confinement steel. SL16 consisted of two #8 upset-headed bars cast in place in a specimen with a reinforcement pattern identical to the single line grout pocket specimens. Because each specimen accommodated two tests, SL15 and SL16 were cast into the same specimen, thus providing a good comparison

between a cast-in-place and grout pocket anchorage. SL17 and SL18 were grout pocket tests utilizing spiral and WWF pocket confinement steel.

Figure 5.15 shows the load-bar slip behavior of each of the multiple-bar tests. The basic grout pocket behavior is exhibited by the response of specimen SL15. Typical splitting cracks transverse to the beam axis appeared at low load levels, around 12 to 16 kips. In addition, another splitting crack formed at a load of 22 kips on a direct line between the bars along the beam axis. Cracks emanating from the pocket corners formed at approximately 26 kips, and the anchorage reached a peak load of 31 kips before mobilizing a concrete breakout failure. The failure cone involved both bars, consistent with the CCD group pyramid failure [17]. As the cone was pulled out under further loading, a large crack formed along the specimen side at approximately the level of the longitudinal reinforcement. Figure 5.16 shows the failed SL15 grout pocket specimen.

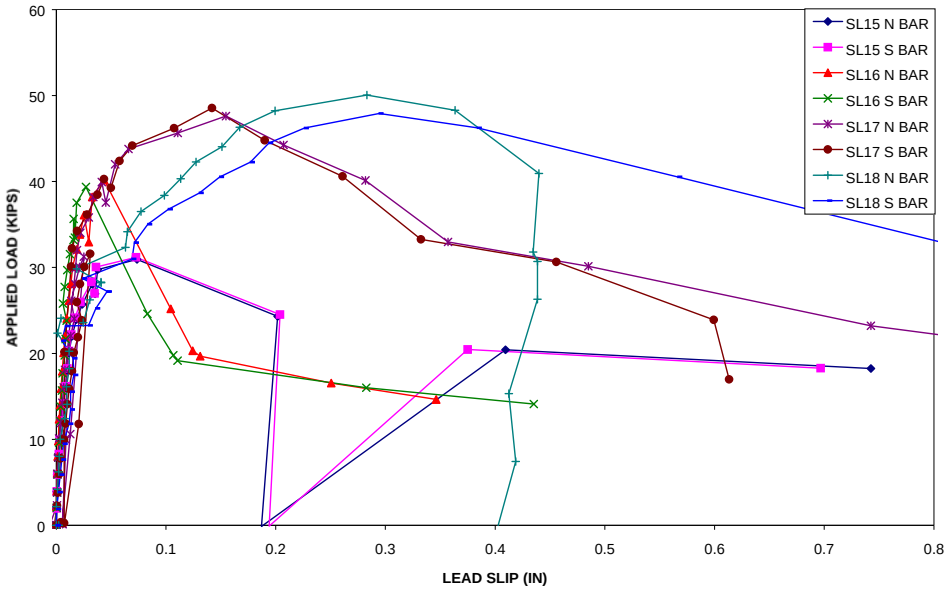

Figure 5.15: Load-Bar Slip Behavior for 2-Upset Head #8 Bars in SLGP

A comparison of the behavior of SL15 with SL16 demonstrates the effect of grout pockets on headed bar anchorages. Though splitting cracks formed at the same load levels as for SL15, the cast-in-place SL16 specimen of did not develop the pocket corner cracks as in grout pocket specimens. As illustrated in Figure 5.17, this allows an overall tension field to develop, rather than the separate fields formed due to the influence of corner cracks. The cast-in-place specimen reached a peak load of 39 kips before forming a classic group-failure pyramid [17].

Figure 5.16: SL15 Breakout Surface Cracks

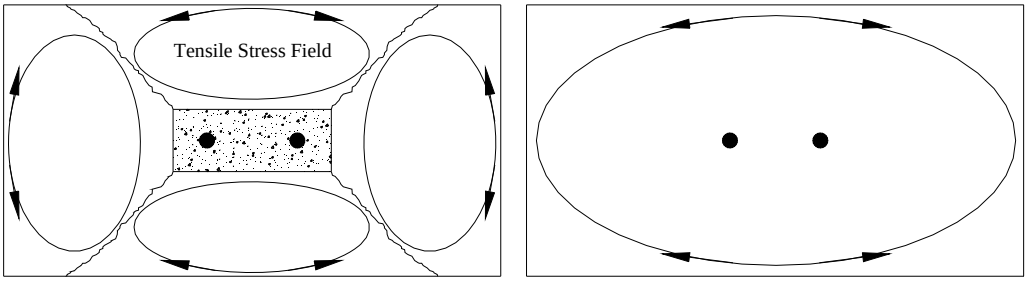

Figure 5.17: Grout Pocket vs. Cast-in-Place Tensile Stress Fields

The addition of pocket confinement steel added both capacity and ductility to the grout pocket anchorage. This steel became effective once the conical failure surface was mobilized and cracks began to open. Because the pocket

confinement steel crossed the cone failure planes, it contributed to the load carrying capacity of the anchorage once the ultimate tensile strength of the concrete breakout surface was reached.

As can be seen in Figure 5.15, the behavior of the specimens with pocket confinement steel was similar to unconfined specimens up to the failure load of the unconfined specimens. The concrete then shed its load to the confinement steel, which allowed the anchorage to reach an ultimate capacity of approximately 50 kips in SL17 and SL18. However, this increase in capacity is associated with the large deformations required to mobilize the confinement steel. Figure 5.18 shows SL17 at ultimate load.

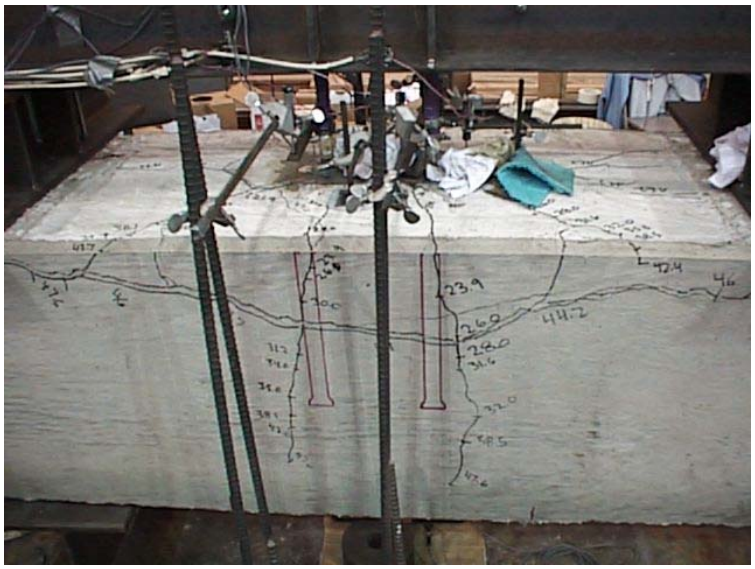

Figure 5.18: SL17 Spirally Confined Grout Pocket at Failure

Slight differences were observed between spiral and WWF pocket confinement steel. Though the specimens with different confinement steel reached an ultimate load of approximately 50 kips, the WWF confinement required a larger deformation to develop the ultimate strength. However, the WWF confinement was able to sustain higher loads at large deformations than the spiral confinement.

It is interesting that specimens with the two confinement types developed the same ultimate load even though the spiral confinement had a much higher volumetric reinforcement ratio (ρ_s = 0.010) than the WWF mesh (ρ = 0.003). This can be explained by considering how the pocket confinement steel intersects with the concrete breakout surface. Because the spiral is composed of a single coiled bar, it can only cross the breakout surface at a limited number of locations. With WWF, the steel is uniformly distributed, so all of the vertical steel crosses the breakout surface cracks.

The distribution of force between the bar head and bar shaft for multiple-bar tests is shown in Figure 5.19. Because less cracking occurs, the cast-in-place specimen resists less load at the head than in the control grout pocket test (SL15). Figure 5.19 also shows the load redistribution effect in the specimens with pocket confinement steel. Near the ultimate load, the force resisted by the head dropped off as the primary load resistance shifted to the confinement steel.

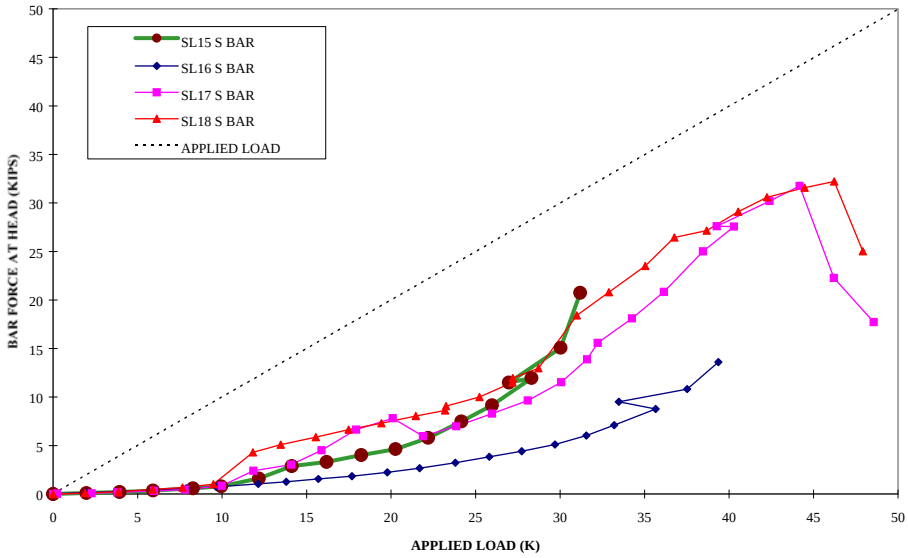

Figure 5.19: Bar Force Distribution for Multiple-Bar Tests

5.4 CONCLUSIONS

Pullout tests of single and multiple bars in single line grout pockets exhibited steel yield and concrete breakout behavior. The type of grout used had little effect on the capacity or behavior of the specimens, provided consistent grout strength was maintained. The major effect of the grout pocket versus a cast-in-place anchorage was the cracks that resulted due to stress concentrations at the pocket corners. These cracks served to break up tensile stress fields in the concrete, forcing breakout behavior similar to that of headed anchorages in cracked concrete. Though bar yield was achieved at relatively short embedment depths, an increased embedment depth served to reduce cracking at service load levels - an important consideration for the durability of grout pocket connections.

Confinement from the wedging effect of the grout pocket served to increase the anchorage capacity of straight bars above what would be expected for cast-in-pace bars. However, excessive bar bending in one straight bar test (SL13) rendered the results somewhat dubious. Additional straight bar tests are discussed in Chapters 6 and 7.

Pocket confinement steel enhanced both capacity and ductility of single line grout pocket anchorages. Due to the geometry of the steel, WWF confinement was found to be much more efficient than spiral confinement for resisting breakout forces. Pocket confinement steel was demonstrated to be a promising option for providing ductility in grout pocket anchorages. More pocket confinement steel parameters are discussed in Chapter 6.

CHAPTER 6

DOUBLE LINE GROUT POCKET TESTS

6.1 SUMMARY OF RESULTS

The double line grout pocket test series is summarized in Table 6.1. Four tests of upset-headed bar groups were conducted for an embedment of 6 inches, and two tests of straight bars were conducted for an embedment of 9 inches. Double line grout pocket tests examined the effects of longitudinal versus transverse moment and pocket confinement. Each of the headed bar tests resulted in a concrete breakout failure, and each of the straight bar tests produced a pullout failure.

Table 6.1: Summary of Double Line Grout Pocket Tests

Test ID	Type	Bar Type	Bar Size	Grout	h_{ef} in	Confinement	f'_c conc ksi	f'_c grout ksi	P_{max} kips/bar	P_{yield} kips
DL01	DLGP-TM	upset-head	#6	MF928	6	-	5.1	4.2	24	*
DL02	DLGP-LM	upset-head	#6	MF928	6	-	5.1	5.9	20	*
DL03	DLGP-LM	upset-head	#6	MF928	6	Spiral	5.6	6.0	22	*
DL04	DLGP-LM	upset-head	#6	MF928	6	WWF	5.6	5.4	24	*
DL05	DLGP-LM	straight	#6	MF928	9	Spiral	5.7	6.3	24	*
DL06	DLGP-LM	straight	#6	MF928	9	WWF	5.7	6.4	28[A]	28

* Concrete Breakout Failure

MF928 = Masterflow 928

Notes: A. pullout failure simultaneous with bar yield

TM = Transverse Moment

LM = Longitudinal Moment

All DLGP tests were of 2 bars

6.2 TRANSVERSE AND LONGITUDINAL MOMENT BEHAVIOR

Connections between precast bent caps and columns must be capable of transferring longitudinal moments (in the direction of the superstructure) and transverse moments (perpendicular to the longitudinal axis of the superstructure) between each bent cap and column, as discussed in Section 1.3. Differences in the behavior of transverse and longitudinal-moment connections are illustrated by tests DL01 and DL02. DL01 was a test of a transverse moment connection that loaded 2-#6 upset-headed bars embedded 6 inches. DL02 had the same bar parameters, but the bars were arranged to resist longitudinal moment. See Figure 4.17 for a description of the bar arrangements.

6.2.1 Transverse Moments

The same basic behavior that was observed during single line grout pocket tests resurfaced in the double line tests. For DL01, the first cracks that formed at approximately 15 kips were splitting cracks within the grout pocket. Corner cracks formed almost simultaneously with the splitting cracks. The corner cracks formed only at the outside pocket corners, and at first formed only adjacent to the loaded bars. The splitting cracks then extended down the side of the specimen at a load of 20 kips. Figure 6.1 shows the specimen at this point.

At a load of 22 kips a splitting crack formed between the loaded bars, across the two separate pockets. The load reached a peak of 24 kips, and failure corresponded with the formation of shallow cones along the beam axis. The failed specimen is shown in Figure 6.2.

Figure 6.1: Splitting and Corner Cracks in DL01

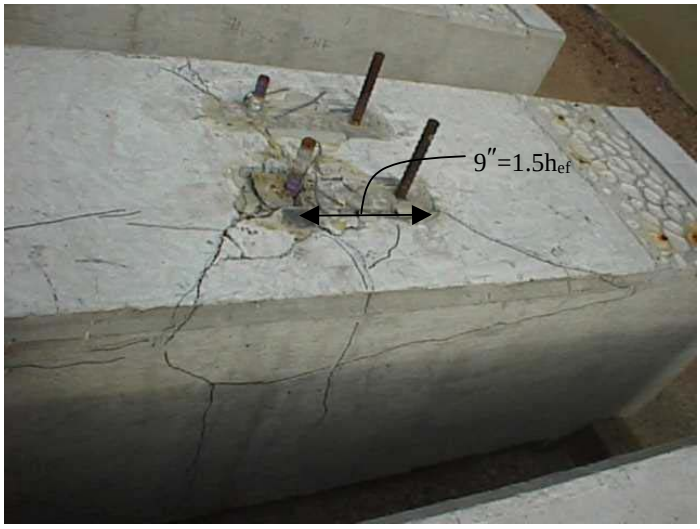

Figure 6.2: Failed Transverse Moment Specimen (DL01)

The failure mode illustrates the effect of the pocket shape. For the double line grout pockets, the maximum inclination of the sides of each pocket was along the beam axis, while the single line grout pockets had maximum inclination of the sides of the pockets transverse to the beam axis. The double line grout pocket shape forced the breakout cones to form along the beam axis, as shown in Figure

6.3. Corner cracking adjacent to the unloaded bars in Figure 6.2 further illustrates this effect. The cracks extended well past $1.5h_{ef}$ (9”) from the test bar, suggesting that the anchorage was not behaving monolithically, but rather the wedging effect of the grout pocket pulling through the surrounding concrete had a major influence on the behavior. This effect was not as apparent in single line tests because the pocket shape forced the cone to the sides of the specimen. Because there was little material present to resist the wedging action, the anchorage behaved similar to a monolithic connection influenced by edge effects.

There was little effect of two separate pockets on the connection behavior. The pullout behavior simulated that of a bar group, and the group acted as if it was in one large grout pocket with cracking occurring only at the outside pocket corners.

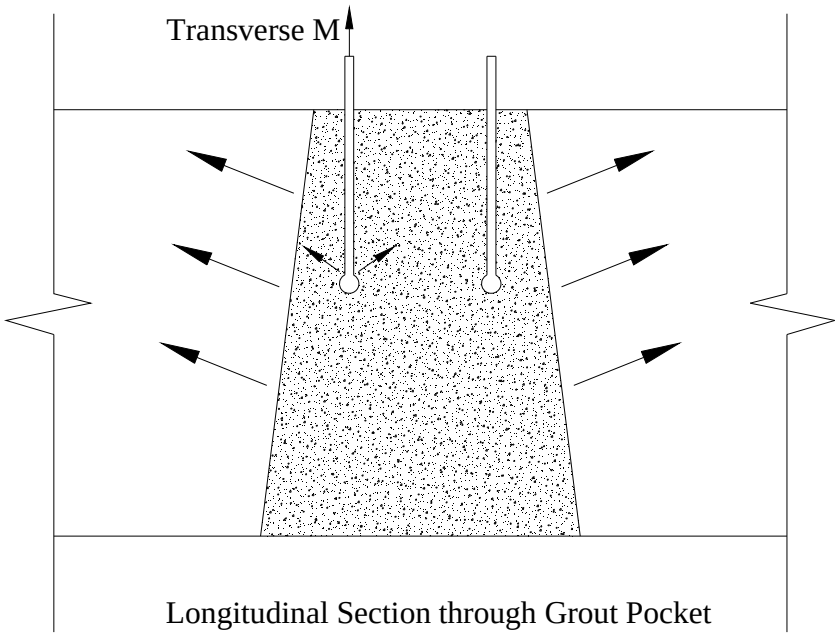

Figure 6.3: Wedging Influence in Double Line Grout Pockets

6.2.2 Longitudinal Moments

The behavior of the two bar anchorage for resisting transfer of longitudinal moment resembled the same group behavior observed in the transverse moment test. Splitting cracks first formed in the pocket at a load of 14 kips, followed by corner cracks at the pocket side adjacent to the edge at a load of 16 kips. Smaller corner cracks appeared at the other side of the loaded pocket at a load of 18 kips. Because only one pocket was loaded in the longitudinal moment configuration, corner cracks were observed only for the loaded pocket. The bar group failed as one splitting crack extended down the side of the beam and the corner cracks extended to form a conical failure surface. Figure 6.4 shows the crack pattern near failure, and Figure 6.5 shows the cone that was pulled out with further loading.

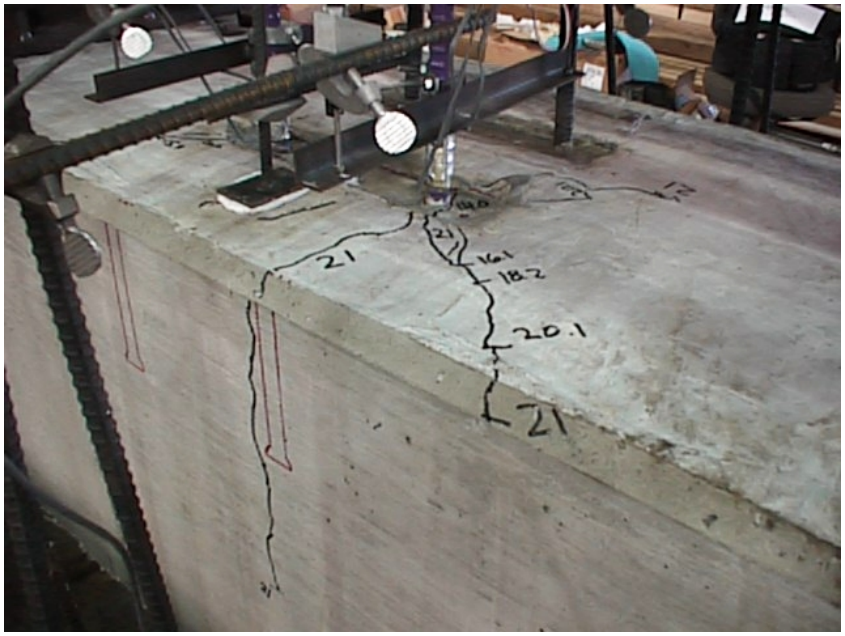

Figure 6.4: DL02 Cracking Near Failure

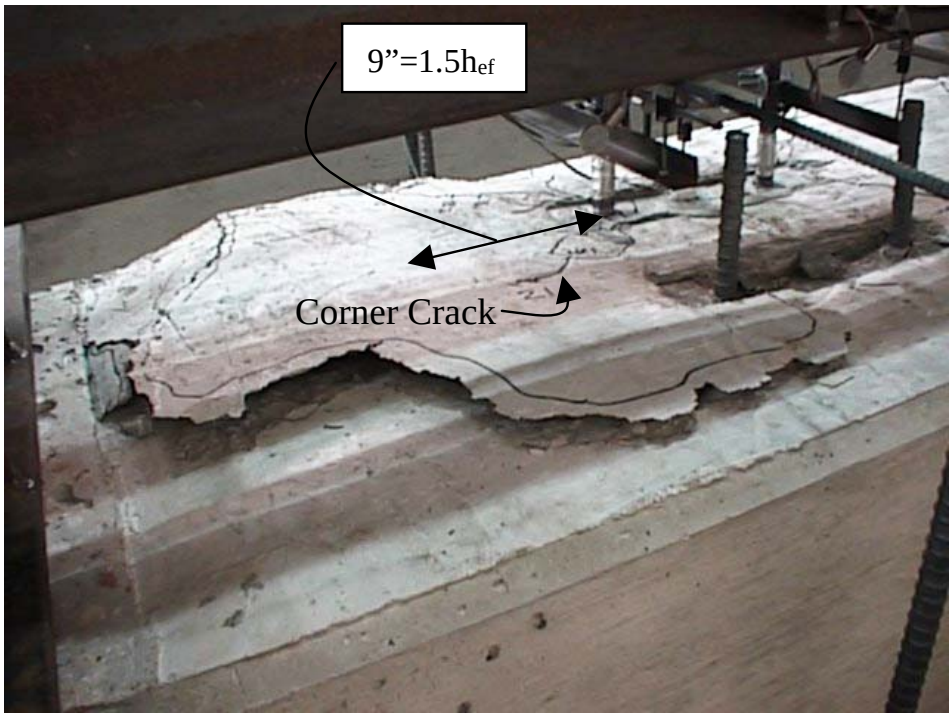

Figure 6.5: DL02 Breakout Surface

As shown in Figure 6.5, the shape of the grout pocket again forced the cone to form along the beam axis. In this case, the placement of the bars near one edge allowed the cone to form fully on the side away from the edge. The unloaded pocket had no effect on the breakout cone since no corner cracks formed. Figure 6.5 also shows that the corner cracks that formed in the loaded pocket away from the edge were not significant enough to separate the breakout cone. The corner cracks that formed near the pocket edge separated the tensile stress fields into three fields as shown in Figure 6.6.

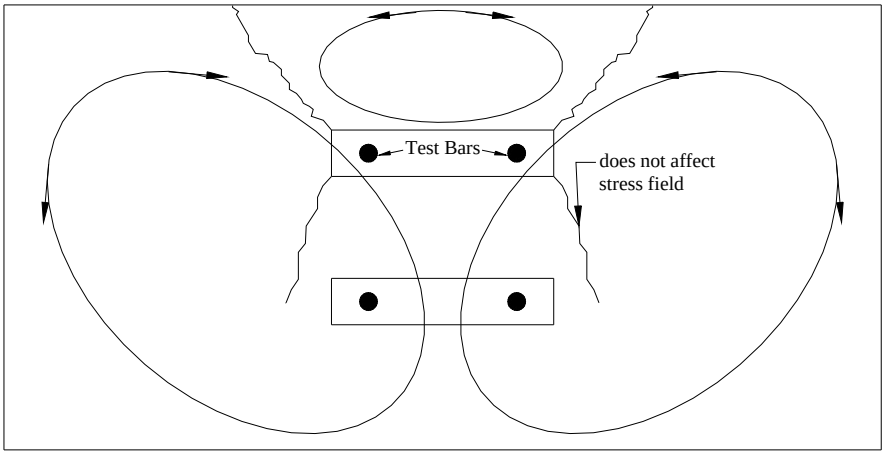

Figure 6.6: Tensile Stress Fields in DLGP Resulting from Longitudinal Moment

Figure 6.7 compares the load-bar slip behavior of DL01 and DL02. The difference in peak load was mainly due to geometry, which is accounted for in the edge effect factors of the CCD method. Bar slips at peak load were similar, but DL01 was able to attain a larger post-peak bar slip than DL02. As shown in Figure 6.8, the force at the head of each bar was very similar for a given load.

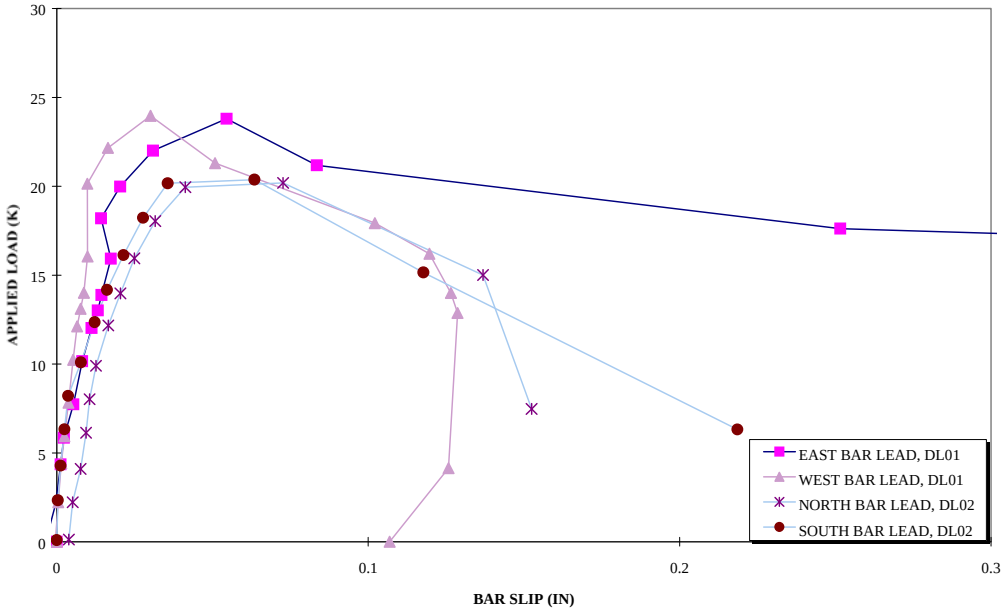

Figure 6.7: Transverse (DL01) vs. Longitudinal (DL02) Moment Load-Bar Slip

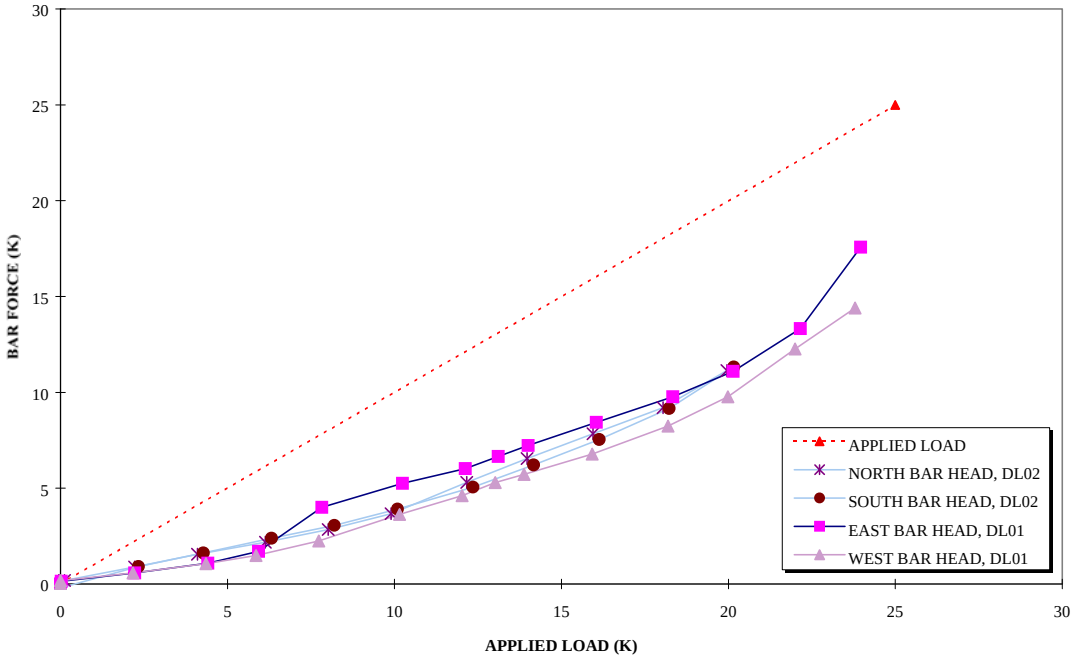

Figure 6.8: Transverse (DL01) vs. Longitudinal (DL02) Moment Head Force

6.3 EFFECT OF POCKET CONFINEMENT STEEL

Spiral and WWF pocket confinement steel were used in DL03 and DL04, respectively, to enhance the capacity and ductility of the anchorage group tested in DL02 under simulated longitudinal moments. Some aspects of behavior of specimens with pocket confinement steel were similar to behavior observed for DL02. Cracks typically formed at the same load levels as described in Section 6.2.2, though the bar group reached slightly higher loads. DL03 failed at a load of 22 kips, while DL04 reached a load of 24 kips. The failed specimens are pictured in Figures 6.9 and 6.10.

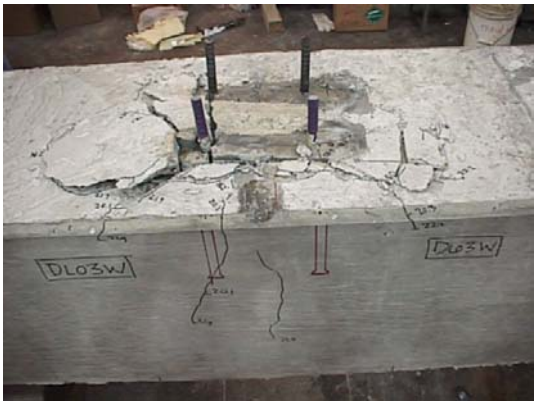

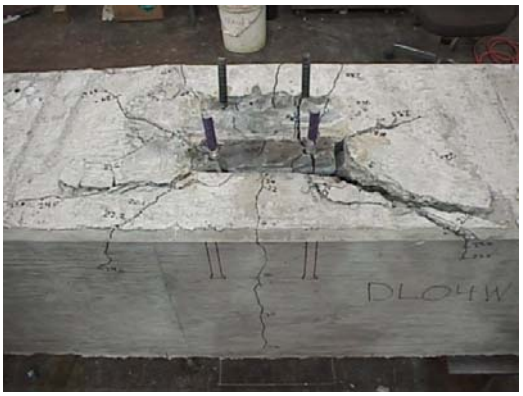

Figure 6.9: DL03 Breakout Surface ***Figure 6.10: DL04 Breakout Surface***

Figure 6.11 compares the load-bar slip behavior of the longitudinal moment tests with and without pocket confinement steel. With the confinement, the bar group reached slightly higher loads, but also required slightly larger bar slips to reach these loads. In the post-peak range, the tests with pocket confinement unloaded gradually, reaching large ultimate bar slips. Load in the unconfined pocket dropped off rapidly.

Figure 6.12 compares the bar load distribution for the longitudinal moment tests of specimens DL02, DL03, and DL04. Again, the distribution is similar at comparable loads for each case. The bar force at the head versus applied load response for confined pockets follow the response curves for the unconfined pocket up to the unconfined failure load, then the head resists an increasing share of the load. Strain readings for the North bar head force in DL03, from which bar forces were extrapolated, were lower than for the other tests, but this is probably due to an error in the strain gauge reading. Initial readings at low loads yielded negative bar strains.

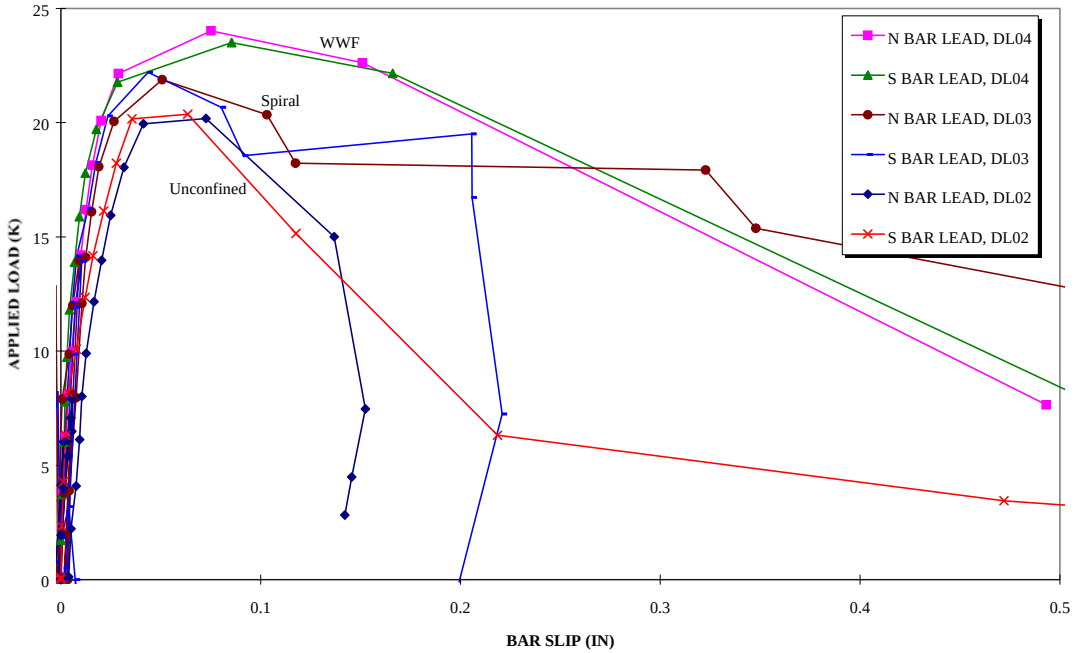

Figure 6.11: Effect of Confinement on Longitudinal Moment Tests

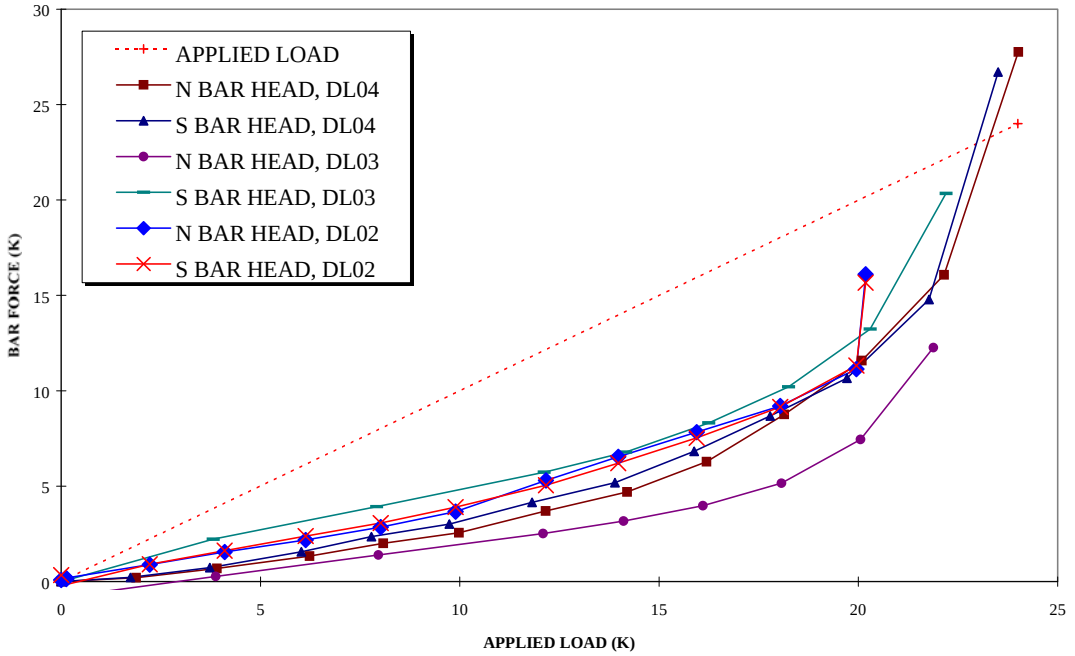

Figure 6.12: Effect of Confinement on Bar Force at the Upset Head

For single line grout pocket tests, the use of pocket confinement steel provided a 60% increase in bar group capacity over the unconfined test. It is surprising, then, that for double line pockets the increase was almost negligible. However, the difference can be explained by examining the geometry of the breakout surface. The embedment depth for the double line tests was only 6 inches, while in single line confinement tests the embedment was 12 inches. As shown in Figure 6.13, the short embedment depth produced a breakout surface that was only able to engage the top of the pocket confinement steel. Because the confinement did not extend above the cap longitudinal reinforcement, it did not intercept a significant portion of the failure surface and thus was largely ineffective. For pocket confinement steel to be effective in resisting breakout forces, the embedment depth of the bars must be sufficient to engage the confining steel.

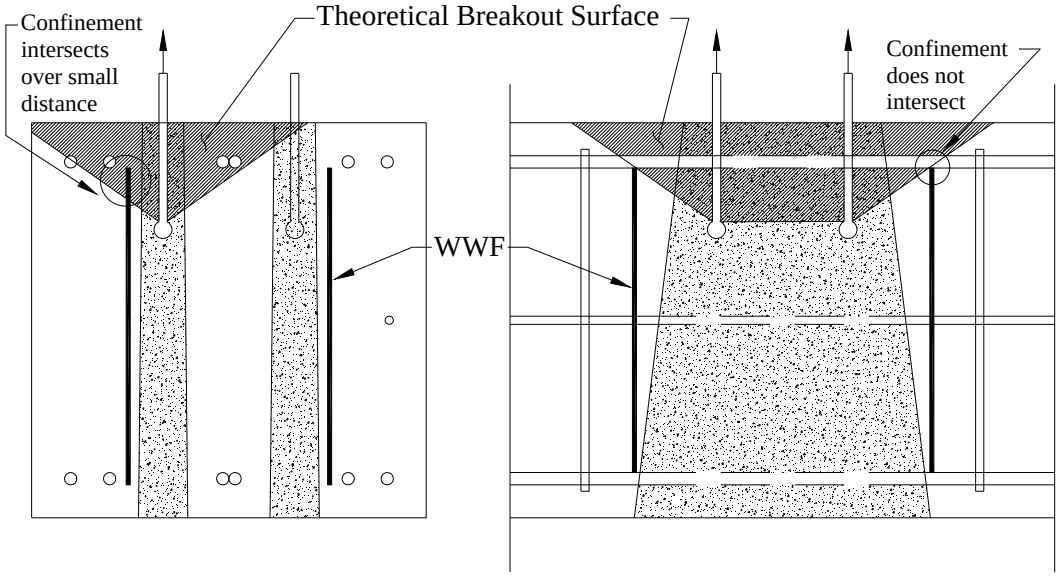

Figure 6.13: Ineffective Confinement for Short Embedment Depths

6.4 STRAIGHT BAR TESTS WITH CONFINEMENT

Straight bar tests under simulated longitudinal moments were conducted to determine both the behavior of straight bars in double line pockets and the depth at which confinement becomes effective. DL05 and DL06 were tests of two #6 bars with spiral and WWF confinement at an embedment depth of 9 inches. Similar behavior was observed for the two tests.

At a load of approximately 8 kips, splitting cracks formed in the grout pocket between the bar and pocket edges, both transverse and longitudinally in the pocket. These were followed by corner cracks at a load of 18 kips in the loaded pocket. At a load of 20 kips, what appeared to be flexural cracks formed on both sides of the specimen between the bars. These cracks later joined with splitting cracks emanating from the loaded bars. Additional splitting cracks spread into the concrete specimen at higher loads, and the anchorage failed by pulling out a shallow-depth cone. DL05 failed at a peak load of 24 kips, while DL06 reached 28 kips. Figure 6.14 shows DL06 near the failure load.

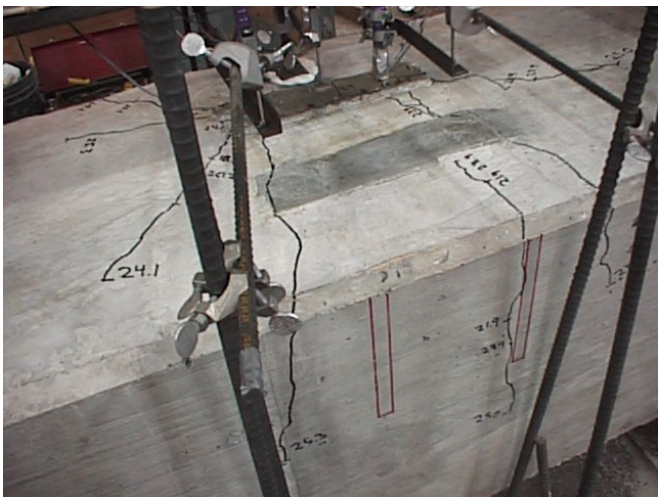

Figure 6.14: DL06 Cracking at Failure

Figure 6.15 compares the applied load-bar slip response of DL05 and DL06. This plot shows that the behavior was almost identical up to the DL05 failure load of 24 kips. At this point the deteriorating concrete redistributed load to the confinement steel. The spiral confinement in DL05 did not provide additional capacity, but allowed the anchorage to maintain the peak load up to a bar slip of 0.10″. The WWF confinement used in DL06 developed additional capacity, but required approximately the same bar slip of 0.10″ to reach the peak load. As first discussed in Section 5.3, the WWF confinement provided greater capacity at a much lower volumetric reinforcement ratio than the spiral confinement.

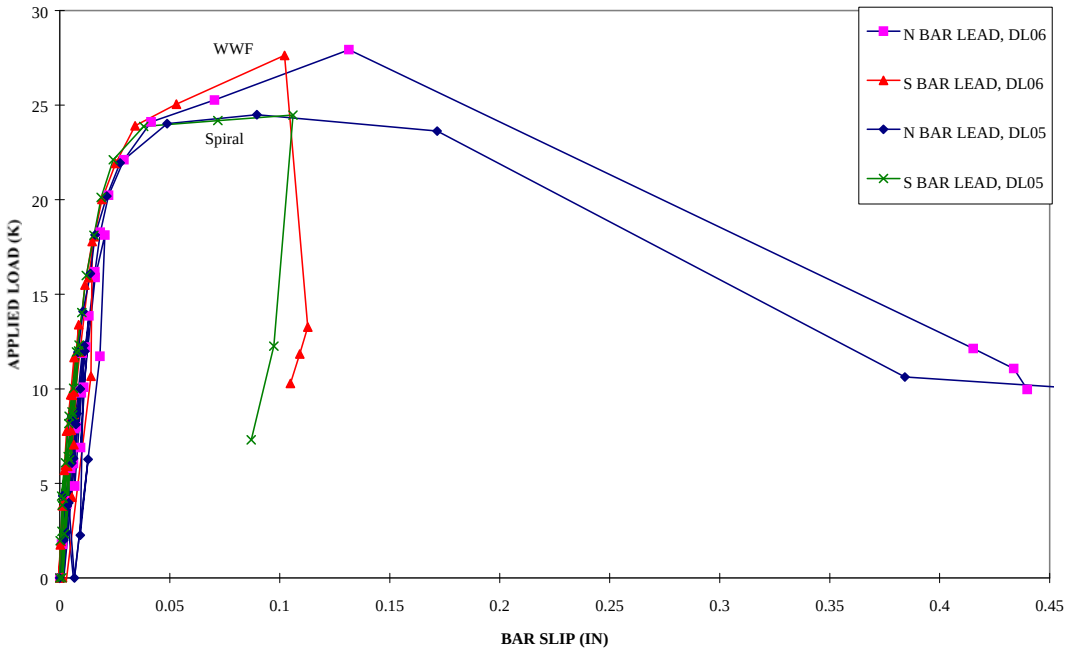

Figure 6.15: Applied Load-Bar Slip for Straight Bar Tests with Confinement

The wedging effect of the grout pocket again enhanced the capacity of the straight bar anchorage. Equation 3-6 predicts a 16″ development length for a #6 epoxy coated bar, suggesting that the anchorage should have failed at 15 kips. The additional strength observed is related to the confinement provided by the wedging action of grout pocket.

6.5 CONCLUSIONS

The same basic behavior observed in single line tests was observed for double line grout pocket tests. Loaded grout pockets formed corner cracks, but loading of one pocket did not affect an unloaded pocket. Tensile stress fields resulting from the anchorage will be broken up according to which pockets are loaded. The shape of the pocket also affected the anchorage behavior. Inclination of the pocket sides in the longitudinal direction of the bent forced a conical failure surface to form along the specimen axis.

Tests using grout pocket confinement steel showed that the bars must be embedded a sufficient depth to engage the confinement steel. For cases of small embedment depth, concrete will simply fail within the confinement steel. Also, test results again showed WWF confinement to be more efficient than spiral confinement.

Confined straight bar tests exhibited similar behavior to that observed for single line straight bar tests. The anchorage exhibited additional capacity beyond that predicted by Equation 3-6 due to the lateral confinement provided by the wedging action of the grout pocket. WWF and spiral confinement provided additional ductility but little capacity gain for straight bar anchorages.

CHAPTER 7

GROUTED VERTICAL DUCT TESTS

7.1 SUMMARY OF RESULTS

The grouted vertical duct test series is summarized in Table 7.1. All tests were conducted on single, epoxy-coated #11 bars grouted in a 4″ diameter corrugated duct, as described in Chapter 4. The basic development length of a straight #11 epoxy-coated bar from Equation 3-6 is 36 inches. Pullout tests were conducted at embedment depths of 12, 18, and 24 inches. Six tests were of straight bars, and the remaining two tests were of upset-headed bars to determine the effectiveness of the head. Three tests resulted in pullout failure, while the remainder of the tests were stopped short of the fracture strength of the bar.

Table 7.1: Summary of Grouted Vertical Duct Tests

Test ID	Type	#Bars	Bar Type	Bar Size	Grout	h_{ef} in	f'_c conc ksi	f'_c grout ksi	P_{max} kips/bar	P_{yield} kips
GVD01	GVD	1	straight	#11	MF928	12	5.4	4.2	76	*
GVD02	GVD	1	upset-head	#11	MF928	12	5.4	4.2	92	*
GVD03	GVD	1	straight	#11	MF928	18	5.6	5.7	120[A]	92
GVD04	GVD	1	straight	#11	EUHF	18	5.6	3.1	94	*
GVD05	GVD	1	straight	#11	S212	18	5.7	4.6	114[A]	93
GVD06	GVD	1	upset-head	#11	MF928	18	5.6	4.8	116[A]	93
GVD07	GVD	1	straight	#11	MF928	24	5.6	5.1	100[A]	94
GVD08	GVD	1	straight	#11	EUHF	24	5.7	4.9	118[A]	93

* Pullout Failure

Notes: A. Test terminated to prevent bar fracture or hydraulic hose failure

MF928 = Masterflow 928
EUHF = Euclid Hi-Flow
S212 = Sika 212

7.2 GENERAL BEHAVIOR

The basic behavior of grouted vertical duct anchorages is illustrated by GVD03, a test of a straight #11 bar embedded 18" in Masterflow 928 grout. No cracking was observed up to a load of 28 kips, at which point a small splitting crack formed at the grout surface. At a load of 56 kips transverse splitting cracks formed in the concrete. These cracks extended upon further loading, and additional cracks formed emanating radially from the duct. The bar yielded at a load of 92 kips, and Figure 7.1 shows the crack pattern at this point. Crack widths were less than 0.010″.

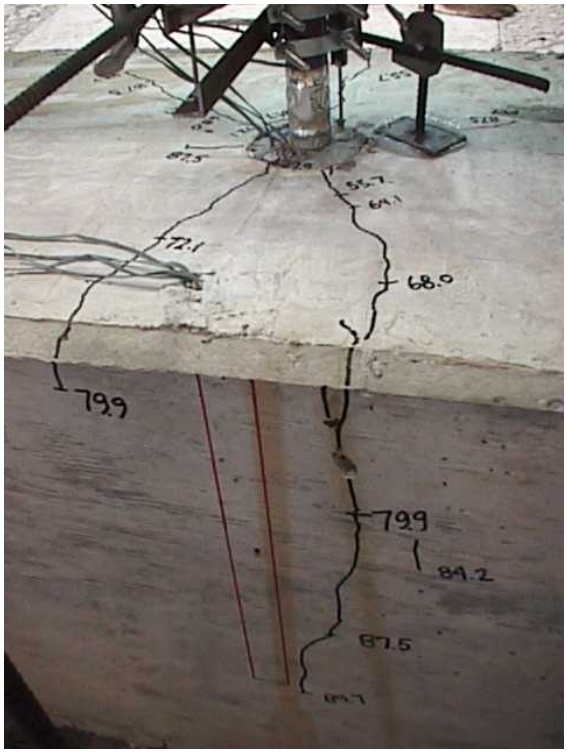

Figure 7.1: GVD03 Crack Pattern at Bar Yield

Further loading opened up existing cracks, some of which turned to form horizontal cracks on the side of the specimen. The surface of the grout lifted noticeably and the concrete immediately surrounding the duct spalled off. Figure 7.2 is a photograph of the top of the duct. The bar was loaded up to 120 kips, at which point the test was terminated to prevent bar fracture. Figure 7.3 shows the crack pattern at peak load.

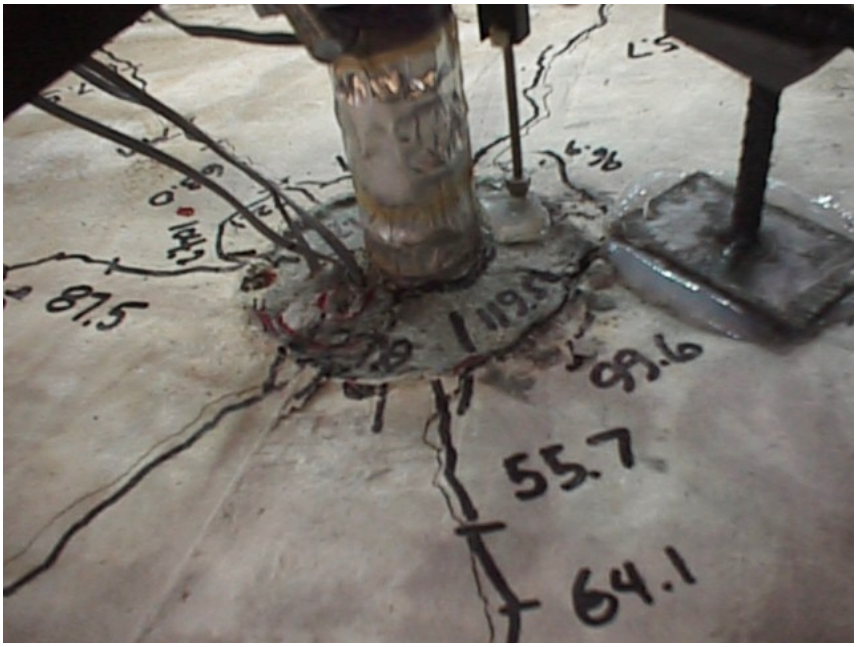

Figure 7.2: GVD03 Cracking at Top of Grout

The applied load-bar slip response of GVD03 is shown in Figure 7.4. The anchorage remained relatively stiff up to the yield point, and then the response was driven by yielding of the bar. Slip of the tail of the bar showed that anchorage slip also contributed to the total lead bar slip in the post-yield range.

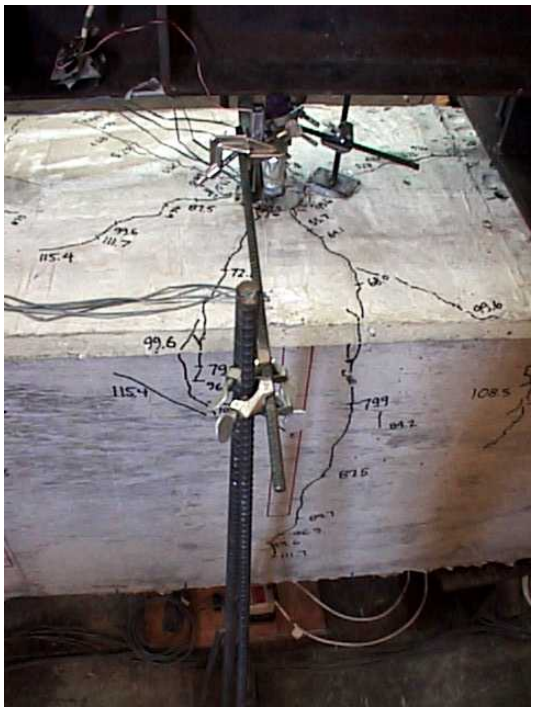

Figure 7.3: GVD03 Cracking at Peak Load

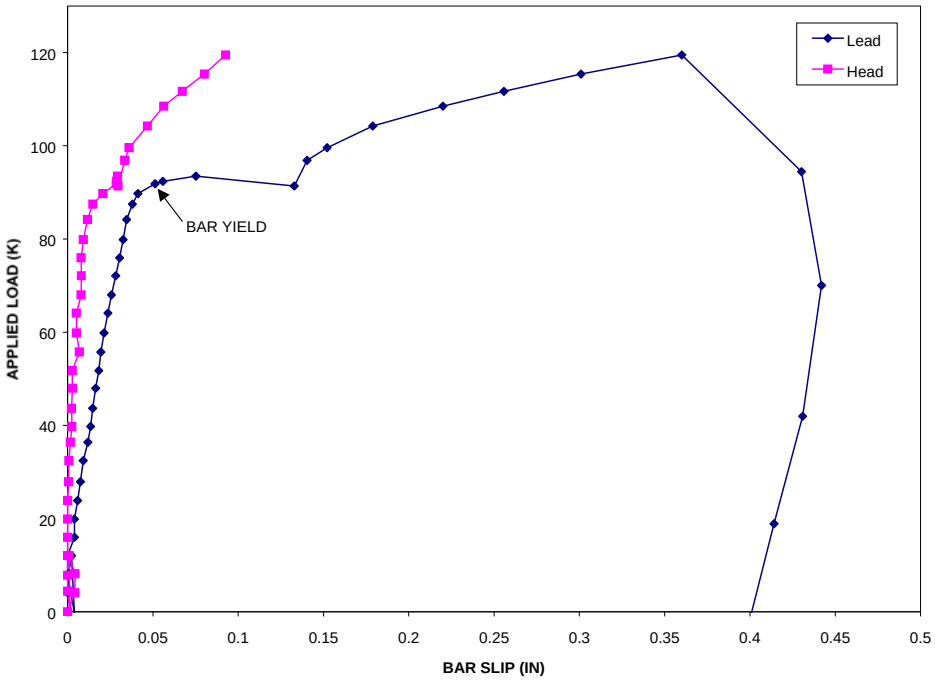

Figure 7.4: GVD03 Applied Load-Bar Slip Response

The cracks observed radiating from the duct were similar to splitting cracks of a bar being pulled out of plain concrete. This suggests that as vertical load was transferred to the duct through the grout, pullout forces on the duct caused splitting cracks to form in the concrete. At the same time, splitting stresses produced by the test bar were confined and restrained by the duct. Thus, as splitting cracks in the concrete widened, the concrete allowed the duct to expand, resulting in a loss of confinement to the grouted bar and slip of the grout. This effect can be seen in the plot of duct strains shown in Figure 7.5. At a load of approximately 88 kips, the circumferential duct strains expanded rapidly, likely due to loss of confinement from the concrete. This corresponds with widespread observed crack extension and formation at 88 kips. The duct expansion allowed

the grout to slip out of the duct. Figure 7.6 shows that slip of the grout from the duct began to increase rapidly at the load corresponding to duct expansion.

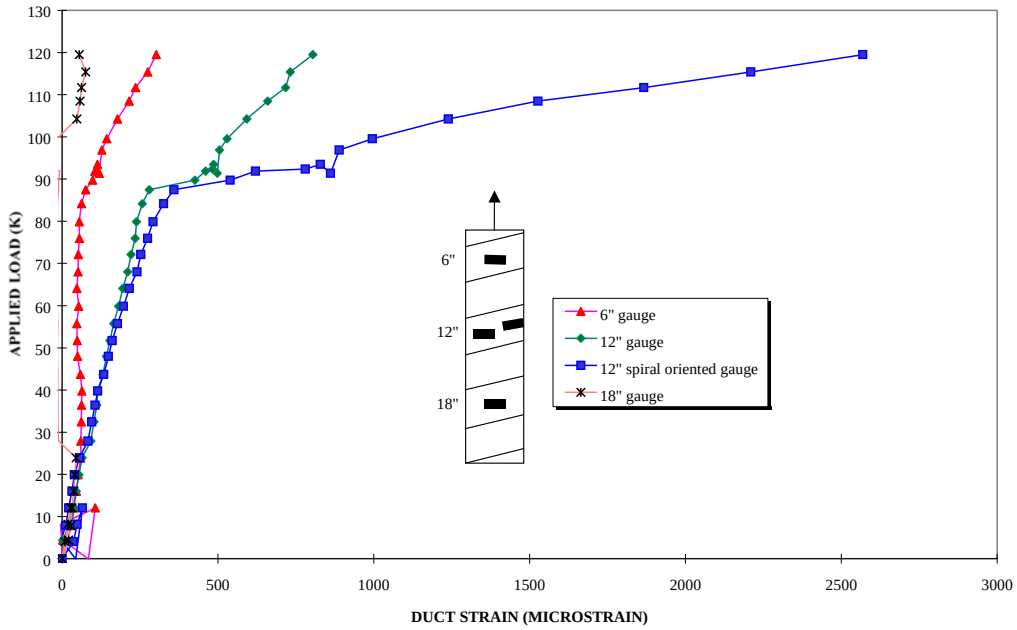

Figure 7.5: GVD03 Duct Strains

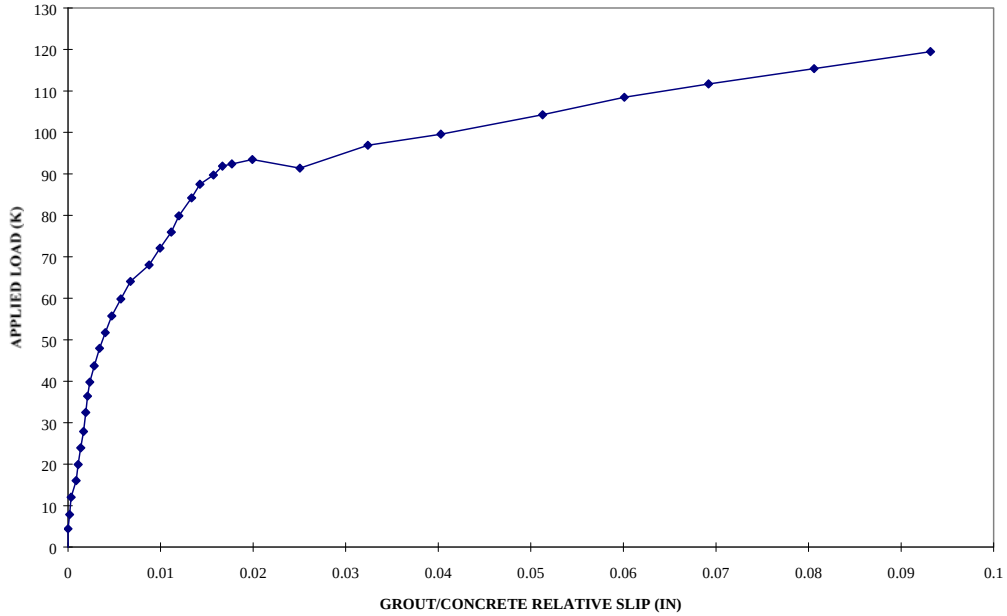

Figure 7.6: GVD03 Grout Slip

The expansion mechanism for the duct is quite complex due to the spiral construction of the duct. The strain gauge oriented parallel to the duct spiral at 12″ yielded the maximum strains, suggesting that the duct expanded by slipping at the seams. It is difficult to determine a duct "strength", and the strain readings reported here should be considered a qualitative measure of duct expansion.

7.3 EFFECT OF EMBEDMENT DEPTH

As discussed above, the strength of a grouted duct anchorage is dependent on the confinement effects of the duct and concrete to resist the splitting forces from the bar. If a bar is embedded deeply, the splitting forces will be well distributed along the length of the bar and the radial confinement demands will be small. Small embedments will require large amounts of confinement.

Tests were conducted at embedment depths of 12, 18, and 24 inches. For straight bars, the 12″ embedment test resulted in a grout pullout failure as described above at a load of 76 kips. Aside from GVD04, the remaining tests at embedments of 18 and 24 inches reached loads well past yield and were terminated due to load limitations in the test setup. Figure 7.7 compares the load-deformation behavior of #11 bars grouted in Masterflow 928 at embedments of 12, 18, and 24 inches. The 12" anchorage failed at a small bar slip due to the large confinement demands over a short duct length. Comparing the head deflections of GVD03 and GVD07, the 24″ embedment of GVD07 was, as expected, stiffer. However, crack widths and bar slips were small at service load levels (<60 kips) for both cases.

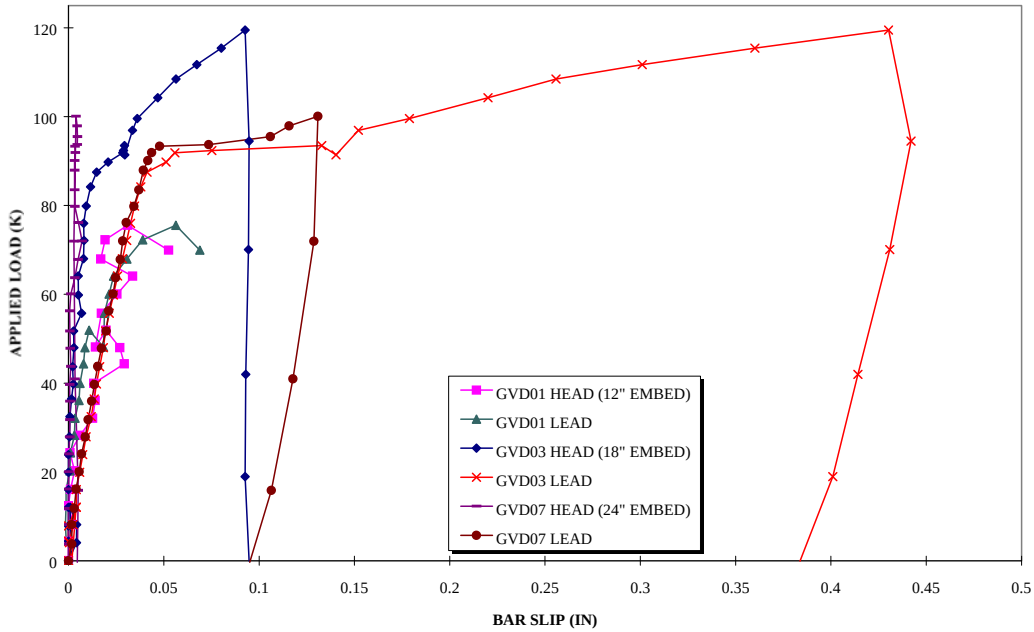

Figure 7.7: Straight Bar Load-Deformation Comparison for h_{ef} = 12, 18, and 24 in.

7.4 EFFECT OF GROUT STRENGTH AND TYPE

Each 18″ embedment test except for GVD04 provided sufficient strength to permit loading the bar well into the strain hardening range. During the grouting procedure, the Euclid Hi-Flow mix used for GVD04 required additional water to be added to the mix in order to achieve acceptable grout fluidity. Ten percent additional water was added, resulting in grout cube strengths of approximately 3 ksi, compared with the strengths between 4.5 and 5.5 ksi for the other 18″ embedment tests. GVD04 formed a grout pullout failure at a load of 94 kips.

Figure 7.8 compares the load-deformation behavior of the 18″ embedment tests with the three different grouts. Though the grout strengths of GVD03 and GVD05 differed by 1 ksi, the behavior was almost identical. However, for

GVD04, which had a significantly lower grout strength, pullout controlled at approximately the yield load of the bar. Lower grout strength implies lower grout stiffness, which results in greater dilation of the grout at a given load and earlier loading of the duct and surrounding concrete. Figure 7.9 shows the increase in duct strains in GVD04 compared with GVD03. This suggests that there should be a minimum grout strength to prevent premature loading of the duct.

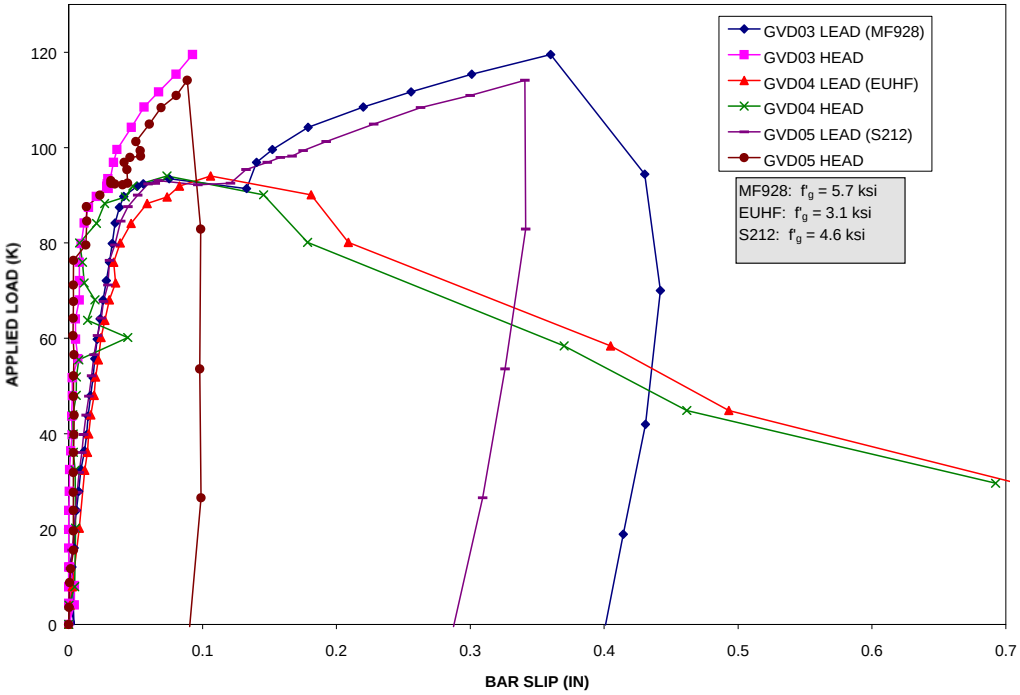

Figure 7.8: GVD Load-Bar Slip Response for Various Grout Types

To ensure that the difference in behavior was not due to the grout type, tests were conducted for an embedment of 24″ to compare Masterflow 928 and Euclid Hi-Flow grouts with the same compressive strength. As summarized in Table 7.1, GVD07 and GVD08 both developed loads in the strain-hardening region before the tests were terminated. Behavior of the two tests was similar.

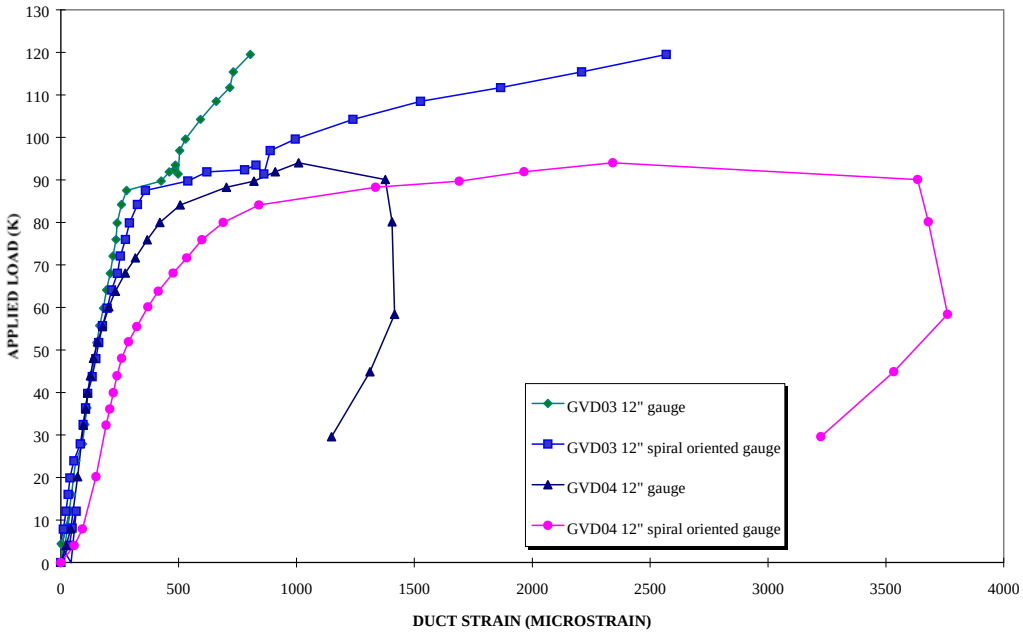

Figure 7.9: Duct Strain Increase in GVD04 Compared with GVD03

7.5 UPSET-HEADED VS. STRAIGHT BAR TESTS

Grouted vertical ducts will typically extend the full depth of a bent cap (28 to 42″), leaving sufficient distance to develop a straight bar as discussed above. However, for cases such as inverted-T caps, reinforcement congestion in the connection region may require shorter duct lengths. For this case, upset-headed bars may be appropriate. Tests of upset-headed bars at embedments of 12 and 18 inches were conducted.

Figure 7.10 compares the load-bar slip response of a straight bar (GVD01) and an upset-headed bar (GVD02) for a 12″ embedment. Both tests resulted in a grout pullout failure, though the headed bar reached a 20% higher load at failure. However, a slip of almost 0.2″ was required to develop the peak load for GVD02. The general behavior of the two anchorages was similar up to the failure load for

the straight bar. The upset-headed anchorage then produced cracks similar to those observed for a breakout cone, and failed as the cracks opened and the grout slipped. Figure 7.11 shows the crack pattern for GVD02 near failure.

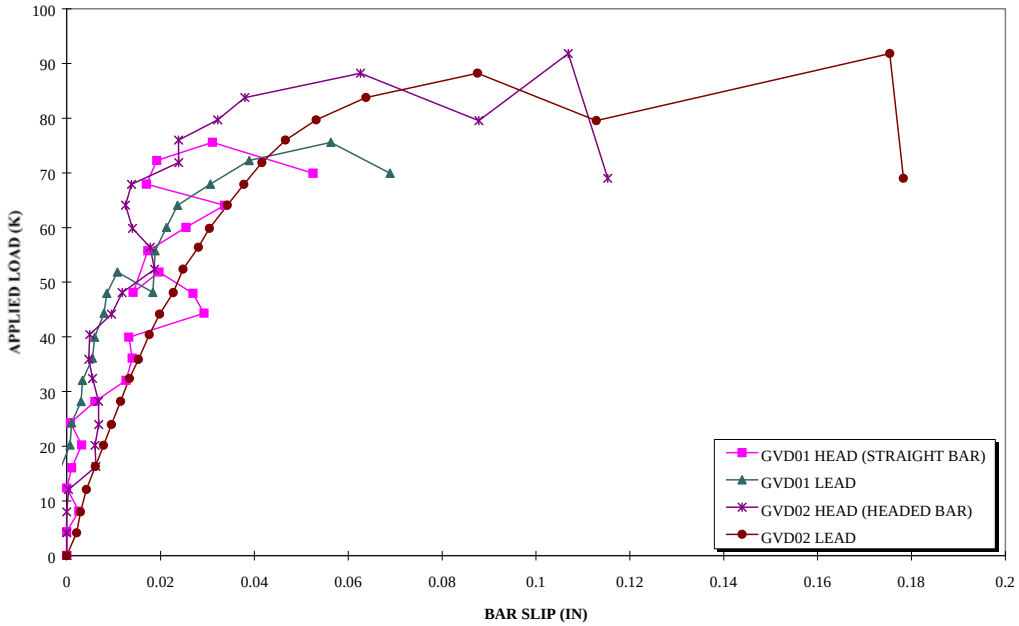

Figure 7.10: Load-Bar Slip Response for Straight and Upset-Headed Bars at h_{ef} = 12″

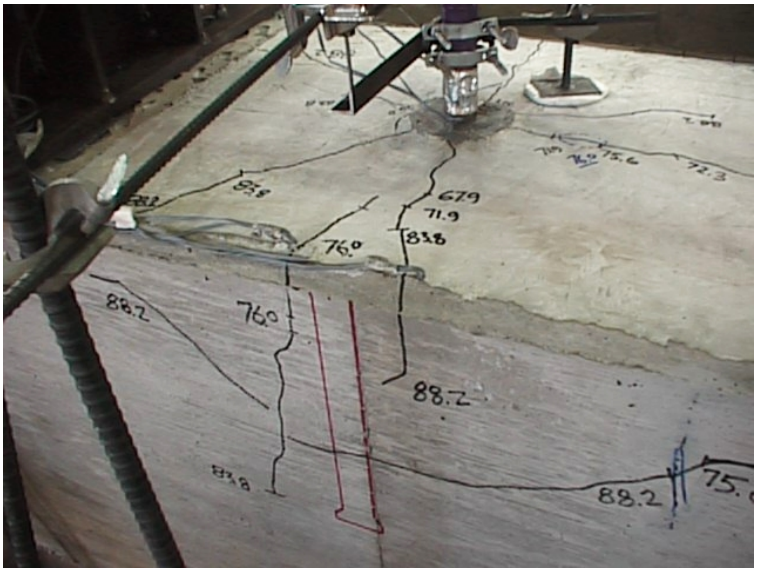

Figure 7.11: GVD02 Cracking at Failure Load

As expected for a short embedment depth, the upset head in GVD02 resisted a large percentage of the applied force. Figure 7.12 shows the bar force distribution. For the majority of the loading history, the head resisted a linearly increasing amount of load.

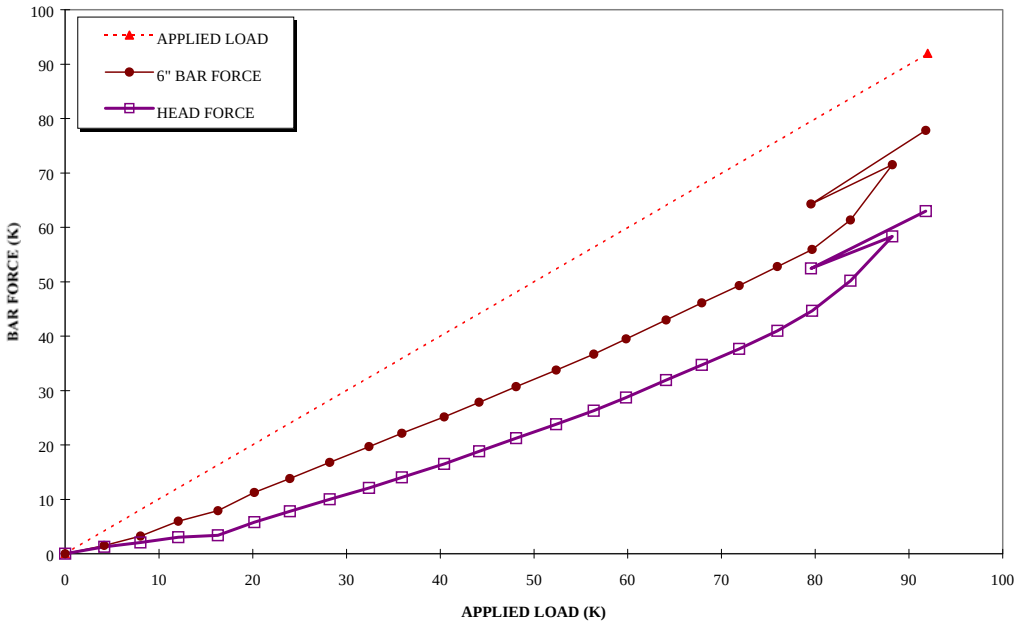

Figure 7.12: GVD02 Bar Force Distribution

Because an 18″ embedment produced acceptable behavior for a straight bar anchorage, provided the grout strength was sufficient, headed bars are not utilized completely and are not necessary at this embedment. Figure 7.13 compares the bar force distribution for straight (GVD03) and upset-headed (GVD06) 18″ embedments. Though the upset head resisted a small amount of force, it did not alter appreciably the distribution of force over the bar length. Therefore, the splitting forces along the duct were similar to those for a straight bar.

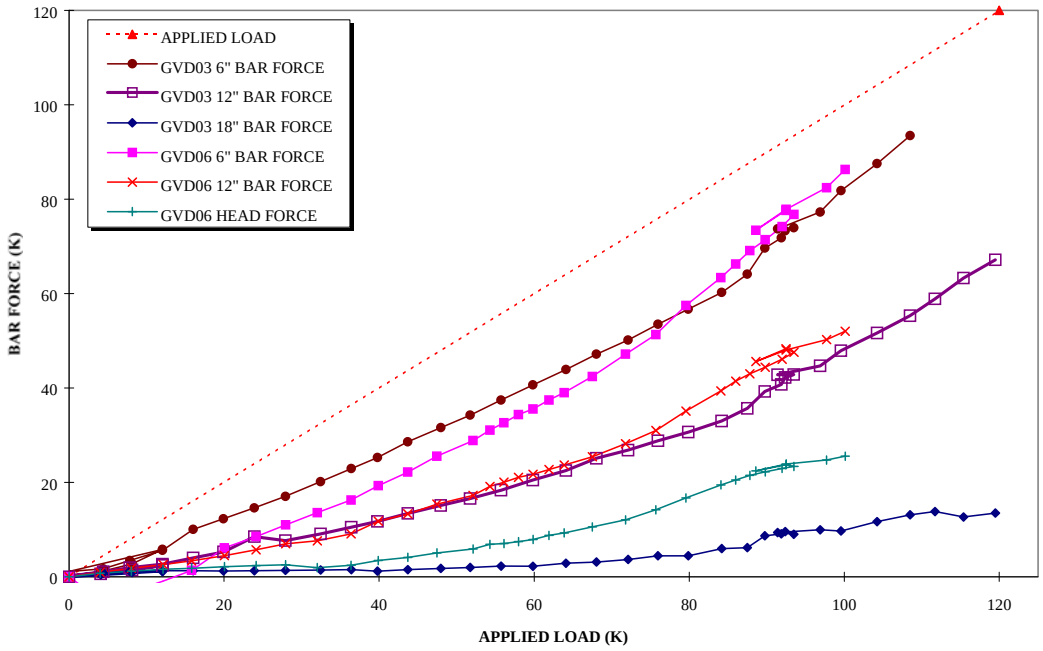

Figure 7.13: Bar Force Distribution for 18″ Embedment With and Without Upset Head

7.6 CONCLUSIONS

Straight bar anchorages in grouted vertical ducts were found to develop bars over much shorter lengths than bars embedded in concrete. Confinement provided by the duct and surrounding concrete enhanced anchorage behavior. The anchorages failed as a result of duct expansion due to loss of concrete restraint. The grout slipped out of the duct as the surrounding cracked concrete dilated.

Low grout strength was found to significantly reduce anchorage capacity. The loss of grout integrity for low strength grout suggests that a minimum grout strength be provided to ensure that duct/concrete dilation controls the anchorage strength.

Upset-headed bars were found to provide additional capacity over straight bars for short embedments, though the anchorage required large bar slips to achieve the strength. At deeper embedments the bar head did not provide additional capacity. A straight bar will provide adequate anchorage and superior economy for deeper embedment depths.

CHAPTER 8

COMPARISON OF GROUT POCKET PULLOUT STRENGTHS WITH EXISTING DESIGN METHODS

8.1 INTRODUCTION

The scope of this research was limited to investigating the major variables affecting selected precast connection anchorage configurations. The limited number of tests precludes development of a new independent design model to predict grout pocket capacities. However, simple modifications to existing anchorage design methods based on observed test behavior may provide useful guidelines for designing anchorages in precast bent cap connections.

Single and double line grout pocket tests of upset-headed bars are easily analyzed by the Concrete Capacity Design (CCD) method described in Chapter 3. This chapter compares the headed bar test results to capacities given by the CCD method. Because the CCD method is based on headed anchor tests in cast-in-place concrete, modifications based on the observed behavior of the grout pocket tests may be required.

The few straight bar grout pocket tests are analyzed using the equations presented in Chapter 3. Modifications to the transverse reinforcement confinement factor may be useful way for accounting for the wedging action of the grout in the pocket during testing.

8.2 CCD METHOD ANALYSIS OF SLGP AND DLGP HEADED BAR TESTS

Sixteen single and double line grout pocket headed bar tests resulted in concrete breakout failures of either single bars or bar groups. This includes tests in which the concrete breakout failure occurred after the test bar yielded. Research conducted by DeVries [8] on headed bars determined that bar yielding had no effect on concrete breakout capacity. The headed bar tests will be analyzed with the CCD method described in Section 3.2.2.

In applying the CCD method to grout pocket anchorages, several issues are not clear. For example, should the concrete or grout compressive strength be used in Equation 3-2? Does the shape of the pocket affect the edge disturbance factor Ψ_1? Is the corner cracking effect on the tensile stress fields adequately accounted for in the CCD adjustment factor for cracking at service load levels? The following sections will attempt to answer these questions by systematic modification of the CCD method and comparing the resulting capacities to the observed test capacities.

8.2.1 Basic CCD Predicted Anchorage Capacities

Table 8.1 summarizes the basic breakout capacities predicted by the CCD method, and the results are plotted against the measured test capacities in Figure 8.1. The basic CCD breakout capacity will be referred to as P_1. P_1 is calculated from Equations 3-2, 3-3, and 3-4 using k=40, the compressive strength of the concrete, and the uncracked modification factor of 1.25. The following illustrates calculation of P_1 for SL03:

Table 8.1: Basic CCD Breakout Capacities, P_1

Test ID	#Bars	h_{ef} in	f'_c ksi	f'_g ksi	P_{test} kips/bar	A_N in^2	A_{N0} in^2	C_1 in	$1.5h_{ef}$ in	Ψ_1	k	Ψ_2	P_1 kips/bar	P_{test}/P_1
SL01	1	6	5.3	6.9	36	324	324	12	9	1.00	40	1.25	53	0.67
SL02	1	6	5.3	6.4	37	324	324	12	9	1.00	40	1.25	53	0.69
SL03	1	12	5.3	6.5	60	864	1296	12	18	0.90	40	1.25	91	0.66
SL04	1	12	5.3	6.3	61	864	1296	12	18	0.90	40	1.25	91	0.67
SL05	1	9	6.3	7.0	46	648	729	12	13.5	0.97	40	1.25	92	0.50
SL06	1	9	6.3	7.1	45	648	729	12	13.5	0.97	40	1.25	92	0.49
SL09	1	4	5.5	7.4	21	144	144	12	6	1.00	40	1.25	30	0.71
SL11	1	6	5.2	6.9	34	324	324	12	9	1.00	40	1.25	53	0.64
SL15	2	12	5.0	5.3	31	1056	1296	12	18	0.90	40	1.25	54	0.58
SL16	2	12	5.0	0.0	39	1056	1296	12	18	0.90	40	1.25	54	0.72
SL17	2	12	5.1	6.2	48	1056	1296	12	18	0.90	40	1.25	54	0.88
SL18	2	12	5.1	5.6	50	1056	1296	12	18	0.90	40	1.25	54	0.92
DL01	2	6	5.1	4.2	24	432	324	8	9	0.97	40	1.25	34	0.71
DL02	2	6	5.1	5.9	20	442	324	8	9	0.97	40	1.25	35	0.58
DL03	2	6	5.6	6.0	22	442	324	8	9	0.97	40	1.25	36	0.61
DL04	2	6	5.6	5.4	24	442	324	8	9	0.97	40	1.25	36	0.66
													average:	**0.67**
													std dev:	**0.11**

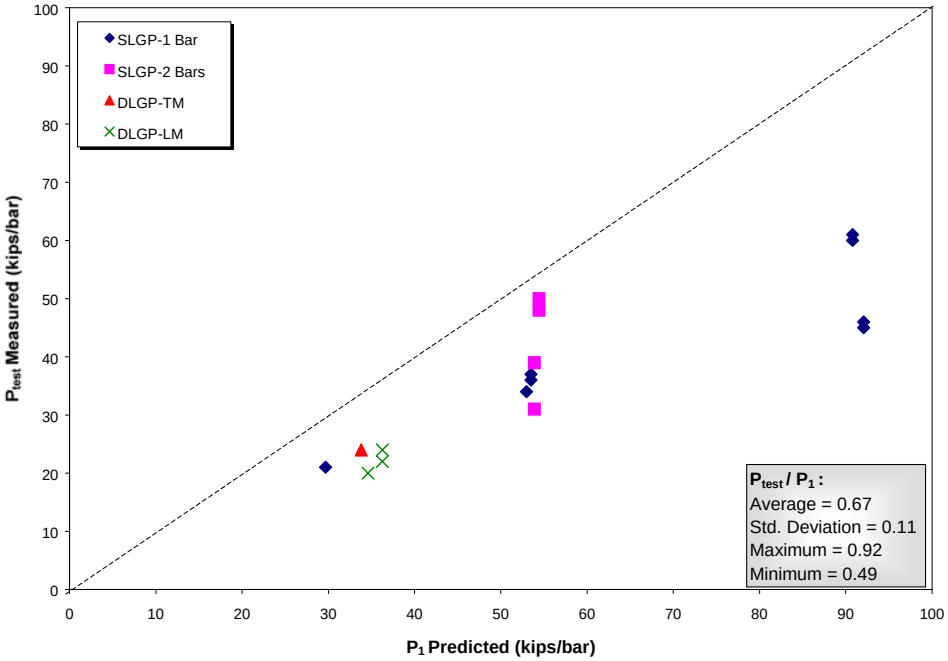

Figure 8.1: Comparison of P_1 Capacities with Test Results

SL03: test failure load = P_{test} = 60 kips

h_{ef} = 12″

f'_c = concrete cylinder strength = 5.3 ksi on test day

from Equations 3-2 and 3-3:

$$P_1 = \frac{A_N}{A_{N0}} \Psi_1 \Psi_2 k \sqrt{f'_c} h_{ef}^{1.5}$$

The available breakout surface area A_N is shown in Figure 8.2:

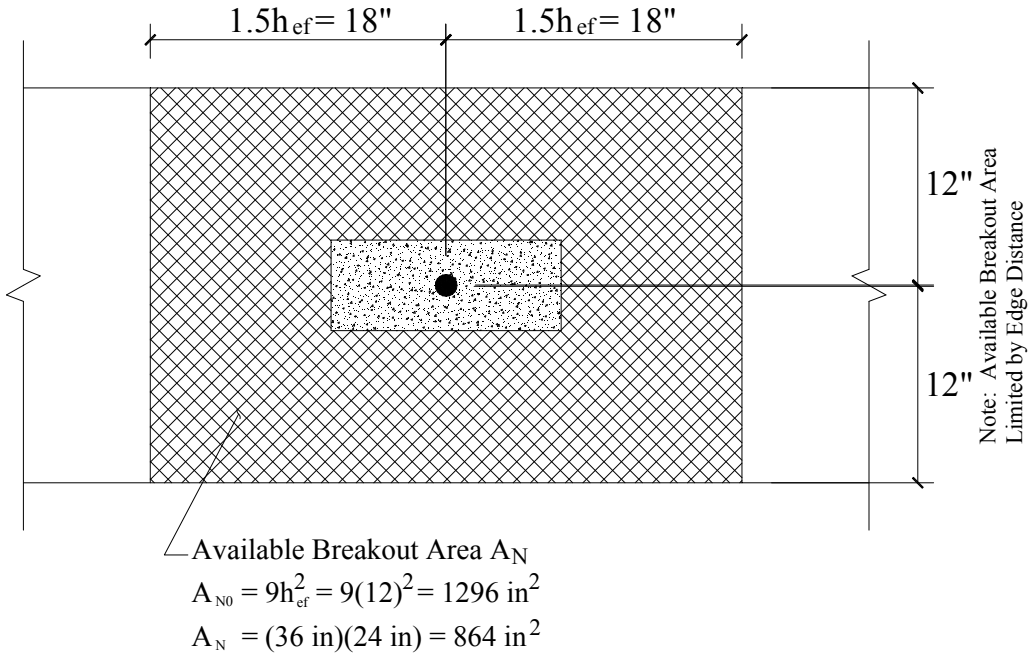

Figure 8.2: Available Breakout Area A_N for SL03

Since the edge is closer than $1.5h_{ef}$ = 18″ to the bar, the edge disturbance factor Ψ_1 applies:

C_1 = 12″

Equation 3-4: $\Psi_1 = 0.7 + 0.3\left(\frac{12}{18}\right) = 0.90$

Ψ_2 = 1.25 assuming no cracking at service loads

k = 40 for best-fit analysis

giving: $P_1 = \frac{864}{1296}(0.90)(1.25)40\sqrt{5300\,psi}(12'')^{1.5} = 90{,}788\ lb. \approx 91\ kips$

The basic breakout capacities summarized in Table 8.1 show that the CCD method without any adjustment factors is very unconservative and inaccurately predicts grout pocket breakout strengths. The most obvious reason for the discrepancy is the service load cracking factor Ψ_2. In all of the tests cracks, which would break up the tensile stress fields, were observed at service load levels ($\approx 0.6P_y$). Both splitting and pocket corner cracks occurred at service levels, and should be accounted for when calculating anchorage capacities.

Table 8.2 summarizes the CCD breakout capacities computed using Ψ_2=1.0, the basic CCD capacity for concrete cracked at service load levels. The results are plotted versus the measured test capacities in Figure 8.3. These capacities will be referred to as P_2. For SL03, P_2 can easily be found from P_1 as:

$$P_2 = \frac{P_1}{1.25} = \frac{91}{1.25} = 73\ kips$$

The P_2 results come much closer to the test results, giving an average P_{test}/P_2 of 0.84. However, the results are still unconservative, suggesting that the extent of cracking caused by the grout pocket corners may warrant an adjustment of the Ψ_2 factor.

Table 8.2: Basic CCD Breakout Capacities in Cracked Concrete, P_2

Test ID	#Bars	h_{ef} in	f'_c ksi	f'_g ksi	P_{test} kips/bar	A_N in^2	A_{N0} in^2	C_1 in	$1.5h_{ef}$ in	Ψ_1	k	Ψ_2	P_2 kips/bar	P_{test}/P_2
SL01	1	6	5.3	6.9	36	324	324	12	9	1.00	40	1.0	43	0.84
SL02	1	6	5.3	6.4	37	324	324	12	9	1.00	40	1.0	43	0.86
SL03	1	12	5.3	6.5	60	864	1296	12	18	0.90	40	1.0	73	0.83
SL04	1	12	5.3	6.3	61	864	1296	12	18	0.90	40	1.0	73	0.84
SL05	1	9	6.3	7.0	46	648	729	12	13.5	0.97	40	1.0	74	0.62
SL06	1	9	6.3	7.1	45	648	729	12	13.5	0.97	40	1.0	74	0.61
SL09	1	4	5.5	7.4	21	144	144	12	6	1.00	40	1.0	24	0.88
SL11	1	6	5.2	6.9	34	324	324	12	9	1.00	40	1.0	42	0.80
SL15	2	12	5.0	5.3	31	1056	1296	12	18	0.90	40	1.0	43	0.72
SL16	2	12	5.0	0.0	39	1056	1296	12	18	0.90	40	1.0	43	0.90
SL17	2	12	5.1	6.2	48	1056	1296	12	18	0.90	40	1.0	44	1.10
SL18	2	12	5.1	5.6	50	1056	1296	12	18	0.90	40	1.0	44	1.15
DL01	2	6	5.1	4.2	24	432	324	8	9	0.97	40	1.0	27	0.89
DL02	2	6	5.1	5.9	20	442	324	8	9	0.97	40	1.0	28	0.72
DL03	2	6	5.6	6.0	22	442	324	8	9	0.97	40	1.0	29	0.76
DL04	2	6	5.6	5.4	24	442	324	8	9	0.97	40	1.0	29	0.83
													average:	**0.84**
													std dev:	**0.14**

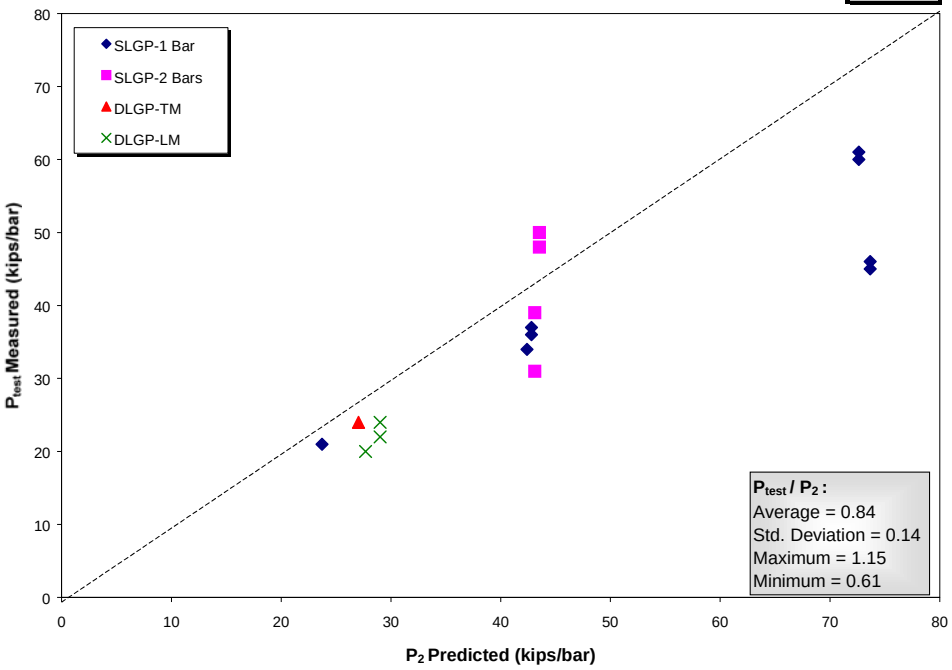

Figure 8.3: Comparison of P_2 Capacities with Test Results

The grout compressive strengths in the grout pocket tests (summarized in Tables 5.1 and 6.1) are greater than the concrete compressive strengths for all but two cases. All else being equal, if the compressive strength of the grout is used in Equation 3-2 in the place of f'_c the resulting capacities will be greater than P_1 (with $\Psi_2 = 1.25$) and P_2 (with $\Psi_2 = 1.0$). Because the P_1 and P_2 methods overestimate test capacities, using the grout compressive strength in the CCD method produces worse estimations of test capacity than using the concrete compressive strength.

8.2.2 Adjustments to the CCD Method for Grout Pocket Anchorages

8.2.2.1 Correction for Pocket Induced Cracking and Pocket Shape

As described in Chapters 5 and 6, corner cracks formed in loaded single or double line grout pockets. The cracking adjustment factor Ψ_1 of the CCD method accounts for flexural type cracks, which would typically break the anchorage forces into two tensile stress fields. However, grout pocket corner cracks can separate the anchorage forces into three and four tensile stress fields (see Figures 5.17 and 6.6). Therefore, it is logical to use a cracking factor Ψ_2 less than 1.0 for grout pocket anchorage design.

Based on statistical analysis of the test results, it is proposed that a Ψ_2 factor of 0.75 be used in design of all grout pocket anchorages. Table 8.3 summarizes the CCD capacities using $\Psi_2 = 0.75$, referred to as P_3 capacities. Figure 8.4 compares the P_3 capacities to the test results. The P_3 method fit the test data well, and is generally conservative. The average P_{test}/P_3 is 1.11, with a standard deviation of 0.19.

Table 8.3: CCD Capacities Modified for Grout Pocket Cracking, P_3

Test ID	#Bars	h_{ef} in	f'_c ksi	f'_g ksi	P_{test} kips/bar	A_N in^2	A_{N0} in^2	C_1 in	$1.5h_{ef}$ in	Ψ_1	k	Ψ_2	P_3 kips/bar	P_{test}/P_3
SL01	1	6	5.3	6.9	36	324	324	12	9	1.00	40	0.75	32	1.12
SL02	1	6	5.3	6.4	37	324	324	12	9	1.00	40	0.75	32	1.15
SL03	1	12	5.3	6.5	60	864	1296	12	18	0.90	40	0.75	54	1.10
SL04	1	12	5.3	6.3	61	864	1296	12	18	0.90	40	0.75	54	1.12
SL05	1	9	6.3	7.0	46	648	729	12	13.5	0.97	40	0.75	55	0.83
SL06	1	9	6.3	7.1	45	648	729	12	13.5	0.97	40	0.75	55	0.81
SL09	1	4	5.5	7.4	21	144	144	12	6	1.00	40	0.75	18	1.18
SL11	1	6	5.2	6.9	34	324	324	12	9	1.00	40	0.75	32	1.07
SL15	2	12	5.0	5.3	31	1056	1296	12	18	0.90	40	0.75	32	0.96
SL16	2	12	5.0	0.0	39	1056	1296	12	18	0.90	40	0.75	32	1.21
SL17	2	12	5.1	6.2	48	1056	1296	12	18	0.90	40	0.75	33	1.47
SL18	2	12	5.1	5.6	50	1056	1296	12	18	0.90	40	0.75	33	1.53
DL01	2	6	5.1	4.2	24	432	324	8	9	0.97	40	0.75	20	1.18
DL02	2	6	5.1	5.9	20	442	324	8	9	0.97	40	0.75	21	0.96
DL03	2	6	5.6	6.0	22	442	324	8	9	0.97	40	0.75	22	1.01
DL04	2	6	5.6	5.4	24	442	324	8	9	0.97	40	0.75	22	1.10
													average:	**1.11**
													std dev:	**0.19**

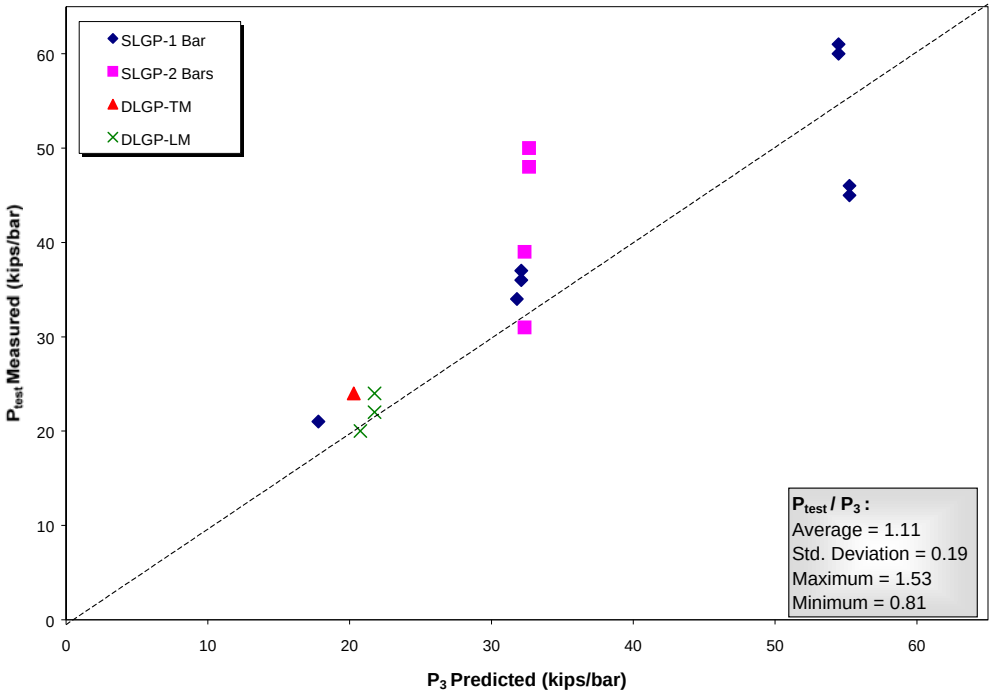

Figure 8.4: Comparison of P_3 Capacities with Test Results

The only tests for which the P_3 method is significantly unconservative are SL05 and SL06, tests of a #8 upset-headed bar at $h_{ef} = 9''$. The average P_{test}/P_3 for these tests is 0.82. This can be explained in part due to the influence of the pocket shape on the edge effect. At an embedment of 9″, the edge effect on the CCD breakout capacity is small for a single line specimen, giving a $\Psi_1 = 0.97$. However, the wedging action of the single line grout pocket shape directs forces to the bent cap specimen edges, as described in Section 6.2.1. Because the CCD edge effects are small for a 9″ embedment, the amplification of edge breakout forces due to pocket wedging are not accounted for. For deeper grout pocket embedments, the CCD method appears to adequately model edge effects.

Because the only data that exhibited this effect are for SL05 and SL06, edge force amplification may be considered part of the scatter. The design equations described in Section 8.2.3, along with load and resistance factors, should provide a sufficiently conservative design.

8.2.2.2 Correction for Grout and Concrete Strengths

The issue of whether to use the concrete or grout compressive strength can be resolved by using a weighted average compressive strength. A rational method for averaging the strengths is weighting the grout and concrete strengths based on the percentage of each in A_N . The resulting compressive strength, $f'_{c,mod}$, is given by Equations 8-1 and 8-2:

$$f'_{c,\mathrm{mod}} = \frac{f'_c A_c + f'_g A_g}{A_N} \qquad \textit{(Equation 8-1)}$$

$$A_N = A_c + A_g \qquad \textit{(Equation 8-2)}$$

where: A_c = area of concrete in projected breakout surface A_N

A_g = area of grout in projected breakout surface A_N

Figure 8.5 shows the areas A_c and A_g for SL03. The modified compressive strength is given by Equation 8-1:

$$f'_{c,\mathrm{mod}} = \frac{(5.3\ ksi)(787\ in^2) + (6.4\ ksi)(77\ in^2)}{864\ in^2} = 5.4\ ksi$$

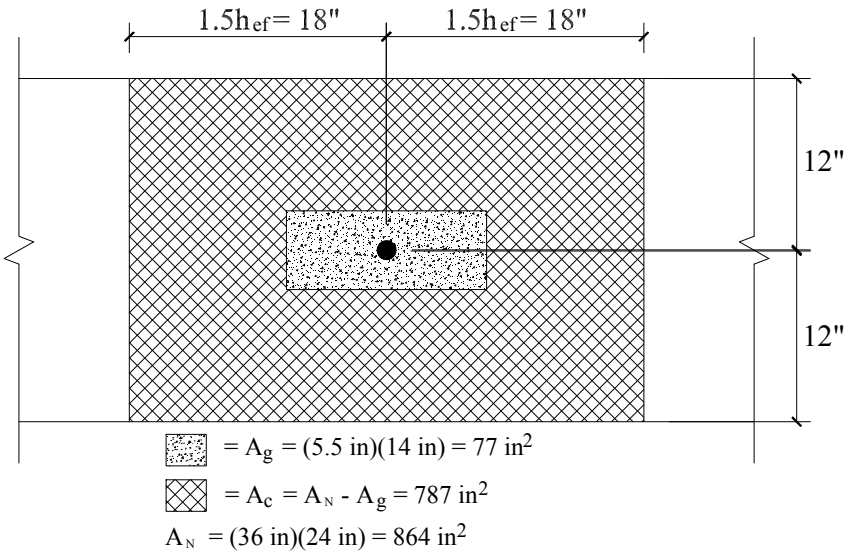

Figure 8.5: A_g and A_c for SL03

Table 8.4 summarizes the CCD capacities P_4, which use $f'_{c,mod}$ and the cracking factor Ψ_2 = 0.75. The results are plotted in Figure 8.6 against the measured test capacities. For SL03, P_4 is given by:

$$P_4 = \frac{864}{1296}(0.90)(0.75)40\sqrt{5400\ psi}(12'')^{1.5} = 54{,}984\ lb. \approx 55\ kips$$

The results shown in Table 8.4 predict the test capacities only slightly better than simply using the concrete compressive strength. In most cases the difference is minimal because A_g is much smaller than A_c. Calculation of $f'_{c,mod}$ should be performed in cases where h_{ef} is small or the difference between grout and concrete

strength is large. However, in most cases it is sufficient to simply use f'_c in Equation 3-2.

Table 8.4: CCD Capacities Using Modified Compressive Strength, P_4

Test ID	#Bars	h_{ef} in	f'_c ksi	f'_g ksi	P_{test} kips/bar	k	Ψ_2	A_g in^2	A_c in^2	$f'_{c,mod}$ ksi	P_4 kips/bar	P_{test}/P_4
SL01	1	6	5.3	6.9	36	40	0.75	77	247	5.7	33	1.08
SL02	1	6	5.3	6.4	37	40	0.75	77	247	5.6	33	1.13
SL03	1	12	5.3	6.5	60	40	0.75	77	787	5.4	55	1.09
SL04	1	12	5.3	6.3	61	40	0.75	77	787	5.4	55	1.11
SL05	1	9	6.3	7.0	46	40	0.75	77	571	6.4	56	0.83
SL06	1	9	6.3	7.1	45	40	0.75	77	571	6.4	56	0.81
SL09	1	4	5.5	7.4	21	40	0.75	77	67	6.5	19	1.08
SL11	1	6	5.2	6.9	34	40	0.75	77	247	5.6	33	1.03
SL15	2	12	5.0	5.3	31	40	0.75	77	979	5.0	32	0.96
SL16	2	12	5.0	0.0	39	40	0.75	0	1056	5.0	32	1.21
SL17	2	12	5.1	6.2	48	40	0.75	77	979	5.2	33	1.46
SL18	2	12	5.1	5.6	50	40	0.75	77	979	5.1	33	1.53
DL01	2	6	5.1	4.2	24	40	0.75	55	377	5.0	20	1.20
DL02	2	6	5.1	5.9	20	40	0.75	57	385	5.2	21	0.95
DL03	2	6	5.6	6.0	22	40	0.75	57	385	5.7	22	1.01
DL04	2	6	5.6	5.4	24	40	0.75	57	385	5.6	22	1.11
											average:	**1.10**
											std dev:	**0.19**

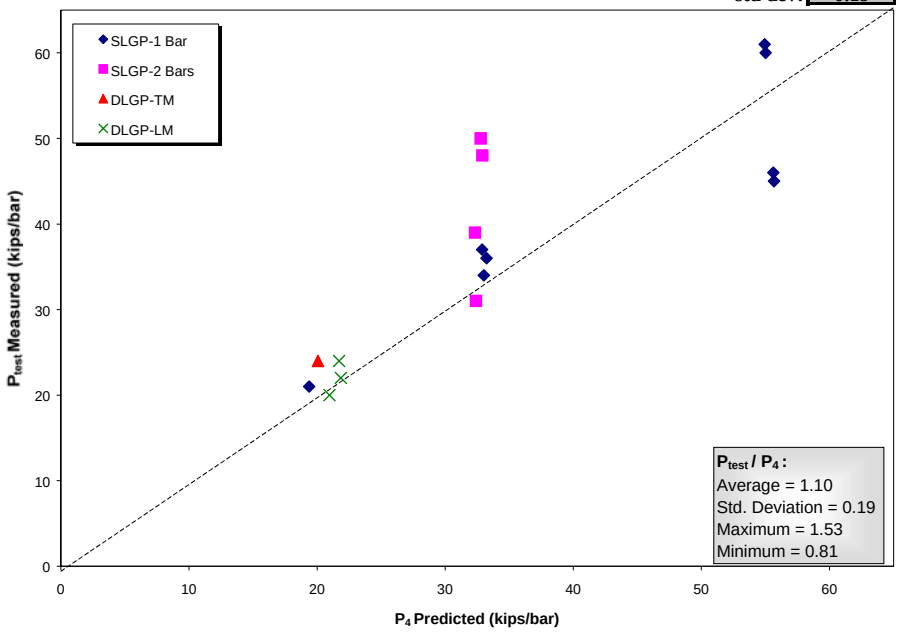

Figure 8.6: Comparison of P_4 Capacities with Test Results

8.2.3 Anchorage Design Equations and Recommendations

The CCD method was used earlier to obtain best-fit predictions of the grout pocket test data. For design, equations consistent with ACI Code proposed CB-30 [13] should be used with the modification factors determined in the previous section. For embedments less than 11 inches, the factor k is taken as 24 to provide a 5% fractile strength, and for embedments greater than 11 inches, k is 16. The following ACI CB-30 equation applies to embedments greater than 11″:

$$P = \frac{A_N}{A_{N0}} \Psi_1 \Psi_2 k \sqrt{f'_c} h_{ef}^{(5/3)} \qquad \textit{(Equation 8-3)}$$

The cracking factor $\Psi_2 = 0.75$ should always be applied in grout pocket anchorage design. The compressive strength used in design may generally be taken as f'_c, though $f'_{c,mod}$ may need to be used in cases of short embedment or large compressive strength difference. Table 8.5 summarizes the design capacities P_5 computed using the design equations and the concrete compressive strength. Results are plotted in Figure 8.7 against the measured test capacities. The average P_{test}/P_5 ratio is 1.85. Table 8.6 summarizes the design capacities P_6 computed using $f'_{c,mod}$ for the compressive strength. The results are plotted in Figure 8.8. The P_6 method gives an average P_{test}/P_6 ratio of 1.82. As an example, the SL03 design capacities are calculated as follows:

$$P_5 = \frac{864}{1296}(0.90)(0.75)16\sqrt{5300\ psi}(12'')^{(5/3)} = 32{,}969\ lb. \approx 33\ kips$$

$$P_6 = \frac{864}{1296}(0.90)(0.75)16\sqrt{5400\ psi}(12'')^{(5/3)} = 33{,}278\ lb. \approx 33\ kips$$

For actual design, a ϕ factor equal to 0.85, as recommended in the CB-30 proposal, should be applied to the above capacities.

Table 8.5: Design CCD Capacities Using f'_c, P_5

Test ID	#Bars	h_{ef} in	f'_c ksi	f'_g ksi	P_{test} kips/bar	Ψ_2	k	P_5 kips/bar	P_{test}/P_5
SL01	1	6	5.3	6.9	36	0.75	24	19	1.87
SL02	1	6	5.3	6.4	37	0.75	24	19	1.92
SL03	1	12	5.3	6.5	60	0.75	16	33	1.82
SL04	1	12	5.3	6.3	61	0.75	16	33	1.85
SL05	1	9	6.3	7.0	46	0.75	24	33	1.39
SL06	1	9	6.3	7.1	45	0.75	24	33	1.36
SL09	1	4	5.5	7.4	21	0.75	24	11	1.97
SL11	1	6	5.2	6.9	34	0.75	24	19	1.78
SL15	2	12	5.0	5.3	31	0.75	16	20	1.58
SL16	2	12	5.0	0.0	39	0.75	16	20	1.99
SL17	2	12	5.1	6.2	48	0.75	16	20	2.43
SL18	2	12	5.1	5.6	50	0.75	16	20	2.53
DL01	2	6	5.1	4.2	24	0.75	24	12	1.97
DL02	2	6	5.1	5.9	20	0.75	24	12	1.61
DL03	2	6	5.6	6.0	22	0.75	24	13	1.69
DL04	2	6	5.6	5.4	24	0.75	24	13	1.84
								average:	**1.85**
								std dev:	**0.31**

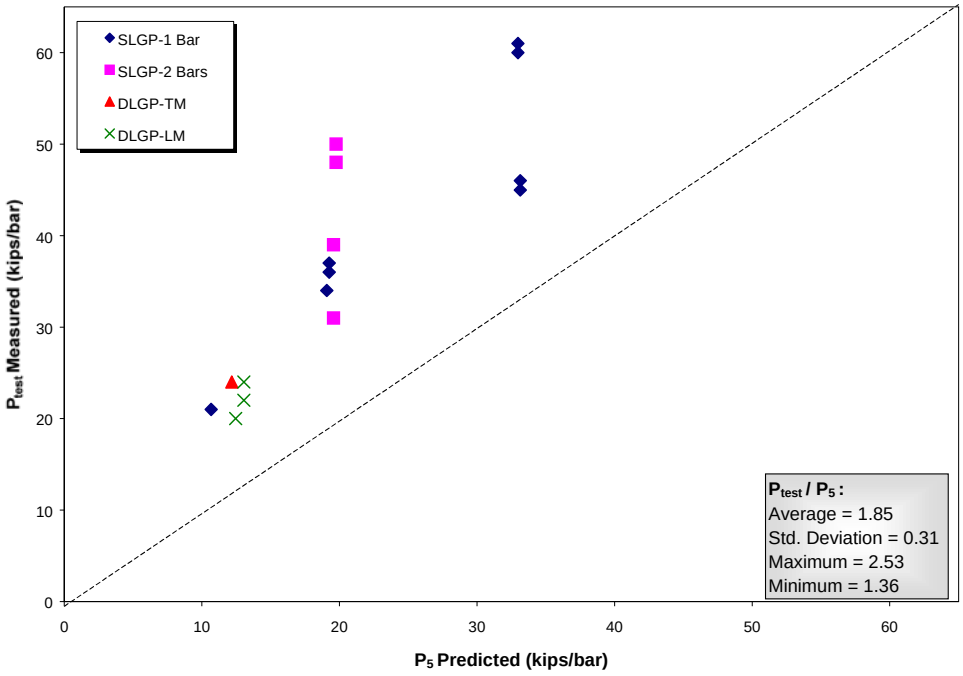

Figure 8.7: Comparison of P_5 Capacities with Test Results

Table 8.6: Design CCD Capacities Using $f'_{c,mod}$, P_6

Test ID	#Bars	h_{ef} in	f'_c ksi	f'_g ksi	P_{test} kips/bar	Ψ_2	A_g in^2	A_c in^2	$f'_{c,mod}$ ksi	k	P_6 kips/bar	P_{test}/P_6
SL01	1	6	5.3	6.9	36	0.75	77	247	5.7	24	20	1.81
SL02	1	6	5.3	6.4	37	0.75	77	247	5.6	24	20	1.88
SL03	1	12	5.3	6.5	60	0.75	77	787	5.4	16	33	1.80
SL04	1	12	5.3	6.3	61	0.75	77	787	5.4	16	33	1.83
SL05	1	9	6.3	7.0	46	0.75	77	571	6.4	24	33	1.38
SL06	1	9	6.3	7.1	45	0.75	77	571	6.4	24	33	1.35
SL09	1	4	5.5	7.4	21	0.75	77	67	6.5	24	12	1.81
SL11	1	6	5.2	6.9	34	0.75	77	247	5.6	24	20	1.72
SL15	2	12	5.0	5.3	31	0.75	77	979	5.0	16	20	1.58
SL16	2	12	5.0	0.0	39	0.75	0	1056	5.0	16	20	1.99
SL17	2	12	5.1	6.2	48	0.75	77	979	5.2	16	20	2.41
SL18	2	12	5.1	5.6	50	0.75	77	979	5.1	16	20	2.52
DL01	2	6	5.1	4.2	24	0.75	55	377	5.0	24	12	1.99
DL02	2	6	5.1	5.9	20	0.75	57	385	5.2	24	13	1.59
DL03	2	6	5.6	6.0	22	0.75	57	385	5.7	24	13	1.68
DL04	2	6	5.6	5.4	24	0.75	57	385	5.6	24	13	1.84
											average:	**1.82**
											std dev:	**0.31**

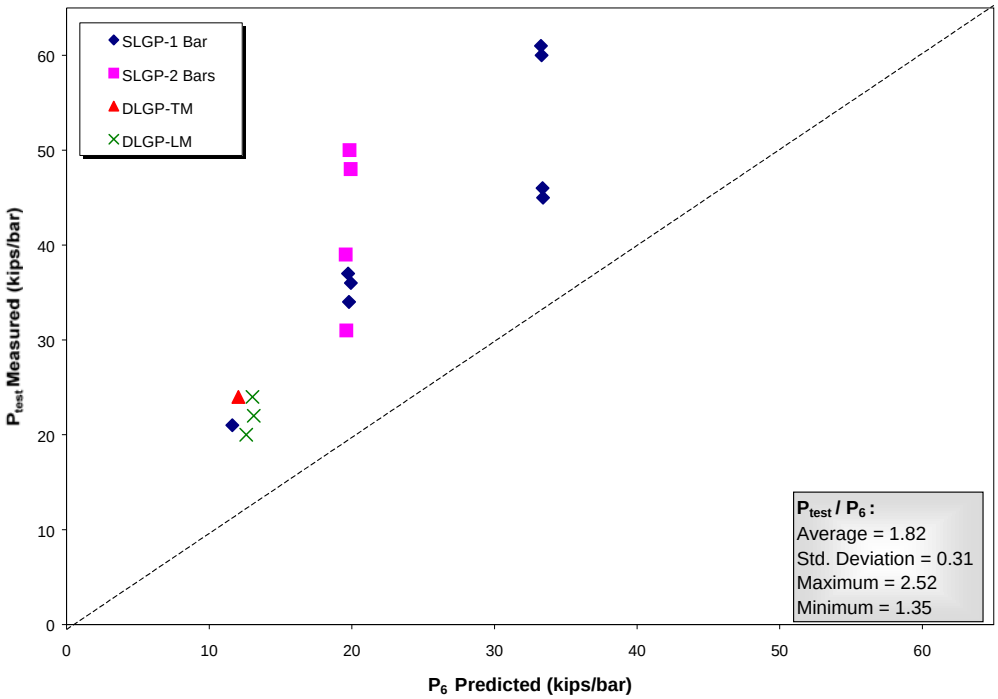

Figure 8.8: Comparison of P_6 Capacities with Test Results

In Tables 8.3 through 8.6, the predicted capacities for specimens SL17 and SL18 are very conservative due to the additional capacity provided by the confinement. However, as discussed in Section 5.3, the breakout surface required large deformations to develop additional capacity from the confining steel. Therefore, confining steel should not be counted on to provide additional capacity in grout pocket anchorages. Confined grout pockets do provide superior ductility to unconfined grout pocket anchorages. Confinement should be used when anchorage ductility is required, as in seismic applications, and for crack control at service load levels.

8.3 ANALYSIS OF STRAIGHT BAR TESTS

Equation 3-6 gives the basic development length for straight bars without confinement from transverse reinforcement. Since there is no transverse reinforcement crossing potential splitting cracks near the bar in grout pockets, it seems reasonable to compute development lengths with Equation 3-6. However, bars in grout pockets are retrained by the wedging action of the grout pocket rather than transverse reinforcement. Research by Orangun et. al. [20] found that Equation 3-6 may be modified for the effects of transverse reinforcement by a factor K as follows:

$$l_d = \frac{12{,}250 d_b}{\sqrt{f'_c}\left(1.2 + 3.0\frac{c}{d_b} + \mathrm{K}\right)} \qquad \textit{(Equation 8-4)}$$

where: $\mathrm{K} = \frac{A_{tr} f_{yt}}{500\, s\, d_b} \le 2.5$ *(Equation 8-5)*

The terms in equation 8-5 refer to the transverse reinforcement parameters. The limit of 2.5 was imposed to account for pullout-type failures. Since grout pocket bars are typically not near an edge, pullout failure should control, as observed in the single and double line tests. Therefore, using a value of K=2.5 for straight bar grout pocket anchorages should account for the restraint provided by wedging action in the grout pocket.

Table 8.7 summarizes the straight bar anchorage capacity predictions, P_s, from Equation 8-4 using K=2.5 and the grout compressive strength. The capacity P_s is approximated by computing a simple ratio of the embedment length to l_d multiplied by the yield strength of the bar. The following example illustrates the calculation for DL05, a 9″ embedment of a #6 bar in Masterflow 928 grout:

Table 8.7: Straight Bar Anchorage Capacities Using K=2.5, P_s

Test ID	#Bars	h_{ef} in	f'_c ksi	f'_g ksi	P_{test} kips/bar	A_b in^2	d_b in	c in	c/d_b	K	α	β	γ	λ	l_d in	P_s kips/bar	P_{test}/P_s
SL13	1	12	5.2	6.9	56	0.79	1.00	12	2.5	2.5	1.0	1.2	1.0	1.0	15.8	36	*
SL14	1	18	5.2	6.9	73	0.79	1.00	12	2.5	2.5	1.0	1.2	1.0	1.0	15.8	54	*
DL05	2	9	5.7	6.3	24	0.44	0.75	8	2.5	2.5	1.0	1.2	0.8	1.0	9.9	24	1.00
DL06	2	9	5.7	6.4	28	0.44	0.75	8	2.5	2.5	1.0	1.2	0.8	1.0	9.8	24	1.16

*Test terminated before failure occurred

DL05: test failure load = P_{test} = 24 kips

h_{ef} = 9″

f'_g = 6.3 ksi on test day

d_b = 0.75 in. for #6 bar

c = 8″ = minimum of bar to edge spacing and bar to bar spacing

c/d_b = 8/0.75 = 11 > 2.5, therefore use c/d_b = 2.5

K = 2.5 for grout pocket anchorages

modification factors from Equation 3-5:

α = 1.0 for vertical bar

β = 1.2 for epoxy-coated bar

γ = 0.8 for #6 bar

λ = 1.0, assume no lightweight aggregate effect for grout

Equation 8-4: $l_d = \dfrac{(12{,}250)(0.75'')(1.0)(1.2)(0.8)(1.0)}{\sqrt{6300\ psi}\left(1.2 + 3.0(2.5) + 2.5\right)} = 9.9\ inches$

yield strength of a #6 bar = 0.44 in^2 (60 ksi) = 26.4 kips

$P_s = \dfrac{9''}{9.9''}(26.4 kips) = 24.0\ kips$

$P_{test}/P_s = 1.0$

The method described above worked well in predicting the pullout strengths of the straight bar grout pocket tests that failed, DL05 and DL06. DL06 reached a peak load of 28 kips, but the deflections increased rapidly at a load of 24 kips. As described in Section 6.4, pocket confinement steel provided in DL06 resulted in the additional capacity. As for headed anchorages, confinement should only be used to provide ductility and crack control, not to provide additional capacity.

The computed development lengths in Table 8.7 are up to 55% conservative for the two straight bar tests in single line grout pockets. Both of these tests were terminated before reaching failure, but each attained a substantially higher load than predicted by the P_s method. For SL13, capacity

may have been enhanced by prying action associated with the large amount of bending observed in the test bar.

Equation 8-4 is a best-fit equation. For design, the ACI expression given in Equation 3-5 [11] should be used. To account for the restraint provided by the wedging action and since grout pocket bars are not near an edge, the term $(c + K_{tr})/d_b$ in Equation 3-5 may be taken as 2.5. This gives the following design expression for straight bar grout pocket anchorages:

$$\frac{l_d}{d_b} = \frac{3}{100}\frac{f_y \alpha \beta \gamma \lambda}{\sqrt{f'_c}} \qquad \textit{(Equation 8-6)}$$

8.4 CONCLUSIONS

With a few simple modifications, the CCD method accurately predicts grout pocket anchorage capacities for upset-headed bars. To account for grout pocket corner cracking, the factor Ψ_2 = 0.75 should be applied to all headed anchorages. To account for the difference in concrete and grout strength, the weighted average compressive strength $f'_{c,mod}$ given by Equation 8-1 may be used in Equation 3-2. However, in most cases it is sufficient to simply use the concrete compressive strength. In cases of shallow embedment or large grout and concrete strength difference it may be necessary to use the modified compressive strength.

Existing straight bar anchorage equations may be used to predict grout pocket anchorage capacities provided confinement of the grout by wedging action in the pocket is accounted for. Equation 8-4 with the confinement factor K = 2.5 accurately predicted straight bar pullout capacities of #6 bars in a double line

grout pocket specimen, and was conservative for tests of #8 bars in a single line grout pocket specimen.

For design of headed bar anchorages the proposed ACI CB-30 [13] equations may be used with the modifications listed above. Straight bar grout pocket anchorages may also be designed by the existing ACI method, which reduces to Equation 8-6 when accounting for confinement. For both types of anchorage, grout pocket confinement steel should not be used to provide additional capacity since that capacity only develops under large deformations. Pocket confinement steel should be used to provide crack control and ductility.

CHAPTER 9

ANALYSIS OF GROUTED VERTICAL DUCT TESTS

9.1 INTRODUCTION

The six straight bar and two upset-headed bar grouted vertical duct tests showed promise for using the confinement provided by the duct to develop bars in much shorter distances than would be required for bars in plain concrete. Because the duct confines the grout well beyond the level assumed in the existing ACI expression for straight bar anchorage in concrete, a new expression is needed. Though only a few variables were studied and limited data were available, the expressions developed in this chapter should be applicable to the typical range of anchorage applications for grouted vertical ducts.

9.2 ANALYSIS OF STRAIGHT BAR GROUTED VERTICAL DUCT TESTS

Of the six straight bar tests summarized in Table 7.1, only GVD01 and GVD04 reached a clearly defined failure. In the remaining four tests the loading was terminated at loads corresponding with the strain hardening range of the bar to either prevent bar fracture or prevent cracks from spreading to the area surrounding an adjacent test specimen. One test, GVD07, with a 24″ embedment had small crack widths (<0.005″) and small deflections (<0.02″) when the loading was terminated. This test clearly did not fail. However, the remaining tests that were terminated in the strain hardening range showed head and grout/concrete

deflections of approximately 0.10″, with widespread cracking up to 0.030″ in width. These tests may be considered to have been on the verge of failing. Thus, five tests, GVD01, GVD03, GVD04, GVD05, and GVD08, are available to calibrate an anchorage design expression.

9.2.1 Modification of Existing Anchorage Expressions

The expression developed by Orangun et. al. [20] for development length given in Equation 3-6 is based on splitting failure controlling the anchorage strength. However, the observed duct failure was essentially a pullout failure, as the grout slipped out of the duct when the duct and concrete could no longer restrain the grout. Though the current ACI expression does not directly address pullout failure, expressions published in earlier codes drew primarily on pullout tests of bars in mass concrete. These bars typically failed by pullout, accompanied by splitting cracks [27]. ACI 318-71 [28] included an expression for development length similar to the following:

$$l_d = \frac{0.034 A_b f_y \Omega \beta}{\sqrt{f_c'}} \qquad \textit{(Equation 9-1)}$$

where: Ω = 0.8 for bars at least 3″ from an edge

β = 1.2 for an epoxy-coated bar (not in ACI 318-71)

In order to provide a best-fit expression, Equation 9-1 does not include the 1.25 factor that was applied as a factor of safety in ACI 318-71. For an epoxy-coated #11 bar with A_b=1.56 and f_y=60,000 psi, Equation 9-1 reduces to the following:

$$l_d = \frac{3055}{\sqrt{f_c'}} \qquad \textit{(Equation 9-2)}$$

Another interesting comparison with results of the grouted vertical duct tests is with the expression developed at the University of Kansas described in Section 3.3.1 [22]. Though the Kansas tests were generally controlled by splitting failure related to small edge distances, they retained the basic premise of pulling a grouted bar out of a preformed hole. By rearranging terms in Equation 3-7 and letting the anchorage strength T_n equal the bar yield force P_y, the following expression is obtained for development length:

$$l_d = \frac{A_b f_y \beta}{30\sqrt{f_c'}} = \frac{3744}{\sqrt{f_c'}} \text{ for an epoxy-coated \#11 bar} \qquad \textit{(Equation 9-3)}$$

Note the similarity between equations 9-2 and 9-3, consisting of a constant divided by a measure of the concrete tensile strength. The difficulty in applying Equations 9-2 and 9-3 to grouted vertical duct pullout tests is that neither equation accounts for the confining effects of the duct on the grout. If the compressive strength f'_c in Equations 9-2 and 9-3 is taken as the grout compressive strength f'_g from cube tests, the development lengths will be severely overestimated because the cube tests do not take into account the strength increase resulting from confining pressure.

Tests by Richart, Brandtzaeg, and Brown at the University of Illinois found that axial compressive strength of cylinders under radial confining pressure increased approximately in proportion to the radial confining pressure [29]. In an attempt to account for the passive confinement of the grout provided by the duct, the grout strength is modified by the following expression developed by Richart et. al.:

$$f'_{g\,\mathrm{mod}} = f'_g + 4.1 f_r \qquad \textit{(Equation 9-4)}$$

where: f'_{gmod} = compressive strength of grout under radial confining pressure

f_r = radial confining pressure

Equation 9-4 will be used for the compressive strength in Equations 9-2 and 9-3. Substituting Equation 9-4 into Equations 9-2 and 9-3 gives the following expression:

$$l_d = \frac{Z}{\sqrt{f'_g + 4.1 f_r}} \qquad \textit{(Equation 9-5)}$$

where: Z = 3055 for the ACI 318-71 expression

= 3744 for the University of Kansas expression

The radial confining pressure required to develop a bar may be found by rearranging Equation 9-5 to give the following expression:

$$f_r = \frac{\left(Z/l_d\right)^2 - f'_g}{4.1} \qquad \textit{(Equation 9-6)}$$

The development length (l_d) in Equation 9-6 corresponds to an embedment depth that would develop exactly the yield stress in the bar. However, the specimens failed at various values of bar stress either above or below the yield stress. To solve for the radial confining pressure in the tests at failure, a length should be substituted in Equation 9-6 for l_d that reflects the actual stress in the bar at failure. At pullout failure, bond stress is typically assumed to be uniformly distributed, giving a bar stress distribution that varies linearly from a maximum at the embedment lead to zero at the embedment tail. Therefore, an equivalent development length for use in Equation 9-6 may be found by modifying the actual embedment depth by the ratio of yield load to failure load:

$$l_{d,eq} = h_{ef} \frac{P_y}{P_{test}} \qquad \textit{(Equation 9-7)}$$

where: h_{ef} = embedment depth of test bar

P_y = Yield load of test bar = 1.56 in^2 (60 ksi) = 93.6 kips for a #11 bar

P_{test} = Failure load or maximum load recorded during test

Table 9.1: Required Radial Confining Pressures for ACI 318-71 and KU Methods

Test ID	grout	h_{ef}	P_{test}	P_y	$l_{d,eq}$	f'_g	Z_{ACI}	f_r	f'_{gmod}	Z_{KU}	f_r	f'_{gmod}
		in	kips	kips	in	psi		psi	psi		psi	psi
GVD01	928	12	76	94	14.8	4200	3055	9368	42609	3744	14584	63995
GVD03	928	18	120	94	14.0	5700	3055	10224	47617	3744	16053	71518
GVD04	EUHF	18	94	94	17.9	3100	3055	6348	29128	3744	9914	43749
GVD05	S212	18	114	94	14.8	4600	3055	9270	42609	3744	14487	63995
GVD08	EUHF	24	118	94	14.8	4900	3055	9197	42609	3744	14413	63995

Table 9.1 summarizes the equivalent development lengths, radial confining pressures, and modified grout compressive strengths for each straight bar duct test that was deemed to have failed. The radial pressures in each case are extremely high, and there is not a consistent confining pressure at failure between the tests. In fact, the radial confining pressures are well outside the range used to develop Equation 9-4. The maximum ratio f_r/f'_c studied by Richart et. al. was only 1.2, whereas the values listed in Table 9.1 result in ratios as high as 3.5. Clearly, Equations 9-2 and 9-3 are not suitable for application to grouted vertical duct anchorages.

9.2.2 Development of a New Expression for GVD Design

Since existing expressions are not easily modified to suit the grouted vertical duct behavior, a more fundamental approach is taken in developing an expression for design of duct anchorages. The main factor driving the anchorage capacity of bars grouted in ducts is the confinement provided by both the duct and surrounding concrete. At some point, the duct and concrete dilate sufficiently to permit the bar and grout to slip out of the duct. As described in Chapter 7, the grout gradually slipped out of the duct at failure. In the cases noted above in which testing was terminated before a clear failure was reached, large amounts of grout slip occurred as the anchorage load increased slightly, resulting in reduced stiffness beyond a certain point in the loading history.

The confinement demand at a particular load level and location is a function of the local bond stress along the bar. Because it is impossible to measure local bond stresses, a useful index of the confinement demand is the average bond stress over the entire bar, given by the following expression:

$$u = \frac{P}{h_{ef}\,\pi\,d_b} \qquad \textit{(Equation 9-8)}$$

where: u = average bond stress

P = load in reinforcing bar

d_b = bar diameter

The confinement demand is also a function of the grout tensile strength, typically taken as a multiple of $\sqrt{f'g}$. The term $\sqrt{f'g}$ is traditionally given units of psi. Because confinement demand is a function of both average bond stress and grout strength, the average bond stress should be nondimensionalized for the

grout tensile strength. This gives the nondimensionalized average bond stress, $\frac{u}{\sqrt{f'_g}}$, which will be defined as Γ.

Figure 9.1 plots Γ versus the maximum recorded duct strain for each test. Because the duct tended to unwind spirally, in most cases the maximum duct strains were measured with the gauge oriented parallel to the spiral. The exceptions were for GVD08 and GVD01. In GVD08, a 24″ embedment test, the duct strains at 12″ from the bar lead measured with the circumferentially-oriented and spirally-oriented gauges were very similar, most likely because the bond stress had more length over which to distribute. The circumferentially-oriented gauge measured slightly higher strains, and these strains are used in Figure 9.1. For GVD01, the bar was only embedded 12″. Therefore, the spirally-oriented gauge at 12″ from the bar lead measured small strains because the bond stress was essentially zero at the end of the embedment. Unfortunately, the duct was instrumented only in the circumferential direction at 6″ from the bar lead. The strains along the spiral at 6″ were likely much higher than the values shown in Figure 9.1.

Because the duct strains for GVD01 were measured circumferentially at a depth of 6″, it is not surprising that the measured strains do not resemble the maximum strain responses measured on the ducts of the other specimens (see Figure 9.1). At a value of Γ just below 15, the apparent duct stiffness deteriorates rapidly. This is most likely due to loss of restraint by the surrounding concrete. The loss of restraint by the duct and surrounding concrete allows the grout to begin to slip out of the duct. Figure 9.2 plots Γ versus the slip recorded at the end

of the embedment (head slip). Though the readings are somewhat erratic, in general the anchorage begins to slip significantly once Γ exceeds 15.

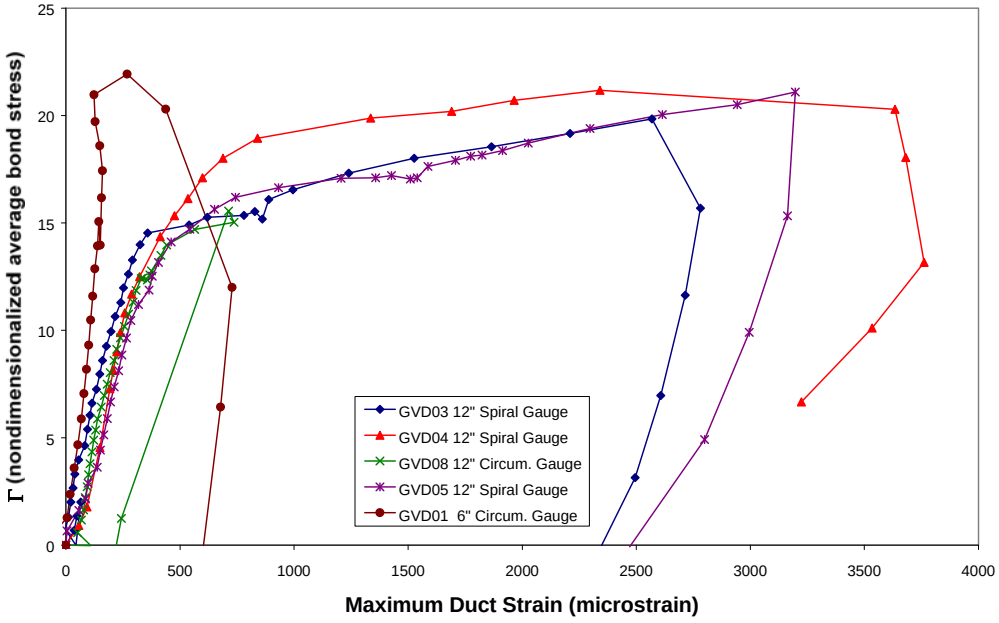

Figure 9.1: Nondimensionalized Average Bond Stress Γ vs. Maximum Duct Strain

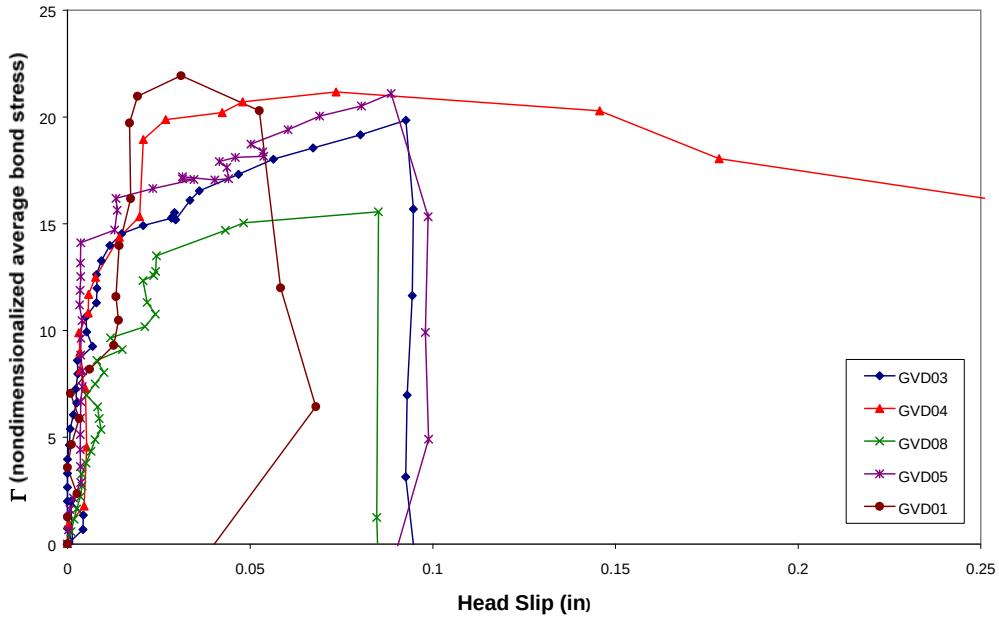

Figure 9.2: Nondimensionalized Average Bond Stress Γ vs. Head Slip

Based on Figures 9.1 and 9.2, it is proposed that for design of grouted vertical duct anchorages the nondimensionalized average bond stress Γ be limited to 15. An important distinction should be made here: this is a design recommendation, not a method for predicting anchorage failure loads. Figures 9.1 and 9.2 clearly show that significant capacity exists past Γ=15. However, it is at this point that the stiffness of the anchorage system is drastically reduced due to dilation of the duct and surrounding concrete. If loading reached this point in a precast bent cap system, irrecoverable large deformations would occur. This is analogous to limiting the stress in steel to the yield stress; significant capacity remains in the steel, but the inelastic deformations are undesirable.

Taking Γ=15, an expression for development length may be derived as follows:

$$\Gamma = 15 = \frac{u_{\max}}{\sqrt{f'_g}}$$

$$u_{\max} = 15\sqrt{f'_g} = \frac{P_{\max}}{h_{ef} d_b \pi}$$

setting $P_{max} = P_y$ and $h_{ef} = l_d$:

$$l_d = \frac{P_y}{15\sqrt{f'_g} d_b \pi}$$

$$l_d = \frac{A_b f_y}{47 d_b \sqrt{f'_g}} \qquad \textbf{(Equation 9-9)}$$

Table 9.2: Summary of Development Lengths and Capacities from Eq. 9-9

Test ID	h_{ef} in	A_b in^2	f_y psi	d_b in	f'_g psi	l_d in	P_d kips	P_{test} kips	P_{test}/P_d
GVD01	12	1.56	60000	1.41	4200	21.8	52	76	1.47
GVD03	18	1.56	60000	1.41	5700	18.7	90	120*	1.33
GVD04	18	1.56	60000	1.41	3100	25.4	66	94	1.42
GVD05	18	1.56	60000	1.41	4600	20.8	81	114*	1.41
GVD08	24	1.56	60000	1.41	4900	20.2	111	118*	1.06

*test terminated at large bar slips before a peak load was reached

Table 9.2 summarizes the development lengths calculated from Equation 9-9 for the grouted vertical duct tests. Using the same assumptions as in Equation 9-7, a predicted test capacity may be found by using the following relationship:

$$P_d = P_y \frac{h_{ef}}{l_d} \qquad \textit{(Equation 9-10)}$$

where: P_d = maximum design tension in the bar at the embedment lengths tested

As expected, the values of P_{test}/P_d listed in Table 9.2 are conservative for all cases.

9.3 HEADED BAR DUCT TESTS

The pullout tests of straight bars in grouted vertical ducts demonstrated that straight bars can be developed in lengths that are easily accommodated within the depth of a precast bent cap. Therefore, headed bars are probably not necessary in typical bent caps. However, in some cases reinforcement congestion will limit the depth of the cap that can accommodate ducts, and in these cases headed bars may be desirable. The two upset-headed grouted vertical duct pullout tests, GVD02 and GVD06, showed that upset heads improve anchorage capacity over straight bars. Since the failure mode of upset-headed duct anchorages was similar to that of straight bar anchorages, a design expression could be developed

by the same method as for straight bars. However, an expression based on only one test failure (GVD02) would be meaningless. If application of straight bars in duct anchorages show that congestion is a problem, additional tests should be conducted in order to develop a design methodology for upset-headed grouted vertical duct anchorages.

9.4 CONCLUSIONS

Existing methods for design of straight bar anchorages were found to be inadequate for design of grouted vertical duct anchorages since they do not account for the restraint provided by the duct and surrounding concrete. In the absence of existing design methods, it is suitable to limit the corrected average bond stress to levels which preclude large inelastic bar slip. Taking the nondimensionalized average bond stress equal to 15, Equation 9-9 is the proposed development length expression for straight bar anchorages in grouted ducts.

Upset-headed anchorages in grouted vertical ducts provide additional capacity and stiffness over straight bar anchorages. However, since straight bar anchorages performed well, the additional cost of upset-headed bars may not be justified. If use of grouted vertical duct connections indicate the need for upset-headed bars to limit congestion, additional testing should be conducted to determine a design expression.

The design recommendations described here should cover the typical range of application of ducts in precast bent cap connections. Though only #11 bars were studied, precast bent cap connections will probably require a minimum #8 bar size simply to transfer typical loads. This range of bar sizes should behave

in a similar manner to the tests reported here. A standard 4″ corrugated duct will most likely be required to provide adequate erection tolerances for the expected range of bar sizes. The use of ducts that will reduce confinement, i.e. ducts of larger diameter or thinner walls, should be carefully considered if the expressions developed here are used.

Ducts show great promise for applications in precast connections, but additional variables should be examined to develop a comprehensive understanding of duct anchorage behavior. The effect of duct diameter and thickness should be determined, and the effect of the strength of the duct spiral seam should be examined. The relationship between confinement provided by the surrounding concrete and that provided by the duct is another issue that is not well understood. Future research should address these issues to provide a complete understanding of duct anchorage behavior.

CHAPTER 10

SUMMARY & CONCLUSIONS

10.1 SUMMARY

Details developed for precast bent cap connections in Chapter 2 facilitate rapid bridge erection and provide a viable and economical alternative to traditional cast-in-place substructures. The results of the anchorage component pullout tests for grout pocket connections and grouted vertical duct connections have shown that adequate anchorage can be achieved in a precast bent cap through the use of upset-headed and straight reinforcing bars. Based on these tests, anchorage design recommendations that address development length, pocket cracking effects, grout strength, duct restraint, and pocket confinement steel were developed.

Eighteen tests simulating single line grout pocket connections were conducted, covering upset-headed and straight bars in single and multiple bar arrangements. Six tests of multiple upset-headed and straight bars simulating double line grout pockets under simulated transverse and longitudinal-moment loading were also conducted. Depending on the embedment depth, capacities of upset-headed anchorages were controlled by either concrete breakout or steel failure. Similarly, capacities of straight bar anchorages transitioned from pullout failure for short embedments to steel failure for deep embedments.

Eight tests simulating grouted vertical duct connections were conducted on straight and upset-headed bars. Similar failure modes were observed in both straight and upset-headed bar tests. Duct expansion triggered by loss of concrete restraint allowed the bar and grout to slip out of the duct.

10.2 CONCLUSIONS AND ANCHORAGE DESIGN RECOMMENDATIONS

10.2.1 Single and Double Line Grout Pocket Connections: Upset-Headed Bars

Based on the twenty tests of upset-headed bars in single and double line grout pockets, the primary factors affecting anchorage capacity were embedment depth and pocket confinement steel. The type of grout used had little effect on the capacity or behavior of the specimens, provided consistent grout strength was maintained. Concrete breakout failure controlled for shallow embedment depths, while steel yield governed the connection capacity for deeper embedment depths. Pocket confinement steel provided capacity increases of up to 60% provided the bar embedment was sufficiently deep to engage the confining steel. However, the capacity gain provided by the confining steel developed only under large anchorage deformations. Due to the geometry of the steel, welded wire fabric confinement was found to be much more efficient than spiral confinement for resisting breakout forces.

The breakout behavior of upset-headed anchorages was driven by cracks that formed at the grout pocket corners due to the stress concentrations caused by the wedging action of the grout in the pocket. These cracks served to break up tensile stress fields in the concrete, forcing breakout behavior similar to that for

headed anchorages in cracked concrete. Pocket corner cracks formed in every loaded grout pocket, but did not form in unloaded grout pockets.

Based on the observed pullout behavior during tests, simple modifications to the cracking factor in the Concrete Capacity Design method provided accurate predictions of the test capacities. The anchorage design recommendations for upset-headed bars in grout pockets are as follows:

for $h_{ef} \leq 11''$:

$$\phi P_n = \phi \frac{A_N}{A_{N0}} \Psi_1 \Psi_2 24 \sqrt{f'_{c,mod}} h_{ef}^{1.5} \qquad \textit{(Equation 10-1)}$$

for $h_{ef} > 11''$:

$$\phi P_n = \phi \frac{A_N}{A_{N0}} \Psi_1 \Psi_2 16 \sqrt{f'_{c,mod}} h_{ef}^{(5/3)} \qquad \textit{(Equation 10-2)}$$

where: ϕP_n = anchorage design strength

$\phi = 0.85$ for concrete breakout

A_N = available projected breakout area at concrete surface (see Figure 3.5)

A_{N0} = basic projected breakout area = $9h_{ef}^2$

Ψ_1 = edge disturbance factor from Equation 3-4

Ψ_2 = grout pocket cracking factor = 0.75

$f'_{c,mod}$ = weighted average concrete strength from Equations 8-1 and 8-2

$f'_{c,mod}$ may be taken as simply f'_c for most cases, but should be calculated for cases of shallow embedment or large difference between grout and concrete strength

h_{ef} = upset-headed bar embedment depth as defined in Figure 3.3.

The anchorage design strength should also be limited to the nominal yield strength of the bar.

Because the anchorage capacity increase provided by pocket confinement steel develops only under large deformations, pocket confinement steel should not be used to provide additional anchorage capacity. However, pocket confinement steel should be used to provide ductility and crack control in grout pocket anchorages. The embedment depth of the anchored bar should be sufficiently large to engage the pocket confinement steel. This can be checked by ensuring that the theoretical CCD breakout surface cracks cross the confining steel so that allows adequate anchorage of the steel is provided on either side of the breakout surface.

10.2.2 Single and Double Line Grout Pocket Connections: Straight Bars

The results of the four straight bar pullout tests in single and double line grout pockets showed that the wedging action of the inverted pyramidal grout pocket provided restraint that enhanced bar anchorage capacity. Straight bars in grout pockets failed by pullout at loads higher than would be predicted by existing ACI methods for bars in concrete.

The existing ACI expression was modified to account for the restraint provided by the wedging action of the grout pocket by taking the transverse reinforcement factor equal to the maximum of 2.5. This modification provided excellent predictions of the test capacities for the two double line grout pocket straight bar tests, but was significantly conservative for the two single line grout pocket tests. Capacity increase due to prying of the bar during the test may explain the high capacity of one of the single line grout pocket tests.

Considering the restraint factor, the existing ACI expression for straight bar development length reduces to the following proposed design equation for straight bars in grout pockets:

$$\frac{l_d}{d_b} = \frac{3}{100}\frac{f_y \alpha\beta\gamma\lambda}{\sqrt{f'_c}} \qquad \textit{(Equation 10-3)}$$

where: l_d = development length

d_b = bar diameter

f_y = steel yield strength

$\alpha,\beta,\gamma,\lambda$ = adjustment factors for reinforcement location, epoxy-coating, bar size, and lightweight aggregate (see Section 3.3.1)

The anchorage design strength should again be limited to the nominal yield strength of the bar.

10.2.3 Grouted Vertical Duct Connections: Straight Bars

Results of the six straight bar grouted vertical duct pullout tests showed that duct confinement allows much shorter development lengths than required in plain concrete. Straight bars in ducts pulled out when the dilation of the grout due to splitting forces could no longer be restrained by the duct and concrete. The primary variables affecting anchorage capacity were embedment depth and grout strength. Short embedment depths produced larger splitting forces and a corresponding increase in duct restraint demand. The reduced stiffness of the lower grout strengths resulted in greater dilation of the grout at a given load. The strain gauge measurements on the duct suggest that the duct expanded by slipping at the seams.

Modifications to existing straight bar design expressions did not adequately predict test capacities. A critical value of normalized average bond stress was identified below which duct expansion and anchorage slip were low. A design expression that produced conservative results was developed based on this critical bond stress. The proposed development length expression for straight bars in grouted vertical ducts is:

$$l_d = \frac{A_b f_y}{47 d_b \sqrt{f'_g}} \qquad \textit{(Equation 10-4)}$$

where: A_b = bar area

f'_g = grout compressive strength

Since only one duct size was used in the test program, application of Equation 10-4 to duct sizes that provide less circumferential resistance (i.e. greater duct diameter and smaller duct thickness) should be carefully considered.

10.3 AREAS FOR FUTURE RESEARCH

This research examined the basic anchorage behavior in grout pocket and grouted vertical duct connections for precast bent caps. A wide range of anchorage types and configurations were studied to simulate typical precast bent cap connections. However, the scope of this research did not allow comprehensive examination of all variables that affect grout pocket and grouted vertical duct anchorage. Therefore, some of the design recommendations developed here, such as for straight bars in grout pockets and ducts, are based on a limited number of tests and are thus necessarily conservative.

Additional tests of straight bars in grout pockets may clear up the discrepancy noted between single line and double line anchorage capacities. A rational method of accounting for the restraint provided by the wedging action of the grout pocket should be developed. Additional straight bar grout pocket variables that were not studied here include grout type, uncoated bars, and confinement steel within the grout pocket.

Only two tests of upset-headed bars in grouted vertical ducts were performed, and only one of those produced a failure. If application of grouted vertical duct connections in future precast bent cap projects indicates that the use of straight bars results in congestion, upset-headed bars may be an effective alternative. Additional tests should be performed in order to develop a design methodology. Additional testing of both straight and upset-headed bars anchored in ducts would provide insight into the relationship between grout dilation, duct restraint, and concrete restraint. Variables not studied here include duct diameter and thickness, bar size, and uncoated bars.

Anchorage behavior is only one component of the performance of precast bent cap connections. A precast bent cap joint will be subjected to a complex state of stress when transverse and longitudinal moments and shears are applied. Future testing should address the performance of the entire connection under various realistic load combinations. The anchorage design recommendations presented here should serve as a guide in developing strut-and-tie models to describe the behavior of the connection region. In addition, full scale connection

testing should address the effects of the bedding layer, precast bent cap post-tensioning, connection shear forces, and bar anchorage in the columns.

The rapid erection process made possible by precast bent caps provides a solution to the growing problem of urban bridge construction. This research has shown that simple connection concepts can accommodate the bridge force-transfer demands. Successful completion of future research should confirm that precast bent caps are a viable and economical alternative to cast-in-place substructures.

REFERENCES

1. American Association of State Highway and Transportation Officials (AASHTO), *Standard Specifications for Highway Bridges*, 16th ed., AASHTO, Washington, D.C., 1992.

2. American Association of State Highway and Transportation Officials (AASHTO), *AASHTO LRFD Bridge Design Specifications: Customary U.S. Units*, 2nd ed., AASHTO, Washington, D.C., 1994.

3. Matsumoto, Eric M.; Waggoner, Mark C.; and Kreger, Michael E, "Development of Precast Bent Cap Systems and Testing Program," *Interim Report 1748-1*, Center for Transportation Research, The University of Texas at Austin, March 1998.

4. LoBouno, Armstrong, & Associates, "Development of Precast Bridge Substructures," Research Report for the Florida Department of Transportation, May 1996.

5. Wolf, Lloyd M. and Friedman, Norman K., "Redfish Bay and Morris & Cummings Cut: Innovations in Bridge Construction and Durability," *Technical Quarterly*, V. 9, No. 2, October 1994, Texas Department of Transportation, Austin, pp. 1-3.

6. Barnes, Robert W., "Development of a High Performance Substructure System for Prestressed Concrete Girder Highway Bridges," M.S. Thesis, The University of Texas at Austin, August 1996.

7. Van der Veen, Theunis, "Precasting the Edison Bridge," PCI Convention, Nashville, October 1992.

8. DeVries, Richard A., "Anchorage of Headed Reinforcement in Concrete," PhD Dissertation, The University of Texas at Austin, December 1996.

9. Wright, Jeffrey L. and McCabe, Steven L., "The Development Length and Anchorage Behavior of Headed Reinforcing Bars," *SM Report No. 44*, University of Kansas Center for Research, September 1997.

10. Choi, Oan Chul; Hadje-Ghaffari, Hossain; Darwin, David; and McCabe, Steven L., "Bond of Epoxy-Coated Reinforcement to Concrete: Bar Parameters," *SL Report 90-1*, University of Kansas Center for Research, 1990.

11. ACI Committee 318, "Building Code Requirements for Structural Concrete and Commentary," *ACI 318-95/ACI 318R-95*, American Concrete Institute, Detroit, 1995.

12. Bashandy, Tarek R., "Application of Headed Bars in Concrete Members," PhD Dissertation, The University of Texas at Austin, May 1996.

13. ACI Committee 318-B, "Fastening to Concrete (Code CB-30)," American Concrete Institute, Detroit, 1998.

14. CEB, *Fastenings to Reinforced Concrete and Masonry Structures: State of the Art Report*, Comite Euro-International du Beton (CEB), August 1991.

15. ACI Committee 349, "Code Requirements for Nuclear Safety Related Concrete Structures," *ACI 349-90*, American Concrete Institute, Detroit, 1990.

16. Precast Concrete Institute, *PCI Design Handbook-Precast and Prestressed Concrete, 4th Edition*, Precast Concrete Institute, Chicago, 1992.

17. Fuchs, W.; Eligehausen, R.; and Breen, J.E., "Concrete Capacity Design (CCD) Approach for Fastening to Concrete," *ACI Structural Journal*, V. 92, No. 1, Jan.-Feb. 1995, pp. 73-94.

18. Eligehausen, R.; Fuchs, W.; and Mayer, B., "Loadbearing Behavior of Anchor Fastenings in Tension," *Betonwerk & Fertigteil-Technik*, No. 12, 1987, pp. 826-832.

19. Eligehausen, R. and Sawade, G., "Fracture Mechanics Based Description of the Pull-Out Behavior of Headed Studs Embedded in Concrete," *Fracture Mechanics of Concrete Structures: From Theory to Applications*, Chapman & Hall, London, 1989, pp.263-281.

20. Orangun, C.O.; Jirsa, J.O.; and Breen, J.E., "Reevaluation of Test Data on Development Length and Splices," *ACI Journal, Proceedings* V. 74, No. 3, March 1977, pp.114-122.

21. Darwin, D.; McCabe, S.L.; Idun, E.K; and Schoenekase, S.P., "Development Length Criteria: Bars Not Confined by Transverse Reinforcement," *ACI Structural Journal*, V. 89, No. 6, Nov.-Dec. 1992, pp. 709-720.

22. Darwin, D. and Zavaregh, S.S., "Bond Strength of Grouted Reinforcing Bars," *ACI Structural Journal*, V. 93, No. 4, July-Aug. 1996, pp. 486-495.

23. Restropo, J.L.; Park, R.; and Buchanan, A.H., "The Seismic Behavior of Connections Between Precast Concrete Elements," *Research Report No. 93-3*, Department of Civil Engineering, University of Canterbury, Christchurch, New Zealand, April 1993.

24. Park, R., "A Perspective on the Seismic Design of Precast Concrete Structures in New Zealand," *PCI Journal*, V. 40, No. 3, May-June 1995, pp. 40-60.

25. Zheng, L.X., "Grouted Precast Concrete Column connections under Reversed Cyclic Bending and Compression," *ACI Structural Journal*, V. 93, No. 3, May-June 1996, pp. 247-256.

26. Einea, A.; Yamane, T.; and Tadros, M.K., "Grout-Filled Pipe Splices for Precast Concrete Construction," *PCI Journal*, V.40, No. 1, Jan.-Feb. 1995, pp. 82-93.

27. ACI Committee 408, "Bond Stress-The State of the Art," *ACI Journal*, Proceedings V. 63, No. 11, Nov. 1966, pp. 1161-1188.

28. ACI Committee 318, "Building Code Requirements for Reinforced Concrete," *ACI 318-71*, American Concrete Institute, Detroit, 1971.

29. Richart, F.E.; Brandtzaeg, A.; and Brown, R.L., "A Study of the Failure of Concrete under Combined Compressive Sresses," *Bulletin No. 185*, University of Illinois Engineering Experiment Station, 1928, 104 pp.